Abstract

Ingle, Nilesh P. Mechanical Performance and Finite Element Analysis of Bi-directional Barbed Sutures (Under the direction of Dr. Martin W. King)

In the current investigation the mechanical performance of barbed sutures made from resorbable and non-resorbable polymer monofilaments were studied. The main objective was to find a method to differentiate between those polymers that form “good” barbs and those that do not. To achieve this objective a suture/tissue pull-out test was developed in which the suture was stressed in a tensile test until it was removed from a tissue simulant specimen. This test was conducted on four resorbable sutures: Biosyn, Maxon, Monocryl & PDS and on three non-resorbable sutures: Ethilon, Novafil & Prolene. Those barbed sutures giving a pull-out load in excess of 1.5 kg were considered to have “good” barbs with adequate mechanical performance. X-ray diffraction, differential scanning calorimetry and tensile testing experiments were performed on the suture polymers in an attempt to identify which microstructural characteristics of the polymer and/or mechanical properties of the monofilament are associated with “good” barb performance. It was found that Maxon, PDS, Ethilon and Prolene sutures gave superior barb performance. Small compactly arranged crystalline structures were found to be the most important factor for the formation of “good” barbs. In addition, the peak tensile elongation of the unbarbed suture was also found to correlate with superior barb performance. The peak tensile force, modulus and toughness of the monofilament appeared to have no effect. It is therefore concluded that the ability of a polymer to form good barbs depends on small crystal size and high tensile elongation. Barb failure was observed to proceed through one of two mechanism; either curling or peeling. Two dimensional finite element analysis of the barb geometry identified the stress concentrations in and near the barbs under load, which were in agreement with the mechanisms of barb failure as observed by image analysis.

Mechanical Performance and Finite Element Analysis of Bi-directional Barbed Sutures

NILESH PANDHARINATH INGLE

A thesis submitted to the Graduate Faculty of
North Carolina State University
in partial fulfillment of the
requirements for the Degree of

Master of Science

TEXTILE TECHNOLOGY & MANAGEMENT

Raleigh, North Carolina

August 2003

Approved by:

David R. Buchanan	**Subhash K. Batra**

Martin W. King
Chair of Advisory Committee

Dedicated to,
my mother and father

Biography

Born in a farmers family, Nilesh Ingle developed an early interest in fibers particularly cotton as a child. He earned Bachelor (May 1997) and Master (December 1999) of Textiles degrees from the University of Bombay (Mumbai), India, where he was the recipient of an All India Council of Technical Education Graduate Aptitude Test for Engineers Scholarship (1997-99). The higher learning of basic textiles and the role of textile fibers further solidified his keen interest in the subject. After working for a year as a marketing and technical manager in the polyester fiber industry, Nilesh decided to pursue fundamental research in fiber science abroad. He joined the College of Textiles at NC State University in August 2001 and is currently a graduate student in the Department of Textile and Apparel Technology and Management. His research work focuses on understanding the biomechanical interactions of biomaterials with living tissue.

Acknowledgements

I wish to thank my advisor Dr. Martin W. King for everything, who made this project possible. His deep interest in the project and his complete attention to every small and simple observation, that I reported to him during the project, inspired me to understand more and more complex phenomenon. His technical support in each and every aspect and guidance at every small step in the project was exceptionally encouraging and gave a new dimension to the project.

I wish to thank Dr. David R. Buchanan for his technical support with his expertise in x-ray diffraction and guidance throughout the project. His keen interest in understanding the composition of crystal size structure in the polymer matrix helped me understand the microstructure of the polymer.

I wish to thank Dr. Subhash K. Batra for his technical support with his expertise in mechanics and guidance throughout the project. His enthusiasm and insight for understanding the filament mechanical behavior in a particular state of existence, made me look at a problem from a clear mechanical perspective.

I wish to thank Dr. Jeff Leung and Mr. Stan Batchlor from Quill medical for supporting the project and providing samples. Dr. Jeff Leung's interesting queries helped us understand the barbed suture. Mr. Stan Batchlor's expertise in creating barbs on a monofilament surface of a specific geometry and well planned schedule for providing samples, helped us to procure and test the samples in time.

I wish to thank Dr. Behnam Pourdeyhimi and Dr. Eunkyoung Shim for their fullest co-operation in providing the Image Analysis facitlity for the project

I wish to thank Dr. John S. Strenkowski for his technical support in finite element analysis in the project.

I wish to thank North Carolina State University for supporting the project. The DHL Library, College of Textiles Library and The Veterinary Library have been a tremendous source of published literature all around the globe. The Unity Computer Laboratories have been very important in providing the computer's and software's needed during the project.

I wish to thank Ms. Birgit Anderson for her full co-operation in performing the experiments with the Differential Scanning Calorimetry technique.

I wish to thank Mr. Chad Graham for his help in performing the experiments with MTS tensile testing machine and unwavering co-operation during the entire project.

I wish to thank Mr. Ferdinand Lundberg for his full help in performing the x-ray diffraction experiments.

I wish to thank Mr. Abhay Mohan for all his help during the entire project.

Nilesh P. Ingle

TABLE OF CONTENTS

List of Figures

List of Tables

1 Introduction

A surgical suture is either a synthetic monofilament or a braided multi-filament structure or alternatively a cut, ground or polished ligature derived from animal intestines, used for tissue approximation or the attachment of an implantable device. Sutures can be made of either resorbable or non-resorbable materials. Resorbable sutures degrade and disintegrate inside the body after exposure to the *in-vivo* environment in a pre-determined time interval, so there is no need for a second surgery to remove the suture after the tissue is healed at the site of the wound. On the other hand the non-resorbable sutures do not degrade, so there is a need to remove them after healing of the wound, unless they are being used as a permanent implant.

The conventional method for securing a suture is by tying the ends together in a single knot, or if the two ends are some distance apart, to tie two or more knots. The main objective while suturing is to effectively distribute the tissue holding forces throughout the suture length. This can be done in various ways, such as using different types of stitches, whereby the length of the suture between the knots can be varied. The frequency of the stitches in the tissue can be used to distribute the forces. Other methods for tissue approximation include the use of tissue adhesives, staples, clips, fasteners, belts, sutures with a preformed loop, and sutures with projections [8,9].

Compared with the conventional knotted suture, the monofilament suture with projections eliminates the necessity to tie a knot. The projections hold the tissue along the entire length of the suture, thus distributing the tissue holding forces over a larger area. The projections grip the tissue at many points and so do not allow slippage of the suture from within the surrounding tissue. This gives an even distribution of forces along the suture length, and through the tissue.

Suture knots themselves present certain disadvantages, once formed inside the body, such as delaying wound healing, constriction of blood flow, and distortion of tissue, which can lead to scar formation. Moreover, because knotting increases local stress concentrations, sutures invariably tend to fail at

the knot. As a result, the clinical performance of a suture is measured in terms of its knot security.

A suture with projections, such as a bi-directional barbed suture, is believed to have certain advantages over conventional sutures. For example, it has the ability to put tension in the tissue with less suture slippage in the wound, as well as to more evenly distribute the holding forces, thereby reducing tissue distortion [1]. Since there is no knot, there is no extra localized mass and volume of suture material, reducing inflammation and hence promoting early wound healing [1].

In such a bi-directional barbed suture barbs can be formed along the length of a monofilament suture by cutting oblique notches in the side of the suture. When cuts are inserted in some types of polymers, such as polydioxanone, polypropylene and polyamide the barbs stand out, whereas with other types of polymers such as polyglycolic acid copolymers, the barbs do not stand up. They fall back immediately into the notch and do not interact mechanically with surrounding tissue.

1.1 Problem Statement:

The problem being studied attempts to identify the most appropriate type of synthetic polymer to be used in the production of monofilament sutures with projections or barbs.

1.2 Goals & Objectives:

The goal of the study is to identify reasons why barbs formed on monofilaments of some polymers stand out and interact mechanically with the surrounding tissue, while those on other synthetic polymers collapse and prevent the monofilament from serving as a barbed, knotless suture. The polymers to be studied are three copolymers of polyglycolic acid, polytrimethylene-carbonate & poly-1,4-dioxane-2-one; polyglycolic acid & polytrimethylene carbonate;

polyglycolic acid & polycaprolactone. Other four polymers to be studied are poly-1,4-dioxane-2-one, nylon 6, polybutester, polypropylene.

The specific objectives to evaluate the above phenomenon are summarized in the following statements:

1. To develop a suture/tissue pull-out test, the results of which can be used to simulate and predict for tissue holding capacity of the suture.
2. To determine the suture/tissue pull-out force for specified resorbable and non-resorbable suture polymers
3. To determine the effect of adding barbs on the suture/tissue pull-out force of selected unbarbed sutures.
4. To determine which micro-structural characteristics of the polymer, measured by x-ray diffraction and DSC, are correlated with superior suture/tissue pull-out force.
5. To determine which tensile and bending properties of the polymer monofilament are correlated with superior suture/tissue pull-out force.
6. To determine the tensile properties of the resorbable or non-resorbable so as to calculate their bending rigidity.
7. To identify mechanisms of barb failure.
8. To use finite element analysis to estimate the relative stress concentrations in and near barbs under load.

1.3 Limitations

1. The barbed and unbarbed suture samples used in this study have been prepared specifically for this investigation in an non-randomized production process. The experimental results therefore apply to this series of samples only and cannot be interpreted by statistical analysis to refer to a larger population of sutures.

2. The suture size (monofilament diameter) and barb geometry of the suture materials used in this study were controlled within a narrow range for reasons of limiting the scope of the experimental design. The results therefore should not be inferred to apply to other suture sizes and barb geometries.

2 Review of Literature

2.1 Classification of sutures

Sutures can be classified into different groups depending on their origin (natural or synthetic), their synthetic (monofilament or braided), their biostability (resorbable or non-resorbable) and whether or not they contain barbs, Figure 2.1.

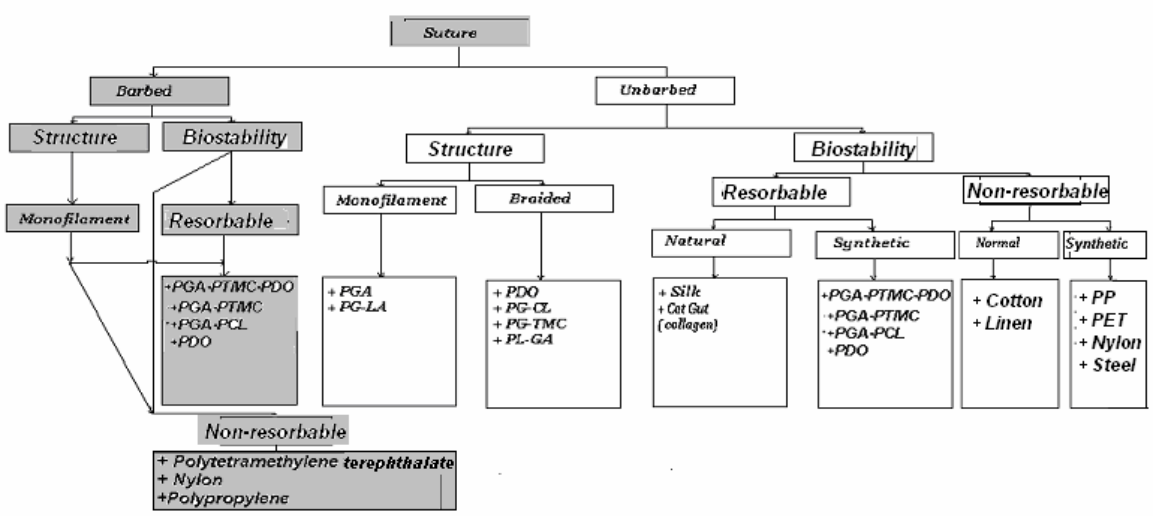

Figure 2. 1: Classification chart for surgical sutures

2.2 Knotted and knotless sutures

Until recently the most sutures were held in place by the tying of a knot. However, because of the disadvantages of having to tie knots, the idea of a knotless suture has been considered over the years.

2.2.1 Disadvantages of knotted sutures

- Delay of wound healing
- Constriction of blood flow
- Distortion of tissue which can lead to scar formation
- Loss of knot security due to increased local stress concentrations

2.2.2 Advantages of barbed knotless sutures

There are a number of innovative ways of securing a suture without the use of a knot. Examples of the these knotless sutures are described in the following sections. However the type of knotless sutures of direct interest to this study is the barbed suture as described in section 2.4. The advantages of barbed sutures are:

- Faster placement – eliminates the necessity to tie a knot
- More distribution of holding forces in tissue
- Elimination of complications associated with knots, e.g. infection and suture "spitting".

2.3 Types of knotless sutures

Various types of knotless suturing methods have evolved over the years. Lemole in 1971 patented a suture which had a needle, a notched suture, and a latched collar. After suturing, the suture is pulled to the correct tension for closure and then locked by the latch and collar [9].

Akiyama in 1978 patented a surgical suture with a plurality of spherical projections on the surface. The suture had a needle on one end and a threading member on the other end. This type of suture can close an opening, such as a blood vessel, without tying a knot. Figure 2.2 shows the mold for producing these spherical projections made of a synthetic resin such as polyvinyl alcohol [7].

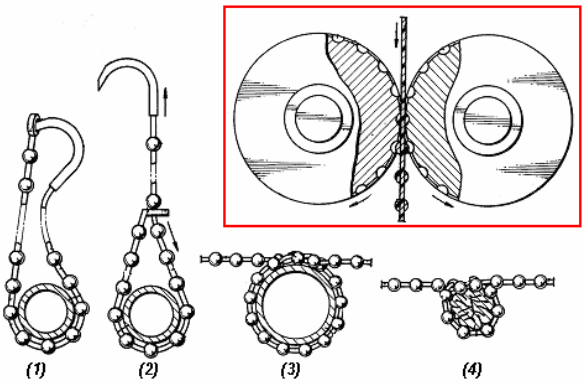

Figure 2. 2: A type of knotless suture with spherical projections[7].

Wilk et al patented a suturing device, Figure 2.3, with a looped end which is shown in the figure below. There are four different types of projections on the suture. By passing the needle through the loop and tightening, the suture can be used for two purposes; for closing an open vessel and for tissue approximation without the need for a knot [6].

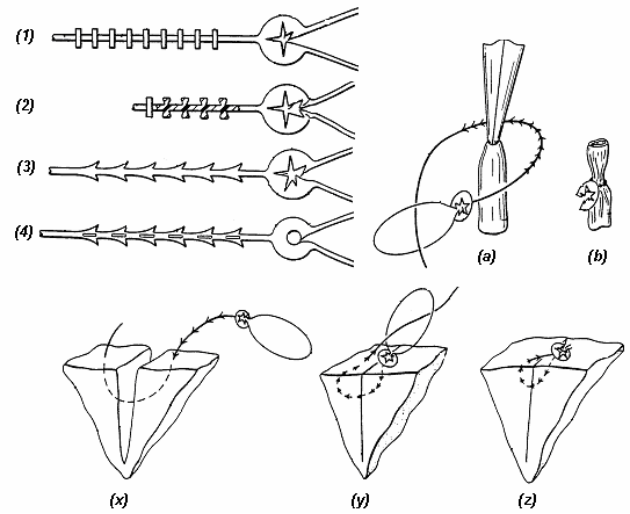

Figure 2. 3: A knotless suturing device[6].

Brotz at al in 1996, Figure 2.4, patented a suturing device which has lateral members with spikes in two directions. These lateral members have a pointed tip, and can penetrate tissue for wound closure. Once inserted the lateral members hold the tissue in position [5].

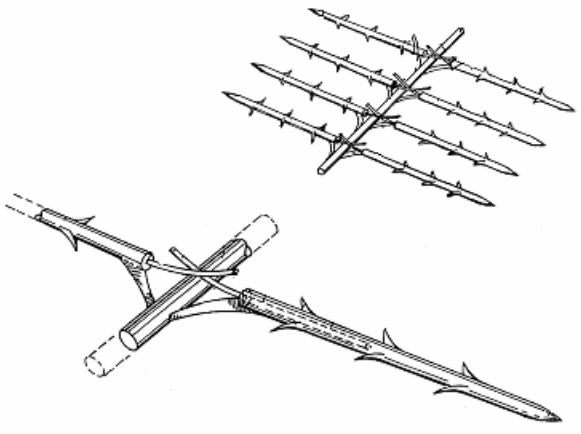

Figure 2. 4: Slender barbed projections fixed on a center filament for tissue approximation[5].

Yoon in 1993 patented a range of suturing devices useful in endoscopic surgery. Figure 2.5 shows various forms of the suturing apparatus. The surface morphology can be varied from barbs to serrated surfaces. These devices are made of bioresorbable polymers. They have a sharp tip, with a slender barbed length to penetrate through the tissue. Instead of a knot, these devices need to be bent and secured in an adjustable plug or loop so as to hold the tissue in position [8].

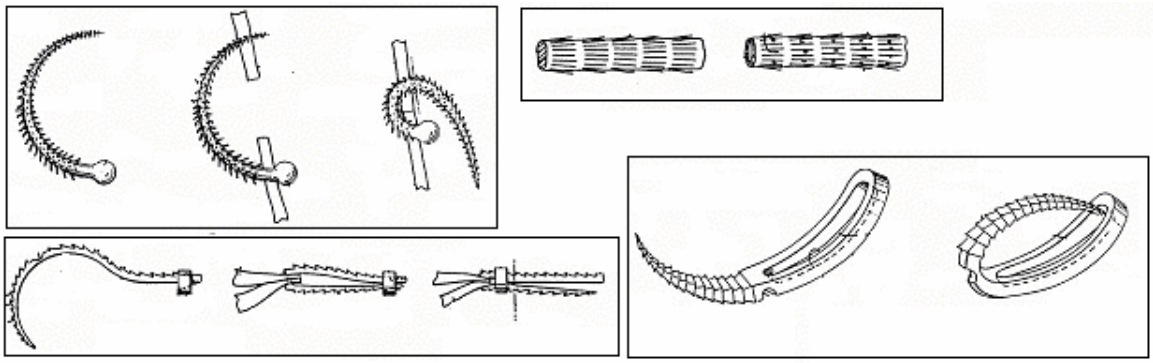

Figure 2. 5: Barbed suturing apparatus[8].

2.4 Changing the surface morphology of a monofilament suture

One of first attempts to acknowledge the importance of surface morphology was made by Cox in 1944. He patented an apparatus for grinding and polishing ligatures. His objective was to make a surgical cat-gut suture with a circular cross-section and a smooth surface, Figure 2.6 [2].

Figure 2. 6: A photomicrograph of a polished surgical cat-gut suture showing grooves [2].

It was in 1958 that Maltin et al patented a method for manufacturing wool-like artificial fibers. The fibers he made had a surface structure as shown below.

It was produced by imparting a intermittent flow to the molten polymer at the spinneret. These pulses traveled beyond the spinneret into the coagulating bath, Figure 2.7 [10].

Figure 2. 7: Wavy filament surface a result of pulsatile polymer flow[10].

Alacamo in 1964 patented a few designs, Figure 2.8, of barbed sutures. The designs described as:

1. barbs/spicules at acute angles (large barbs)
2. barbs/spicules at acute angles (small barbs)
3. projects terminating in curved edges
4. projections at right angles
5. projections having curved edges and alternating directions
6. knurled surface
7. spiral
8. sharp curved edges
9. spherically triangular curved facets
10. annular notched rings
11. sinuous suture body with barbs

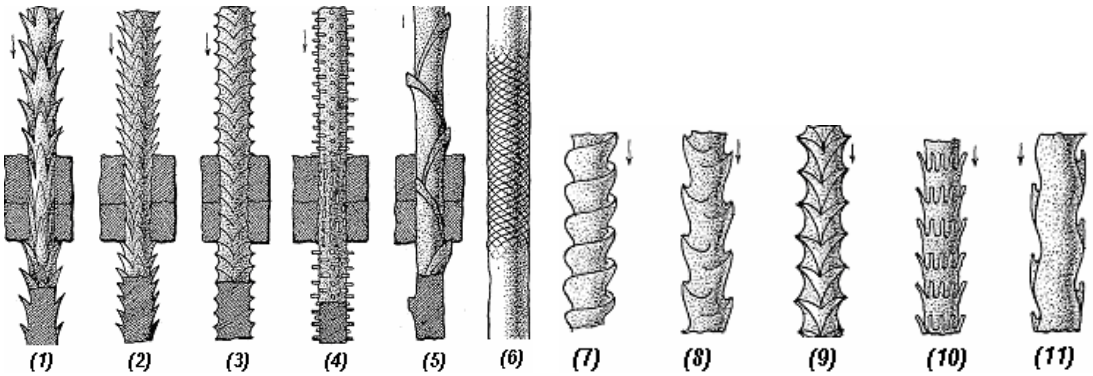

Figure 2. 8: Different types projections on a knotless suture[11].

Buncke in 1999 patented a bi-directional and a uni-directional surgical suture, Figure 2.9. The uni-directional suture had one needle at one end. The bi-directional suture had two needles at both ends of the monofilament suture (Figure 2.9). While suturing with the uni-directional needle, a combination of two sutures in opposite directions had to be used [3].

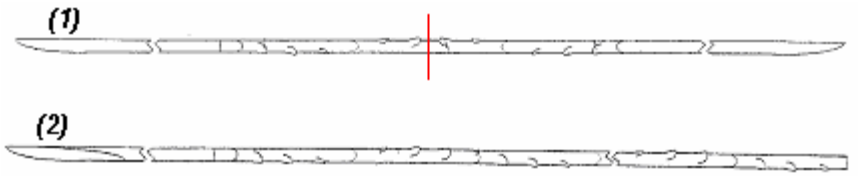

Figure 2. 9: A bi-directional suture (1) & a uni-directional suture (2)[3]

2.5 Methods of creating a barb on a monofilament suture

Buncke in 1999 patented three methods of creating a barb on the surface of a monofilament (diameter: 100 to 500 microns). The first method shown in Figure 2.10, consists of a bar with cutting blades that moves inwards and outwards against the stationery monofilament to produce barbs. The second method consists of a rotating cutting wheel which has blades on the surface. The monofilament is held under tension and the blades from the opposing pair of wheels cut into the monofilament and push it forward to form two rows of parallel barbs [3].

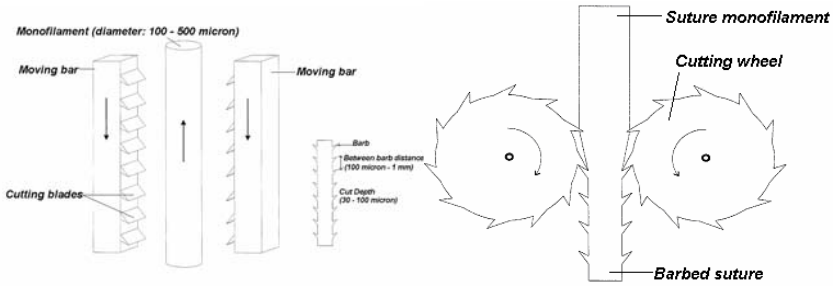

Figure 2. 10: Methods for creating barbs on a monofilament suture[3].

In another embodiment of his apparatus the barbs are created by the use of a laser. As shown in Figure 2.11, a sharp focusing industrial laser is directed at the

cross hatched areas. The laser removes these areas to form barbs. The barbs can be formed in a spiral around the monofilament by keeping it in a twisted form while creating the barbs. When returned to a relaxed state the barbs will then form a spiral around the monofilament suture [3].

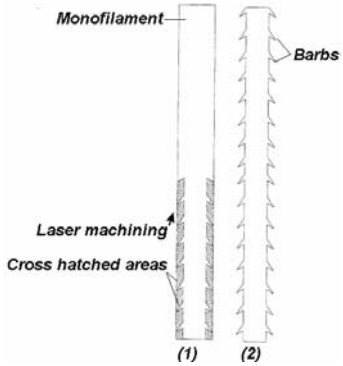

Figure 2. 11: Laser cutting method for creating barb on a suture monofilament[3].

Williams et al in 2003 filed an application for patenting methods of forming barbs on a monofilament surface. As seen in the Figure 2.12- A, B, C, D, the principle of cutting is with the sharp edge of a knife. One method of creating a barb is by Method A, wherein the knife has only one degree of freedom. Hence the knife moves along the x-axis to cut the filament and create a barb. In case of Method B, the knife has 2 degrees of freedom. So the knife moves forward in the y direction as it simultaneously moves along the x-axis. The third Method C, consists of a blade which has 3 degrees of freedom. Here the knife moves forward (y axis) on its way down (z axis), and is then pulled out in the x-axis direction after cutting the barb. The Method D, has a blade also with 3 degrees of freedom. But this time the knife has a zig-zag motion imparted to it as shown in the Figure 2.12[13].

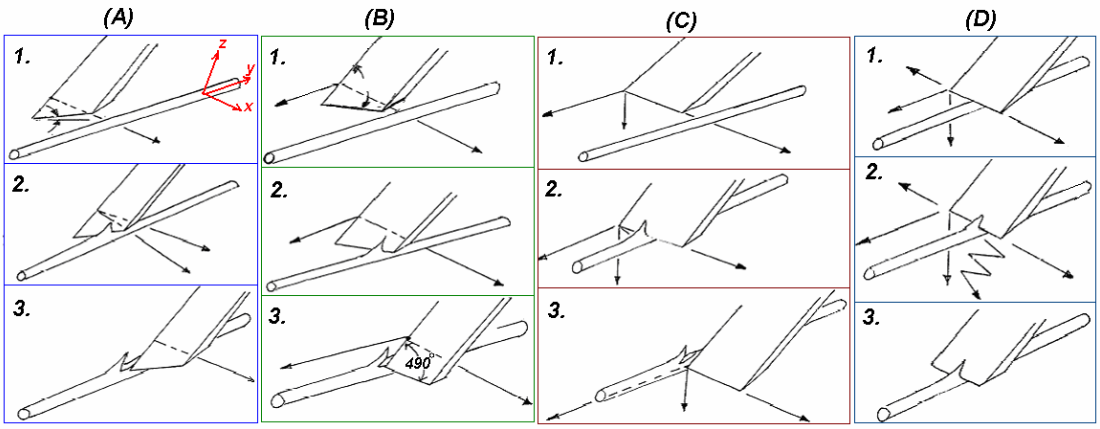

Figure 2. 12: Paths of blade while creating a barb on a monofilament suture[13].

Each of the above methods of cutting barbs with blades having different degrees of freedom creates different barb designs. It is this movement of the blade inside the monofilament suture that decides the final geometry of the barb.

As shown in Figure 2.13 the barb cutting apparatus includes a vise assembly with notches. They hold the monofilament firmly along its whole length. The cross-sectional view is shown in A, B & C. The firm grip of the vise ensures the filament is stationary. A blade then comes to cut into the filament to create the barb. Another view of the vise is shown in I & II. The third inset shows the four stages of the suture while barbs are being created. The inset (1) shows a monofilament before cutting in a relaxed state, where the dotted line is the fiber axis. The stage (2) shows the same suture after insertion of twist. In stage (3) the barbs have just been formed. They all lie along the top of the suture. The inset (4) shows the final barbed suture in a relaxed state. The barbs can be seen formed in a spiral around the monofilament once the twist has been removed [13].

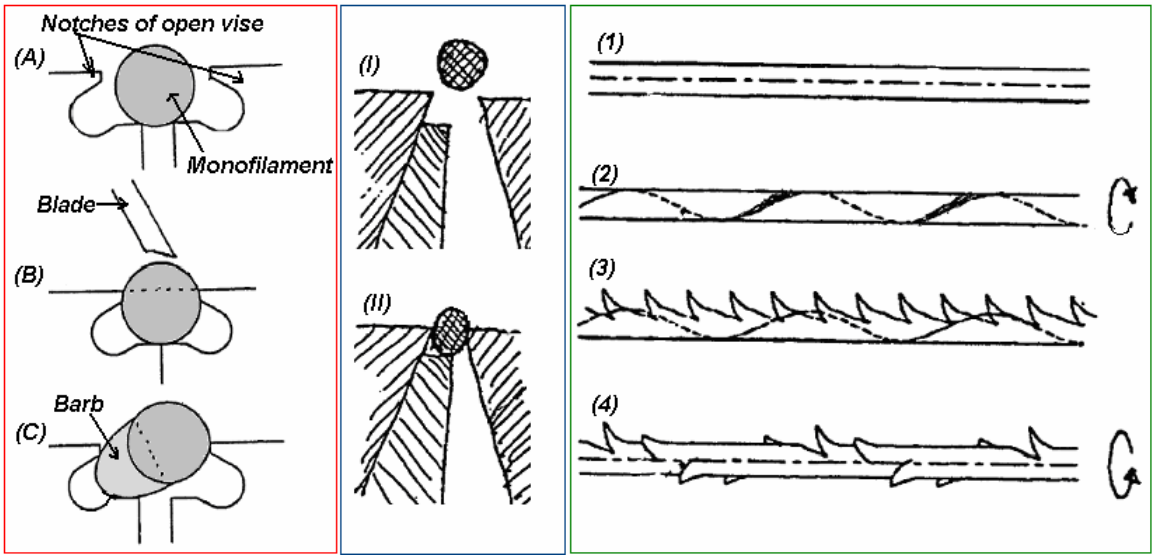

Figure 2. 13: Monofilament suture clamping device for creating barbs[13].

2.6 Suturing techniques with barbed sutures

Buncke used a uni-directional suture to stitch two pieces of tissue together. This type of suture has only one needle. So, one suture has to be stitched in one direction and another suture is used to stitch in the opposing direction so that the opposing barbs of the two separate sutures hold the tissue in position [3].

Kaplan et al in 2003 filed an application for patenting various suturing techniques with a bi-directional barbed suture. His techniques require the use of only one bi-directional suture to approximate tissue. Since this type of suture has two needles, and barbs are facing in opposite directions starting from the center of the suture (marked by arrows in Figure 2.14). The first step in suturing is to put one of the needles through both tissue layers at the center of the wound and to pull the suture through to the center locking point. This is because at this point the first pair of opposing barbs face each other and the suture cannot be pulled further through the tissue against the opposing barbs. To complete the wound closure both ends of the suture can be stitched in various ways such that the entire suture remains concealed beneath the tissue. Figure 2.14 depicts four such suturing techniques [4].

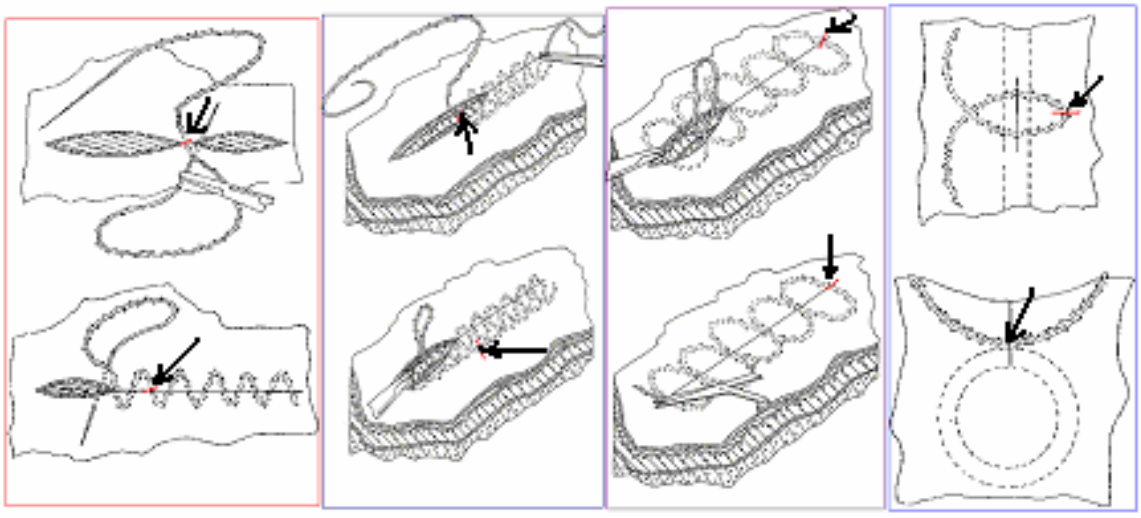

Figure 2. 14: Suturing techniques with a barbed suture[13].

2.7 Tissue holding capacity of bi-directional barbed sutures

Dattilo et al in 2003 studied the effect of barb geometry on the tissue holding capacity of bi-directional barbed sutures. They used a modified running stitch to suture two pieces of tissue stimulant together and loaded the specimens in an Instron constant-rate-of-elongation tensile tester to measure the peak load required to produce a 2 mm gap in between the two pieces of tissue stimulant. They found that a cut angle of 159.9 ± 2.1 degrees and cut depth of 0.15 ± 0.03 mm gave the highest tissue holding capacity at 2.83 ± 0.85 kgf [1].

3 Materials and Methods

This chapter discusses in detail the materials and methods used to perform the experiments. The investigation will be supported by experimental measurements of the physical properties and microstructure of the various polymers and barbed filaments. In addition the mechanical performance of barbed sutures will be measured by a novel suture/tissue pull force test that has been developed specifically for this study. Finite element analysis will be used to understand the distribution of the stresses in the barb and near barb regions.

3.1 Design of Experiments

The design of experiments consists of dependent and independent variables. The effect of each of these independent variables on the dependent variables is studied.

3.1.1 Dependent variables

The dependent variables are:

- Suture/ tissue pull-out force
- Length of suture pull-out

3.1.2 Independent variables

The independent variables are:

Variable defining the microstructure of the suture:

- Crystal size
- Degree of crystallinity
- Herman's orientation factor

Variables defining the mechanical properties of the suture:

- Bending rigidity
- Tensile modulus

- Peak tensile load
- Tensile toughness
- Peak tensile elongation

3.2 Materials

Seven types of sutures were used in this project. They are listed in the Table 3.1.

Table 3. 1: Suture Material

Sr. #	Suture Trade Name	Manufacturer	Polymer Type	Suture Size	50% force retention
1	Biosyn	USSC	Polyglycolic acid (PGA) - Polytrimethylene-carbonate (PTMC)- Poly-1,4-dioxane-2-one (PDO) (60% : 26% : 14%)	0	1-2 w
2	Maxon	USSC	Polyglycolic acid (PGA) - Polytrimethylene-carbonate (PTMC) (67.5% : 22.5%)	0	2 w
3	Monocryl	Ethicon	Polyglycolic acid (PGA)- Poly-caprolactone (PCL) (75% : 25%)	0	1-2 w
4	PDS II	Ethicon	p-dioxanone (100%)	0	~ 8 w
5	Ethilon	Ethicon	Nylon 6 (100%)	1	-
6	Novafil	USSC	Polytetramethylene terephthalate (100%)	0	-
7	Prolene	Ethicon	Isotactic polypropylene (100%)	1	-

All these sutures were supplied in a unbarbed original condition as prepared and packaged by the manufacturer. In addition, barbed sutures of the same size were prepared and supplied by Quill Medical Inc (RTP, NC).

3.3 Methods

Table 3.2 lists the types of tests performed on the unbarbed and barbed sutures.

Table 3. 2: Experimental Tests Performed

Sr. #	Name of Test	Parameters Measured
UNBARBED		
1	Physical Characteristics	i. Linear Density (denier), ii. Density (gm/cc).
2	X-ray Diffraction	i. Crystal size ii. FWHM (degrees) iii. $Cos^2\Phi$ iv. Degree of orientation, (Herman's orientation factor)
3	DSC	i. Degree of crystallinity (%)
4	Image Analysis	i. Diameter (mm)
5	Tensile Testing	i. Peak Tensile Load (gms) ii. Peak Tensile Elongation (%), iii. Tensile Elastic Modulus (gms/denier), iv. Calculated Bending rigidity ($gf*cm^2$) v. Toughness (Joules)
6	Suture/tissue Pull-out Force Test	i. Suture/ Tissue Pull-out force (gms)
BARBED		
1	Image Analysis and Barbed Geometry	i. Cut Depth (mm) ii. Cut Angle (degrees) iii. Calculated Cut Length (mm) iv. Barb Angle (degrees) v. Barb Length (mm) vi. Barb Base Length (mm) vii. Spiral Angle (degrees) viii. Diameter (mm) ix. Distance Between Barbs (mm)
2	Barbed Suture Tensile Testing	i. Peak Tensile Load (gms) ii. Peak Tensile Elongation (%), iii. Toughness (joules),
3	Barbed Suture Pull Test	i. Barbed Suture/ Tissue Pull Force (gms) ii. Suture pull-out length (mm)

3.3.1 Physical Characteristics

A unit length of each monofilament was measured and then weighed in a dry state on a scientific weight balance with a precision of 0.1mg. One measurement of a complete unbarbed monofilament suture type was made. The length and the weight were noted. Then the linear density of the monofilament was calculated. Denier is the mass in grams of 9000 meters of yarn.

The cross-section of the monofilaments was found to be circular when observed at a 90^0 angle in the image analysis system. Hence we considered the monofilament to be a circular cylinder, with *[volume] = [area of circular cross-section]*[length]*. Therefore the *density* (in *gms/cc*) of the monofilament sutures was calculated from: *[density] = [mass]/ [volume].*

Both the linear density and the polymer density were calculated for the unbarbed sutures only. Since the same size sutures were used for making the respective barbed suture, the denier and the density were assumed to remain the same. No loss of material was observed during the barb cutting process.

3.3.2 X-ray Diffraction

3.3.2.1 Apparatus

The Omni ATPS, XRD 1000 (Model # PH268L-25) x-ray apparatus was used. A proportional counter was used to measure both the intensity and position of the x-ray peaks.

3.3.2.2 Operating condition

A copper source was used for the production of x-rays. The wavelength of the Cu k_α was 1.54 A^o.

3.3.2.3 Measurement angle 2θ:

This section will describe a principles for 2θ angle measurement.

3.3.2.3.1 Mounting of the specimen:

The metal ring with the filament wrapped on it was placed on the magnetic circular mount connected to the 'chi-motor' inside the x-ray chamber. The disc was placed inside the x-ray chamber on a circular rotating stage.

3.3.2.3.2 Specimen Preparation

Specimens were mounted on a circular metal ring (~ 1 inch diameter) which was placed in the x-ray machine to direct the incident x-ray beam. For preparing each specimen, the monofilament was cut into lengths equal to the

diameter of the ring. The total number of such lengths amounts to a number that gives a 5mm width when mounted parallel on the ring. It is very important to arrange the filaments exactly parallel to each other without overlapping or cross-crossing to avoid double curves in the images. The free ends of these pieces were fixed by adhesive cellophane tape onto the ring, Figure 3.1.

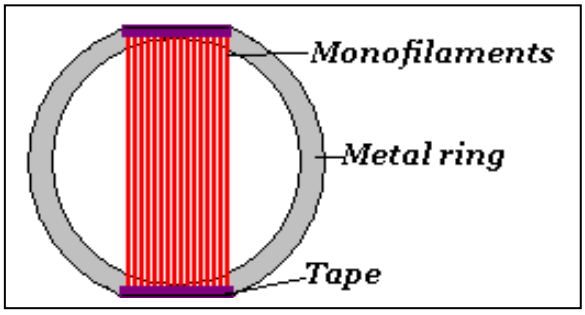

Figure 3. 1: Specimen for x-ray analysis.

3.3.2.4 Crystal Size

The crystal size is calculated from the FWHM (full width at half maximum, see fig.) of the 2-theta curve from the following relation,

$$\Delta(2\theta) = \frac{0.9\,\lambda}{L\cos\theta}$$

where,

$\Delta(2\theta)$ – *Full width at half maximum (FWHM), in radians*

L - *Crystal size, in* $A^{o.}$

λ - *wavelength, in* A^{o}

3.3.2.5 Measurement of angle $\Phi_{1/2}$:

3.3.2.5.1 Imaging Conditions

Suture Type : Unbarbed monofilament suture

Exposure time : 30 minutes

3.3.2.5.2 Specimen preparation:

The specimen of parallel monofilament sutures was mounted on a metal plate with a circular hole. The filaments were carefully arranged parallel to each other, Figure 3.2.

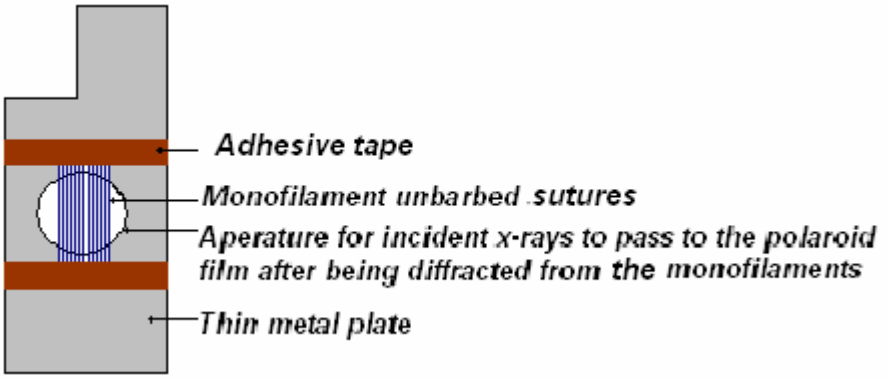

Figure 3. 2: Monofilament suture mounting plate for X-ray imaging

3.3.2.5.3 Method of experimentation:

The specimens mounted on the plate were clamped in a holder in front of the x-ray shutter eye such that the monofilament axis was vertical. A Polaroid film was placed in a clamp facing the x-ray beam. The Polaroid film was slid into the Polaroid apparatus with the 'Expose' knob still inside (not pulled out) and the lever in its upper position. After the film was completely slid inside the apparatus, the 'Expose' knob was pulled out and the film was pulled out as far as possible till it stopped. The film was now ready to be exposed to the oncoming x-rays diffracted through the monofilament specimen. On opening shutter #1, the film was exposed for 30 minutes.

After completion of the exposure the 'Expose' knob was pushed inside. The film was pushed back inside and the lever to unload was turned down. Then the film was pulled out and allowed 30 seconds for developing. On opening the package the image was wiped immediately with a neutralizer and allowed to dry. The image was then ready for measurement of angle *phi.* Then the Herman's orientation factor was calculated. One Polaroid image per suture type was taken for measurements.

3.3.2.5.4 Angle $\Phi_{1/2}$:

The angle phi is the angle shown in the figure below, measured in degrees, which is used to calculate the preferred orientation of the crystalline structure with respect to the fiber axis, Figure 3.3.

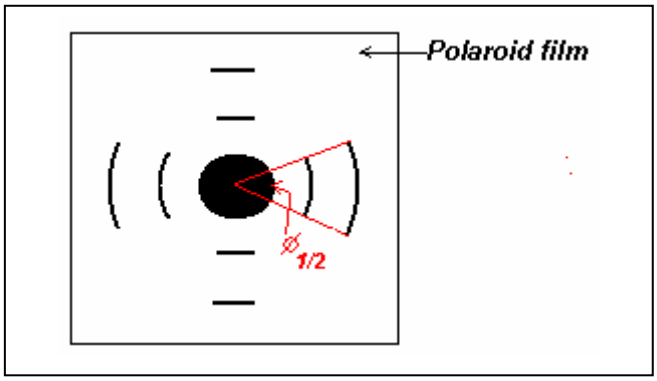

Figure 3. 3: Measuring angle *phi* from image

3.3.2.5.5 Calculating $\cos^2 < \Phi >$ for a normal distribution of Φ:

The cos2<phi> curve is calculated by solving the following integral[22]:

$$\cos^2\phi = \frac{\int_0^{\pi/2} I(\phi)\cos^2\phi\sin\phi\,d\phi}{\int_0^{\pi/2} I(\phi)\sin\phi\,d\phi}$$

where,

$$I(\phi) = \left(\frac{h}{\sqrt{\pi}}\right)e^{-h^2\phi^2}$$

$$\phi_{1/2} = \frac{0.833}{h}$$

$\phi_{1/2}$ = from Polaroid image

$I(\phi)$ = Intensity distribution

3.3.2.5.6 Herman's orientation factor

It is calculated from the following relationship[22]:

$$f = \frac{3 < \cos^2\phi > -1}{2}$$

It gives a measure of the degree of orientation for the crystalline regions in the monofilament. A value of *f=0* indicates random distribution, *f=1* indicates perfect orientation, *f=-1/2* indicates perfect orientation perpendicular to z-direction. The

figure below shows a possible way in which the crystalline and the amorphous regions of the monofilament polymer could be arrange.

3.3.3 Differential Scanning Calorimetry:

A Perkin Elmer (Model: Diamond DSC) differential scanning calorimeter was used to find the degree of crystallinity and melting temperature of the seven unbarbed sutures. Specimens weighing at least 5mg were crimped and sealed in aluminum pans and the heating rate from 25^{o} – 300^{o} C was maintained at a constant rate of 20^{o}C/minute. The temperature and exthoerm scales were calibrated with a known mass of indium.

3.3.3.1 Degree of Crystallinity

The degree of crystallinity refers to the proportion of crystalline material present in a polymer. The higher the degree of crystallinity the higher is the amount of crystals in the polymer. After each run the base line was constructed under the melt peak and the area corresponding to the heat of fusion was calculated.

3.3.3.2 Calculations

The degree of crystallinity was calculated from the heat of fusion of the known mass of polymer tested and the heat of fusion value for the same but 100% crystalline polymer. In case of a co-polymer the heat of fusion data for the major component of the polymer was used[14].

$$Degree\ of\ crystallinity\ (\%) = \frac{Heat\ of\ fusion\ for\ sample}{Heat\ of\ \ fusion\ for\ 100\%\ crystalline\ polymer} \times 100$$

or,

$$Degree\ of\ crystallinity\ of\ copolymer\ (\%) = \frac{Heat\ of\ fusion\ for\ copolymer\ sample}{\mathrm{Pr}\ oportionate\ heat\ of\ \ fusion\ for\ 100\%\ crystalline\ major\ \ polymer} \times 100$$

3.3.4 Image Analysis and Barb Geometry

The barb geometry is one of the most important factors that gives the exact dimensions of a barb design.

3.3.4.1 Apparatus

The following equipment and software were used for the measurement of barb geometry:

- Monofilament holder
- Optem Zoom microscope with upper and lower light source for illumination
- Image analysis software

3.3.4.2 Calibration

The ratio of the number of pixels to the horizontal length in millimeters was calibrated before starting measurements. This was done by focusing a scale at magnifications 1x, 2x and 6x. The number of pixels in 1mm were recorded and used to convert the barb geometry measurements from pixels to mm.

3.3.4.3 Specimen Mounting

A monofilament suture was threaded through the eye of the specimen holder and tightened with a screw. The other end of the suture was passed over a small roller and was fixed to the frame using adhesive tape, to maintain the suture in a straightened position.

3.3.4.4 Characterization

A single bi-directional barbed suture was divided into four zones on each side, as shown in the Figure 3.4 below:

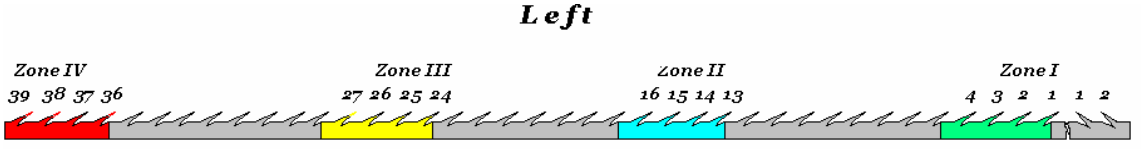

Figure 3. 4: One side of a bi-directional barbed suture, showing barbs to be measured in color.

Each zone thus contained four barbs. Each barb was characterized by the following a set of dimensions,Figure 3.5.

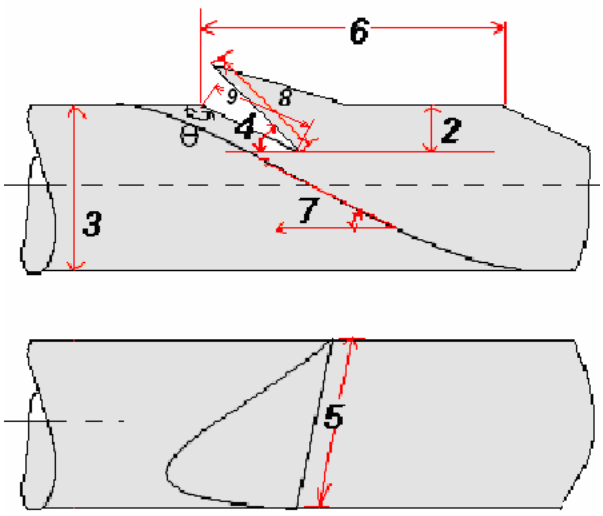

Figure 3. 5: Barbed suture dimensions

Where,

1. θ, Cut Angle
2. Cut Depth
3. Diameter
4. Barb Angle
5. Barb Base Length
6. Distance Between Barbs
7. Spiral Angle
8. Barb Length
9. Cut length (calculated).

3.3.4.5 Measurements:

The monofilament sutures were in a straightened relaxed state, with a nominal turn of 90^{o} while measuring all dimensions, except for the distance between barbs.

All the measurements were taken directly from the image. The distances measured between two points and the angles measured in degrees are depicted in the figure above.

The barb cut length was calculated by the following formula[1]:

$$Cut\ Length,\ \ L_c = \frac{D_c}{Sin(180-\theta)}$$

where,

Dc – Cut depth

Θ – cut angle

3.3.4.6 Focusing views

The measurements were taken from various angles for a single barb, to assure proper focusing and exact measurements. The pictures below, Figure 3.6, show the focusing angles while measuring the dimensions of a barb from:

- Normal side view
- Cut depth view
- Barb angle view
- Top view

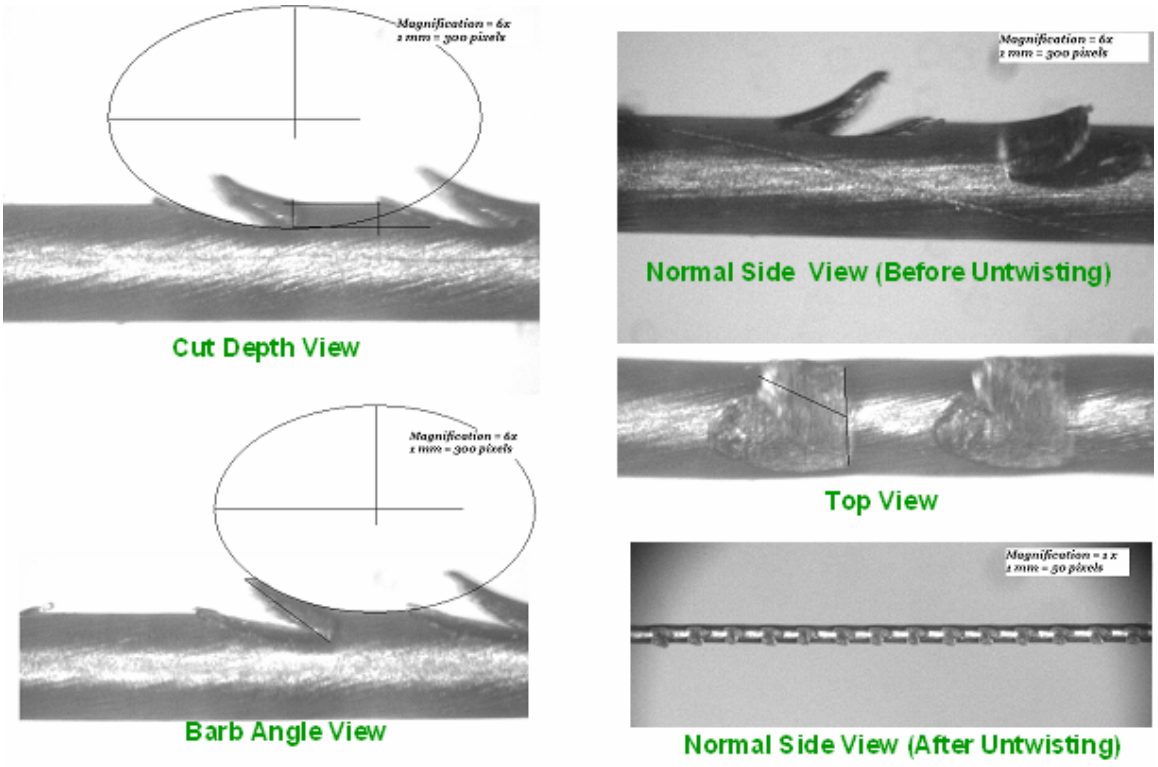

Figure 3. 6: Focusing on the barbs at different angles to measure barb geometry

The 16 measurements thus taken on each suture were then statistically analyzed.

3.3.5 Tensile Tests

An MTS (Model # 1122) tensile testing machine was used to test the

- Tensile load of the unbarbed suture monofilaments
- Tensile load of the barbed suture monofilaments
- Suture/ Tissue Pull-out Test

3.3.5.1 Testing Conditions

Table 3. 3: Tensile testing conditions for monofilament sutures

Sr. #	Condition	Tensile Testing	Suture/ Tissue Pull-out Test
1	Load cell capacity	500 kg	500 kg
1	Gauge Length	16.62 cm	12 cm
2	Cross-head Speed	0.6 mm/sec	1.0 mm/sec
3	Clamp Air pressure	30 psi	30 psi
4	Types of Clamps	Capstan	Capstan and flat jaw
5	Material	Suture monofilament	Suture monofilament, tissue simulant
6	Atmosphere	70^{o}F, 65% RH	70^{o}F, 65% RH

3.3.5.2 Tensile Testing of Un-barbed Sutures

The unbarbed suture monofilaments were tested in the dry state with the use of the intact filaments which were clamped in capstan clamps. After clamping the filaments were loaded at a constant rate of extension. The filament break was set at a sensitivity of 100% and the jaws returned after each specimen broke. The broken specimens were collected for viewing of the fracture plains by image analysis.

3.3.5.3 Tensile Testing of Barbed Sutures

Exactly the same procedure was followed for testing the barbed sutures. The rate of loading was kept the same as the unbarbed sutures so that the data

could be compared. Again the broken specimens were collected for image analysis.

3.3.5.4 Calculation of bending rigidity:

The bending rigidity is the product of Young's modulus and the moment of inertia of a circular rod about its axis[39]. It can also be calculated from the following equation:

$$Bending\ rigidity = \frac{\eta.E.T^2}{4.\pi.\rho} \times 10^{-5}\ (gf.cm^2)$$

$where,$

$\eta - Shape\ factor, (\eta = 1, circular\ cross - \sec tion)$

$E - Initial\ Young's\ Modulus\ (gf / tex)$

$T - Linear\ density, (tex)$

$\rho - Suture\ polymer\ density, \left(g / cm^3\right)$

3.3.6 Suture/ Tissue Pull-out force test

The Figure 3.6 shows a specimen ready to be loaded in the MTS mechanical testing machine to measure the suture/tissue pull-out force. The gray area consists of a tissue simulant which was the size shown in the figure, where D is the diameter of the needle used for suturing through the tissue simulant. A one inch clamping space was kept for clamping the tissue simulant in the lower jaw of the MTS machine, which remained stationary.

This compound specimen type and shape were designed specifically for use in this study. The shape of the suture was a semicircle of the diameter of the suturing needle. This type of suturing method was used to replicated the bending of the suture when stitched by a suturing method inside the body, where it will remain in curved form. This also enables the barbs to be deployed in a protruding or extended fashion. In this study D=1.3 cms, Figure 3.7.

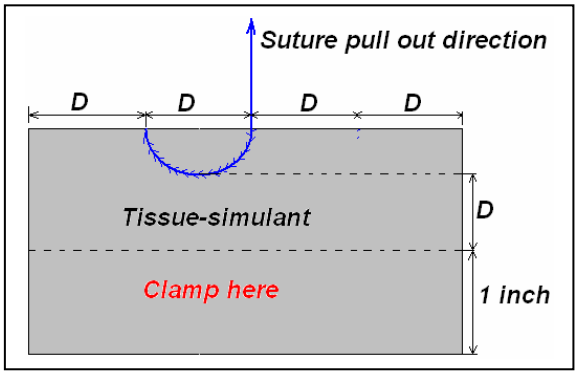

Figure 3. 7: Specimen for Suture/Tissue Pull-out force.

The pull-out force measured was the peak load the suture could sustain inside the tissue simulant before being pulled out. This force is higher than the first peak of the first barb failure and the final breaking force at the suture failure load. The tissue simulant used in the present study was 'Miracle Towel' manufactured by Turtle Wax Accessories, LLC, Chicago, IL 60638 which is a type of fibrous nonwoven sandwiched between two microporous foam layers.

3.3.7 Statistical Analysis

The data was statistically analyzed to determine significant differences between data sets using an f-test, t-test and one way analysis of variance (ANOVA). In addition linear regression analysis was performed so as to identify which variables were closely correlated. Values for α were assumed to be 0.05.

3.3.7.1 F-test

The f-test was used to test whether two population variances were equal or unequal.

Assumptions:

- The values within a sample were independent of each other and were normally distributed
- The two samples were independent of each other

The F-value was interpreted depending if F-calculated was less than F-critical, than the difference was not significant, and vice-versa.

3.3.7.2 T-test

This test was performed on the data to test the level of significance of the means of two sets of data at 95 % level of confidence[40].

$$t = \frac{X_T - X_C}{\sqrt{\frac{\mathrm{var}_T}{n_T} + \frac{\mathrm{var}_C}{n_C}}}$$

where,

X_T, X_C - mean

$\mathrm{var}_T, \mathrm{var}_C$ - covariance

n_T, n_C - number

3.3.7.3 Analysis of Variance:

One way analysis of variance was performed on sets of data to determine if there were significant differences between the sets.

3.3.7.4 Linear Regression Analysis

The Pearson's correlation coefficient r was calculated to find the level of association between two set of variables. It was calculated as the sum of the squares of differences between observed values and the mean values for those sets of data[40].

$$r = \frac{\sum x_1 x_2}{\sqrt{\left\{\left(\sum x_1^{\,2}\right)\left(\sum x_2^{\,2}\right)\right\}}}$$

where,

x_1 , x_2 – standard deviations from respective mean

3.3.8 Finite Element Analysis

The finite element analysis of the barbed suture was performed using Ansys software. The PDS II suture with a density of 1.59 gm/cc was used to run the simulation assuming the barb geometry values listed in the following Table 3.5.

Table 3. 4: Barb Geometry for solid modeling.

Parameter	Value
Cut Angle	166^{o}
Cut Depth	0.13 mm
Cut Length	0.59 mm

3.3.8.1 Assumptions:

1. The barbed filament was considered multi-linear elastic, so the viscoelastic` function of creep and stress relaxation did not apply to the current model.
2. The barbed filament was a two dimensional model
3. The barbed filament properties were considered isotropic.
4. The Poisson's ratio (i.e. the ratio of elongation normal to a compressive stress compared to elongation parallel to a compressive stress) was assumed to be 0.5

The following material properties were used to run the simulation, Table 3.6,

Table 3. 5: Extrapolated stress-strain values for Polydioxanone polymer

Sr. #	Strain (%)	Stress (lb-f)
1	0.00	0.00
2	7.30	0.85
3	14.70	1.45
4	22.03	1.04
5	29.41	2.79
6	36.76	3.39
7	43.50	3.62

3.3.8.2 Ansys two dimensional simulation parameters

- Element : Plane 42, 4 nodes, 2-D space
- Structural Properties: Multilinear Elastic
- Meshing: Area – free

3.3.8.3 Solid Modeling

The two dimensional solid model was designed using the above parameters. The Figure 3.8 shows the meshed two barbed suture with boundary conditions of zero displacement at the four corners or the rectangle.

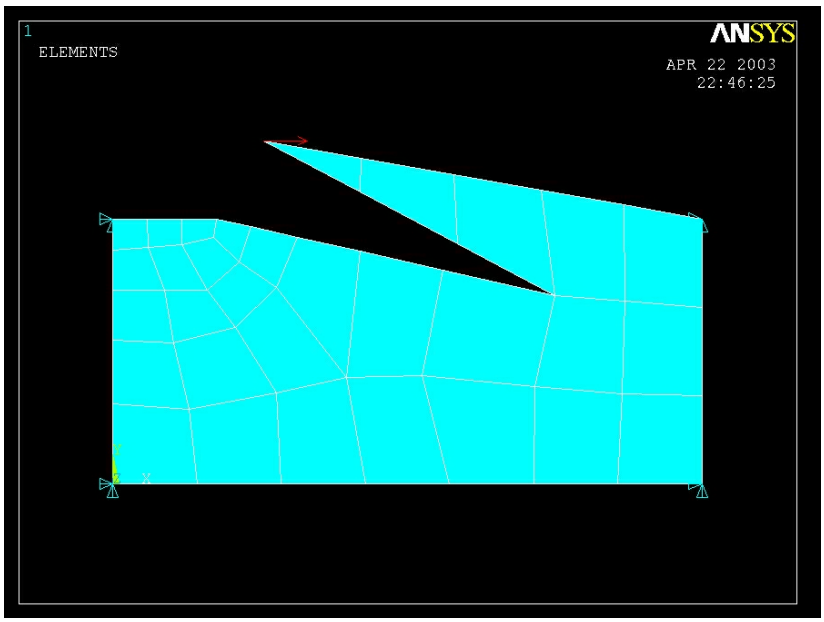

Figure 3. 8: Meshed solid model for a barbed suture.

3.3.8.4 Running the Simulation:

A force of 2.0 lbs was applied at the tip of the barb in the positive x-direction. The results were then analyzed for nodal stress and strain.

4 Results and Discussion

In this chapter all the results from the testing procedures are listed. Possible reasons why some polymers form rigid barbs and others do not form rigid barbs will be discussed in this chapter.

4.1 Results

4.1.1 Physical Characteristics

The suture monofilaments were weighed and measured so as to find their linear density, filament diameter and density, Table 4.1.

Table 4. 1: Physical measurements

	Mass Linear Density (denier)	Filament Diameter (mm)		Density (gms/cc)	
		(present)	(literature)	(present)	(literature)
Biosyn	2191.93	0.440 ± 0.002	-	1.60	-
Maxon	2348.53	0.443 ± 0.002	0.466[59]	1.69	-
Monocryl	2215.63	0.448 ± 0.002	-	1.56	-
PDS II	2070.74	0.443 ± 0.001	0.437[59,60]	1.49	1.45[41]
Ethilon	1769.89	0.459 ± 0.002	0.450[59]	1.19	1.13[44]
Novafil	1484.58	0.384 ± 0.001	0.382[59]	1.42	-
Prolene	1534.46	0.459 ± 0.005	0.457[58,59]	0.96	0.90[43]

4.1.2 X-ray Diffraction

The x-ray diffraction was performed on the seven types of suture polymers. Figures 4.1 - 4.7 show the x-ray diffraction patterns on a Polaroid film. These images depict the arcs which are the reflections from the crystal size axis. The angle Φ measurements were obtained from these images. The convention followed to obtain the orientation of these images was to look for the length of the arc. The smaller the length of these curves, the more oriented is the polymer. A dot in place of an arc indicates very high crystallinity. On the other hand if an arc that extends into a circle is seen in the image it indicates that the material has totally random orientation.

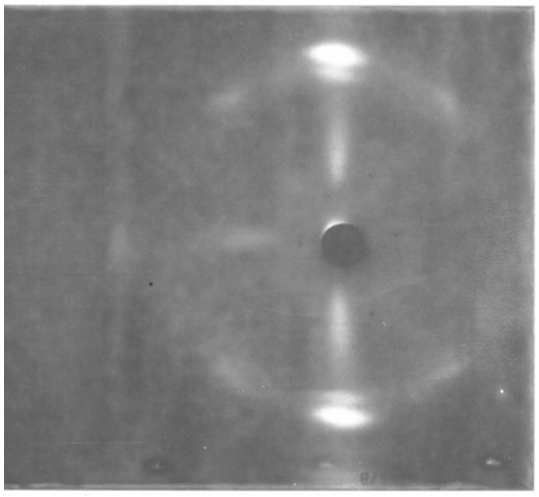

Figure 4. 1: Biosyn x-ray Polaroid image

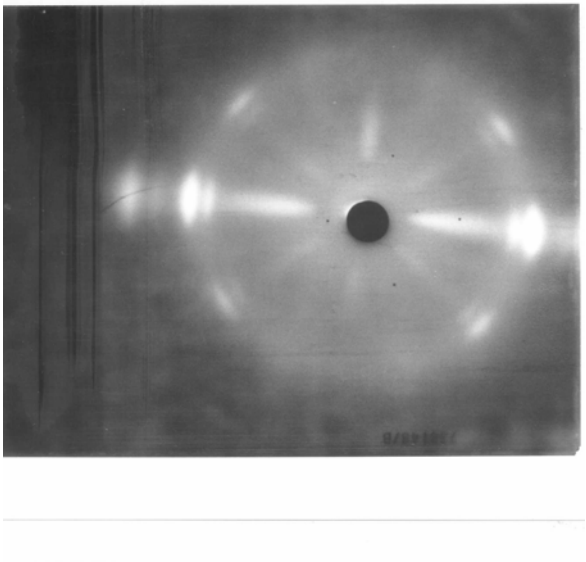

Figure 4. 2: Maxon x-ray Polaroid image.

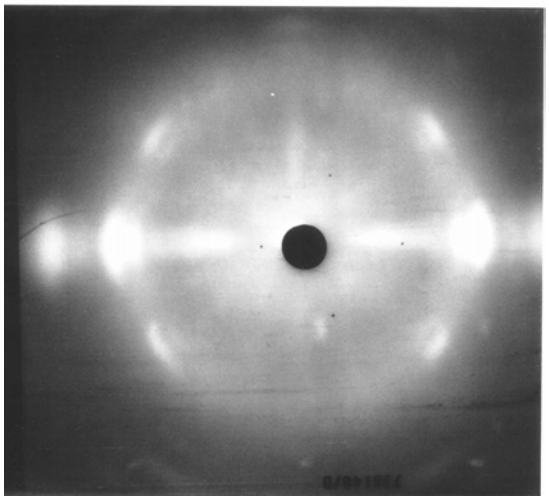

Figure 4. 3: Monocryl x-ray Polaroid image

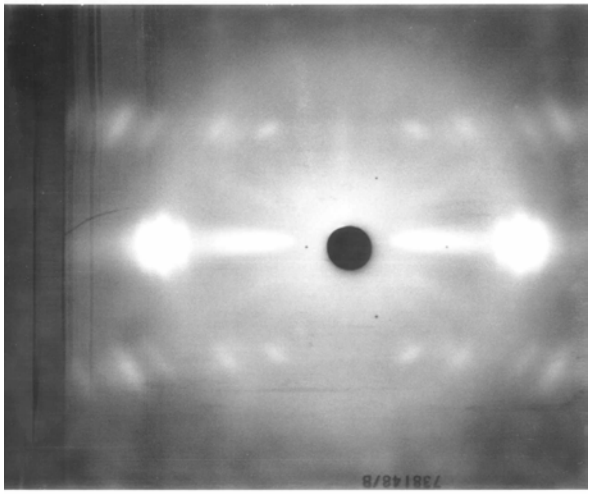

Figure 4. 4: PDS II x-ray Polaroid image

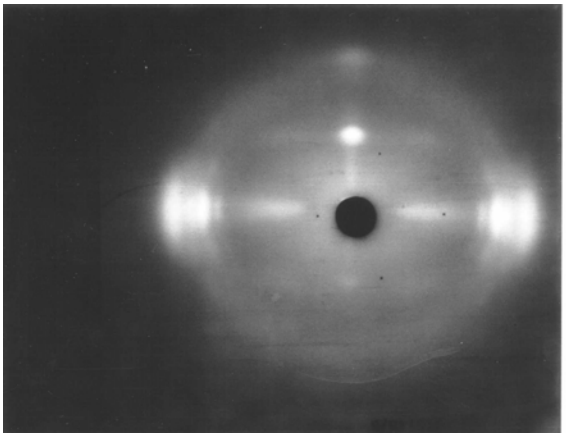

Figure 4. 5: Ethilon x-ray Polaroid image.

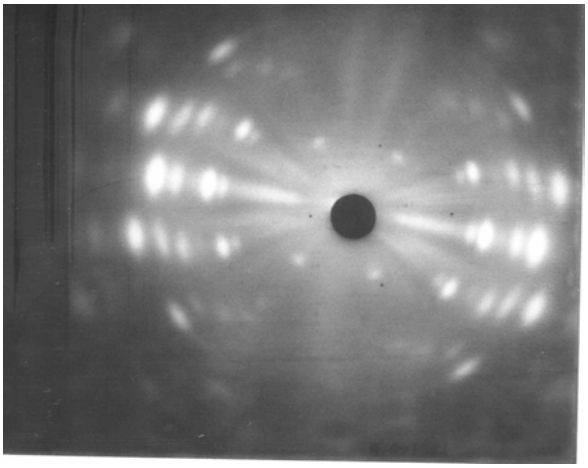

Figure 4. 6: Novafil x-ray Polaroid image.

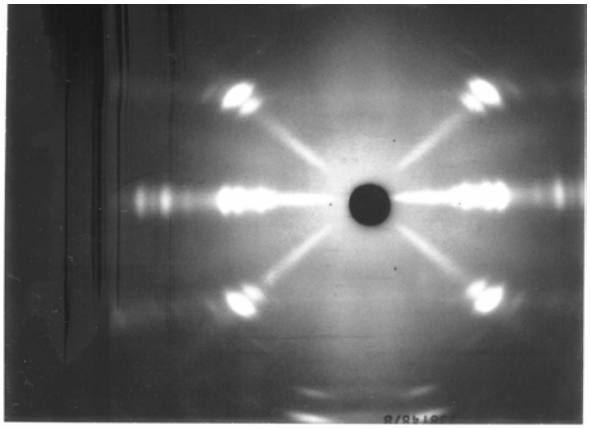

Figure 4. 7: Prolene x-ray Polaroid image

It can be observed from the above diffraction patterns that the length of the arcs is the shortest for the Prolene suture, whereas the arcs for Biosyn, Maxon and Monocryl are comparatively long. Novafil also shows short lengths of arcs similar to Prolene, signifying an oriented structure. The x-ray diffraction curves for the suture types Biosyn, Maxon and Monocryl were found to be similar to the PGA[62] x-ray diffraction peaks. The peaks occurred at the same 2θ degrees. Also the peaks for the Ethilon[64], Prolene[57] showed peaks at the same 2θ degrees, as found by others in the literature.

The tables shown below list the results from the measurements of the arc length and the x-ray intensities measured. Table 4.2 shows the crystal size for each of the seven polymers, and the Table 4.3 shows the values for the Herman's Orientation Factor.

Table 4. 2: Crystal size by x-ray diffraction data from one peak per suture.

Suture Type	2 θ (degrees)	θ (degrees)	θ (radians)	FWHM (degrees)	FWHM (radians)	Crystal size (A^o)
Biosyn	21.76	10.88	0.19	1.5063	0.0263	53.2888
Maxon	21.84	10.92	0.19	1.5798	0.0276	50.8130
Monocryl	22.35	11.17	0.19	1.3446	0.0235	59.7271
PDS II	22.37	11.19	0.20	1.2351	0.0215	65.0236
Ethilon	23.53	11.77	0.21	2.3886	0.0417	33.6570
Novafil	23.09	11.54	0.20	1.2935	0.0226	62.1269
Prolene	19.08	9.54	0.17	1.5843	0.0276	50.5588

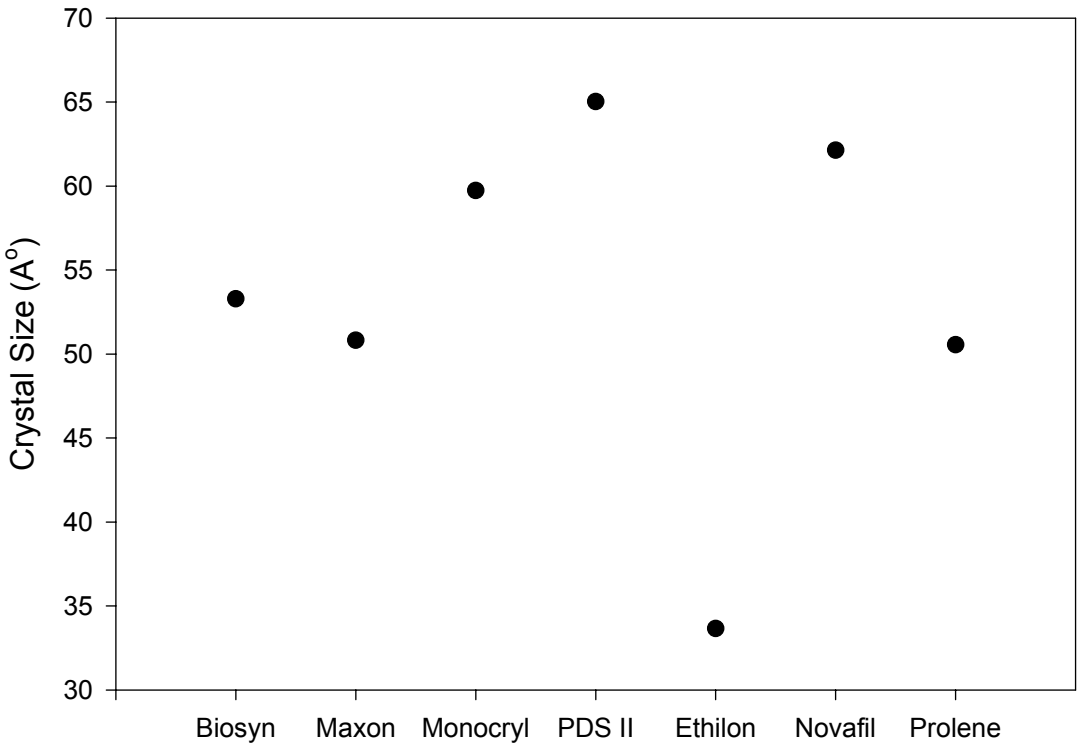

Figure 4. 8: Variation of crystal size with different suture polymer types.

Figure 4.8 shows a graphical representation of the values for crystal size for the different polymers. It can be seen that the crystal size s for these seven

suture polymers vary in the range of 33.6 A^o to 65.0 A^o. All the polymers exhibit a fairly high degree of orientation, see Table 4.3, with the Herman's orientation factor in the range of 0.78 to 0.93. It can be seen that the molecular orientation is higher in the case of the non-resorbable polymers as compared to the resorbable polymers.

Table 4. 3 Herman's Orientation Factor by x-ray diffraction

Suture Type	Angle $\Phi_{1/2}$ (degrees)	$Cos^2< \Phi >$ (degrees)	Herman's Orientation Factor f
Biosyn	17.00	0.8855	0.8283
Maxon	18.00	0.8855	0.8283
Monocryl	19.50	0.8541	0.7812
PDS II	17.50	0.8794	0.8191
Ethilon	13.00	0.9301	0.8951
Novafil	10.00	0.9575	0.9363
Prolene	10.00	0.9575	0.9363

It can be seen from Tables 4.2 and 4.3 that the crystal size is the lowest for Ethilon and is the highest for PDS II. The highest value for the Herman's orientation factor (1.0 indicates perfect orientation) is for Prolene and the lowest for Monocryl. Figures 4.9 graphically depict the variation of Herman's orientation factor for different suture polymers.

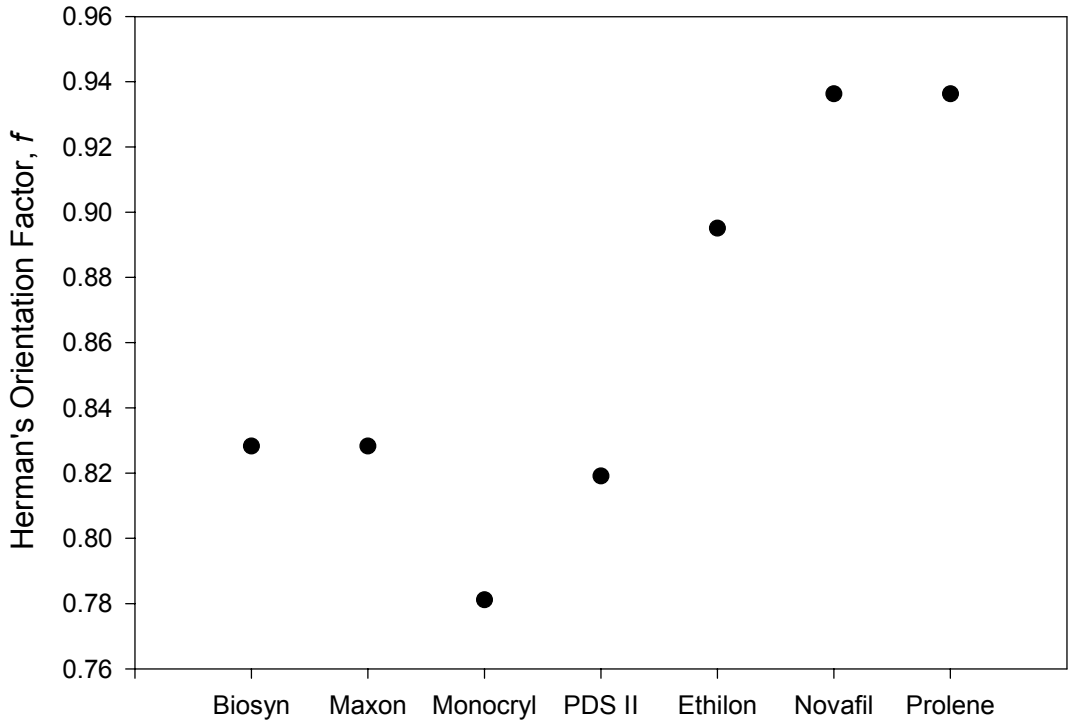

Figure 4. 9: Variation of Herman's Orientation Factor for seven polymer types.

The $\cos^2\langle\Phi\rangle$ is the square of cosine of the angle between the crystal size axis and the fiber axis. It is an average value of all such angles for all crystals. This is shown in the Figure 4.10.

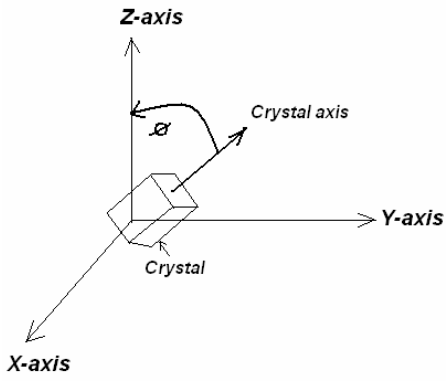

Figure 4. 10: Angle Φ with reference to the crystal size axis and the fiber axis, z.

Thus an angle of 0^o means the crystal size axis is parallel to the fiber axis. This is the case for perfect orientation. This value is attributed to the $\cos^2\langle\Phi\rangle$ value

which becomes 1.0 for perfect orientation. Similarly an angle of 90°, suggests that the crystal size axis is perpendicular to the fiber axis. Here the $\cos^2<\Phi>$ value will be zero. Now referring back to the Figure 4.11 we can say that the crystals in the suture monofilament of the seven polymers are nearly parallel to the fiber axis for non-resorbable polymers (0.93 to 0.95) at an average angle lying between 21.56° to 18.19°. The resorbable polymers on the other hand lie at an average angle in the range of 28.36° to 31.78°.

4.1.3 Differential Scanning Calorimetry

The results from the seven suture polymers tested by differential scanning calorimetry for their thermal properties, are presented in Table 4.4 and 4.5. The melting point for the non-resorbable polymers was higher than for all the resorbable polymers, except for Prolene. This suggests that when heat is supplied to the resorbable polymers, the molecular chains require comparatively less energy to change into a melt. Thus the resorbable polymers soften at a lower temperature than the non-resorbable polymers.

Table 4. 4: Differential scanning calorimetry data for suture polymers[17].

Suture Type	Major polymer component	Proportion of Major polymer (%)	(g/mol)	Heat of fusion at 100%crystallinity (KJ/mol)	(J/g)
Biosyn	Polyglycolic acid (PGA) (60%)	60.00	132.00	11.00	83.30
Maxon	Polyglycolic acid (PGA) (67.5)	67.50	132.00	11.00	83.30
Monocryl	Polyglycolic acid (PGA) (75%)	75.00	132.00	11.00	83.30
PDS II	p-dioxanone (100%)	100.00	104.00	14.40	138.46
Ethilon	Nylon 6 (100%)	100.00	113.01	-	188.00
Novafil	Polytetramethylene terephthalate (100%)	100.00	216.00	31.00	143.52
Prolene	Isotactic polypropylene (100%)	100.00	54.00	9.92	187.70

The x-ray diffraction patter for the sutures Biosyn, Maxon , and Monocryl were similar to 100% PGA x-ray diffraction pattern, i.e. same peaks were observed at the same angle 2θ. Also, there was only one melting peak in DSC. So, we have assumed that the major polymer contributes the most to the crystallinity of the co-polymer. Hence the heat of fusion by DSC with the proportion of the major component of the co-polymer was used to calculate the crystallinity. The method

to calculate the crystallinity of a co-polymer is discussed by Wlochowicz *et.al.*[65] could not be used, since the density or the x-ray diffraction pattern for 100% crystalline and 100% amorphous components of each of the homopolymers was not available.

Table 4. 5: Differential Scanning Calorimetry results.

Suture Type	Heat of fusion (J/g) (present)	Heat of fusion (J/g) (literature)	Proportionate heat of fusion (J/g)	Degree of Crystallinity (%) (present)	Degree of Crystallinity (%) (literature)	Melting Temperature(°C) (present)	Melting Temperature(°C) (literature)
Biosyn	7.62	-	49.98	15.25	-	176.95	175.5[50]
Maxon	41.19	41.19 [45]	56.23	73.26	-	212.49	206.2[49,50]
Monocryl	30.05	56.09 [45]	62.48	48.10	-	205.29	200.8[55]
PDS II	82.29	91.67 [45]	138.46	59.43	57.60[54]	102.12	100[63]
Ethilon	48.43	42-71 [44]	188.00	25.76	18 - 36[52]	225.19	254[44]
Novafil	44.51	-	143.52	31.01	-	215.63	-
Prolene	118.75	118 [43,46]	187.70	63.27	50-70[47,48,56,57,]	168.66	166.2[43,46]

Table 4.5 shows the values for heat of fusion, degree of crystallinity and melting temperature from the present study. These values are similar to those found in the literature.

4.1.4 Image Analysis and Barb Geometry

Barb geometry of the barbed suture was measured in one direction. This was the same direction as was used to suture through the tissue simulant and measure the suture/tissue pull-out force. Tables 4.6 to 4.8 show the important dimensions of the barbs, with an adjacent column for standard error (*SE*). All the measurements were analyzed for Analysis of Variance (ANOVA) by the F-test. The results indicated a significant difference in the values at p = 0.05. This difference can be attributed to the human errors while cutting barbs manually.

Table 4. 6: Image analysis data on barb geometry.

	Cut Depth		Cut Angle		Calculated Cut Length
	(mm)	*SE*	(degrees)	*SE*	(mm)
Biosyn	0.1855	*0.0028*	157.24	*0.46*	0.1855
Maxon	0.1461	*0.0043*	159.87	*0.46*	0.4247
Monocryl	0.1694	*0.0035*	158.45	*0.31*	0.4614
PDS II	0.1488	*0.0038*	160.51	*0.23*	0.4462
Ethilon	0.1562	*0.0041*	156.95	*0.69*	0.3990
Novafil	0.1236	*0.0063*	161.81	*0.45*	0.3981
Prolene	0.1417	*0.0037*	163.72	*0.35*	0.5057

Table 4. 7: Image analysis data on barb geometry

	Barb Angle		Barb Length		Barb Base Length	
	(degrees)	SE	(mm)	SE	(mm)	SE
Biosyn	0.1855	*0.0028*	157.24	*0.46*	0.1855	0.0278
Maxon	0.1461	*0.0043*	159.87	*0.46*	0.4247	0.0128
Monocryl	0.1694	*0.0035*	158.45	*0.31*	0.4614	0.0100
PDS II	0.1488	*0.0038*	160.51	*0.23*	0.4462	0.0092
Ethilon	0.1562	*0.0041*	156.95	*0.69*	0.3990	0.0121
Novafil	0.1236	*0.0063*	161.81	*0.45*	0.39812	0.0000
Prolene	0.1417	*0.0037*	163.72	*0.35*	0.5057	0.0105

Table 4. 8: Image analysis data on barb geometry

	Spiral Angle		Diameter		Distance between barbs	
	(degrees)	SE	(mm)	SE	(mm)	SE
Biosyn	15.4804	0.2450	0.4399	0.0015	0.9728	0.0278
Maxon	13.3700	0.0128	0.4434	0.0128	0.9472	0.0034
Monocryl	13.1851	0.0100	0.4483	0.0100	0.9167	0.0095
PDS II	11.8738	0.0092	0.4330	0.0092	0.9357	0.0047
Ethilon	13.4860	0.0121	0.4379	0.0121	0.9494	0.0075
Novafil	11.6229	0.4797	0.3720	0.0012	0.9282	0.0009
Prolene	6.4218	0.0105	0.4426	0.0105	1.4969	0.4120

4.1.5 Tensile Properties

This section discusses the tensile properties for the barbed and un-barbed sutures, when loaded at constant rate of extension. Ten measurements per suture type were done for barbed sutures and due to limited sample availability, only 8 measurements per suture type were done for unbarbed sutures. All the tensile testing results for the seven suture polymers were significantly different at p = 0.05, by f-test.

4.1.5.1 Unbarbed Suture Peak Tensile Load

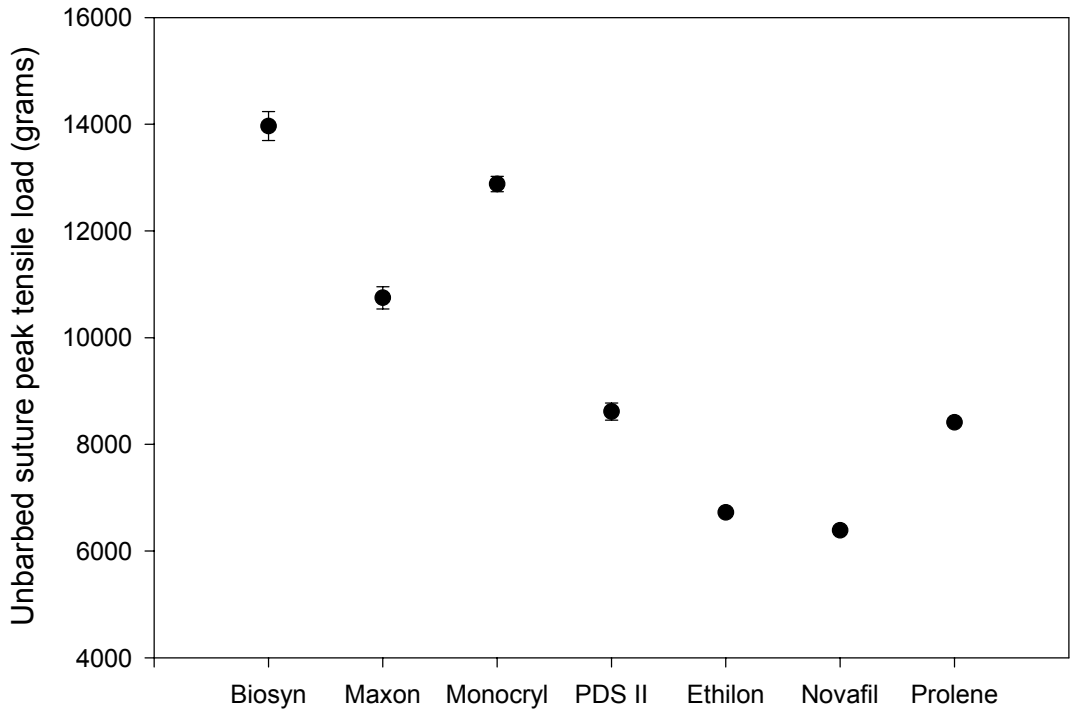

Figure 4. 11: Peak tensile load for unbarbed sutures

Table 4. 9: Peak tensile load for unbarbed sutures of different types(grams)

Sr #	Biosyn	Maxon	Monocryl	PDS II	Ethilon	Novafil	Prolene
1	14393	10866	13262	8167	6597	6394	8596
2	13868	11611	13286	8125	6713	6389	8448
3	12753	9991	13210	8678	6577	6055	8296
4	14389	10898	12542	9143	6701	6335	8379
5	14311	10719	12169	9107	6663	6342	8322
6	12718	11177	13074	8723	6682	6382	8446
7	14198	9805	12908	8945	6773	6389	8319
8	14346	10891	12575	8002	6705	6362	4320
Mean	**13872**	**10745**	**12878**	**8611**	**6676**	**6331**	**8401**
SD	**721**	**592**	**408**	**456**	**63**	**113**	**105**
CV%	**5.20**	**5.51**	**3.18**	**5.30**	**0.96**	**1.80**	**1.25**
variance	**520738**	**349926**	**167234**	**208670**	**4084**	**12986**	**11108**
SE	**255**	**187**	**129**	**144**	**20**	**36**	**33**
(literature)>		*10030*[59]	-	-	*6600*[59]	*6180*[59]	*7010*[59]

Table 4.9 and Figure 4.11, shows that the values found in the present study are similar to those found in the literature for the same suture size. The t-test results show that the peak load for the unbarbed all the sutures is significantly different from each other, except for one case, at p=0.05. No significant difference was found between the peak loads for PDS II and Prolene.

Table 4. 10: Peak elongation for unbarbed sutures of different types (gauge length = 16.62 cms) (percent)

Sr #	Biosyn	Maxon	Monocryl	PDS II	Ethilon	Novafil	Prolene
1	29.48	33.57	37.12	39.29	42.48	28.28	29.66
2	29.66	35.38	36.94	40.13	43.56	28.10	33.87
3	27.02	31.29	36.40	44.04	45.01	28.70	10.11
4	29.84	32.79	35.02	48.92	43.44	28.16	39.17
5	29.36	32.73	34.18	46.81	42.72	28.28	32.37
6	27.02	34.72	36.16	44.95	42.18	28.70	34.84
7	29.12	30.87	36.70	47.65	42.60	28.28	35.50
8	29.60	33.94	35.20	38.33	45.43	27.92	34.60
Mean	**28.89**	**33.16**	**35.97**	**43.77**	**43.43**	**28.30**	**31.27**
SD	**1.18**	**1.57**	**1.05**	**4.06**	**1.20**	**0.27**	**8.96**
CV%	**4.07**	**4.73**	**2.93**	**9.27**	**2.77**	**0.97**	**28.67**
variance	**1.38**	**2.46**	**1.11**	**16.46**	**1.45**	**0.08**	**80.35**
SE	**0.42**	**0.50**	**0.33**	**1.28**	**0.38**	**0.09**	**2.83**

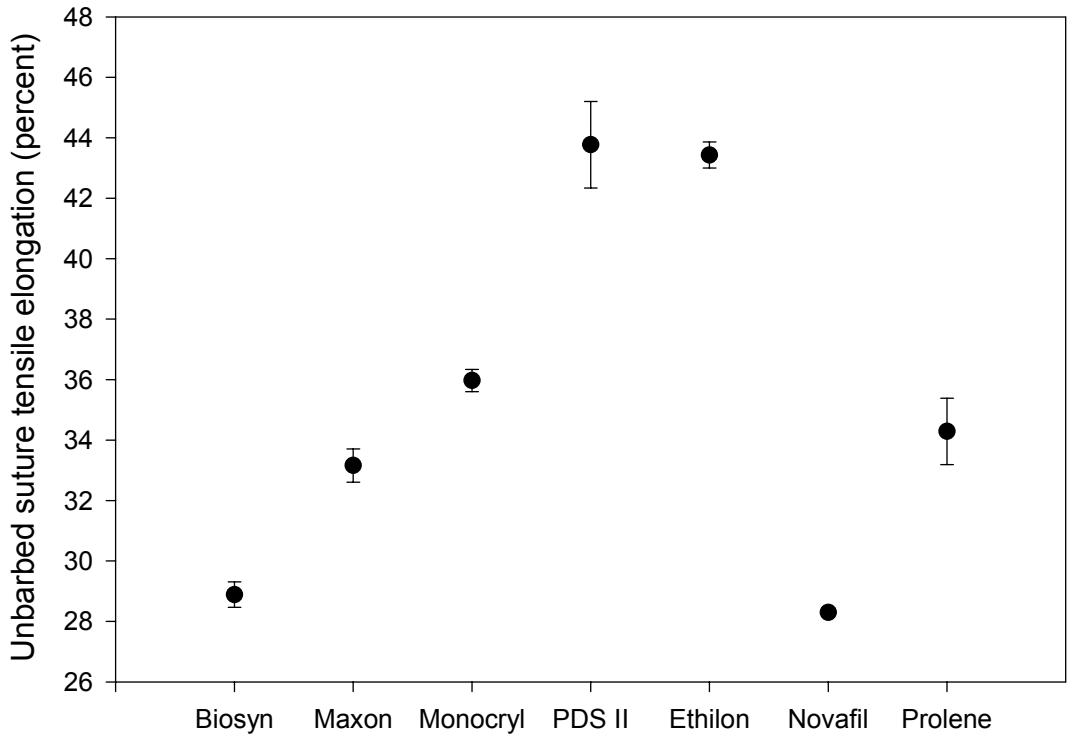

Figure 4. 12: Peak elongation percent for unbarbed sutures of different types (%)

The t-test results, at p=0.05, show that the peak elongation for between all the sutures was significantly different, except for three cases, Table 4.10 and Figure 4.12. There was no significant difference for the peak elongation values between the sutures: Biosyn & Novafil; Maxon & Prolene; and PDS II & Ethilon. The literature values could not be compared since we had used capstan clamps and the gauge length was higher.

4.1.5.2 Barbed Suture Peak Tensile Load

Table 4. 11: Peak tensile load for barbed sutures of different types (grams)

Sr #	Biosyn	Maxon	Monocryl	PDS II	Ethilon	Novafil	Prolene
1	3456	4154	3681	3469	2496	1959	2567
2	3142	3976	3684	2103	2599	1856	2355
3	3359	3822	3671	3389	2441	1871	2389
4	3565	4038	3729	3632	2619	1769	2487.03
5	3529	4106	3821	3401	2679	1788	2532
6	3325	3091	3955	3445	2569	1817	2383
7	3253	4205	3396	3469	2588	1914	2331
8	3335	4144	3702	3173	2612	1816	2585
9	3321	3832	3803	3342	2531	1939	2606
10	3967	4002	3515	3412	2656	1798	2542
Mean	**3425**	**3937**	**3695**	**3283**	**2579**	**1852**	**2478**
SD	**227**	**324**	**155**	**430**	**72**	**66**	**104**
CV%	**6.66**	**8.24**	**4.21**	**13.10**	**2.82**	**3.60**	**4.18**
variance	**51963**	**105178**	**24264**	**185126**	**5304**	**4440**	**10729**
SE	**72**	**102**	**49**	**136**	**23**	**21**	**33**

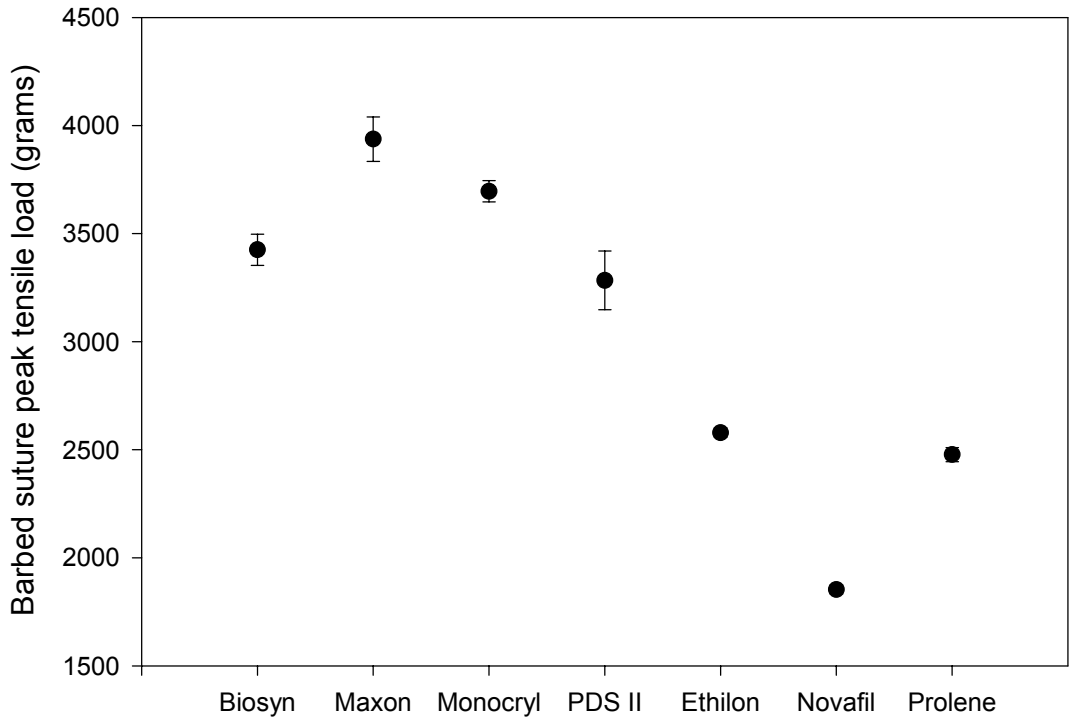

Figure 4. 13: Peak tensile load for a barbed suture

The t-test results at p-value = 0.05 show that the difference between the peak loads between all the sutures is significant, except two cases, Table 4.11 and Figure 4.13. There is no significant difference between the peak load for Biosyn and PDS II. Similarly no significant difference in peak tensile load was found between Maxon and Monocryl.

Table 4. 12: Peak tensile elongation for barbed sutures (gauge length= 16.62 cms) (percent).

Sr #	Biosyn	Maxon	Monocryl	PDS II	Ethilon	Novafil	Prolene
1	15.94	19.68	18.47	19.92	16.37	17.09	8.24
2	14.98	18.65	18.83	18.95	16.67	17.57	6.56
3	15.52	18.23	18.65	19.61	15.82	17.27	6.74
4	15.82	19.37	18.83	19.80	16.85	17.81	6.86
5	15.70	19.19	18.89	20.46	17.51	16.91	6.26
6	15.58	16.25	19.37	19.49	16.67	16.67	5.66
7	15.64	20.34	17.75	20.40	17.27	17.81	6.50
8	15.46	19.92	18.29	18.95	17.39	17.51	7.34
9	16.00	18.77	18.95	19.25	17.21	17.63	7.22
10	16.79	19.01	17.99	19.74	16.79	17.63	7.10
Mean	**15.75**	**18.94**	**18.60**	**19.66**	**16.85**	**17.39**	**6.85**
SD	**0.47**	**1.13**	**0.49**	**0.52**	**0.51**	**0.39**	**0.70**
CV%	**2.95**	**5.99**	**2.61**	**2.66**	**3.05**	**2.25**	**10.19**
variance	**0.22**	**1.29**	**0.24**	**0.27**	**0.27**	**0.15**	**0.49**
SE	**0.15**	**0.36**	**0.15**	**0.17**	**0.16**	**0.12**	**0.22**

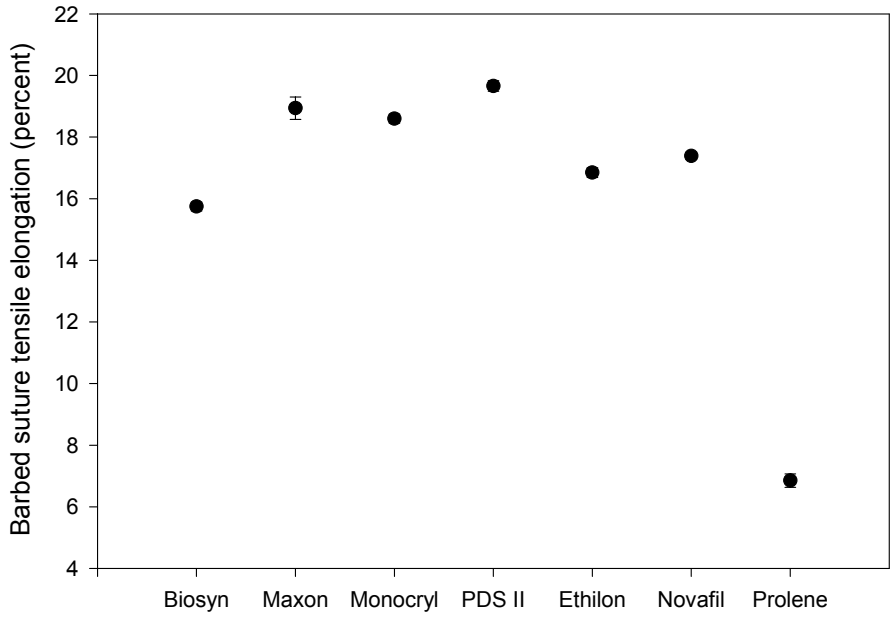

Figure 4. 14: Peak elongation of barbed sutures of different types

The t-test results show that the differences in the peak tensile elongation for the barbed sutures are significant at p=0.05, except for one case, Table 4.12 and Figure 4.14. No significant difference for peak elongation was found between Maxon and Monocryl.

4.1.5.3 Tensile Elastic Modulus (calculated)

The tensile elastic modulus (i.e. the Young's modulus of elasticity) is the slope of the stress-strain curve, Table 4.13 and Figure 4.15.

Table 4. 13: Calculated tensile elastic modulus of unbarbed sutures.

Suture Type	Modulus (grams/denier)	SE
Biosyn	13.48	0.33
Maxon	26.51	0.91
Monocryl	13.41	1.09
PDS II	15.38	0.16
Ethilon	13.41	0.37
Novafil	18.96	0.15
Prolene	48.75	3.72

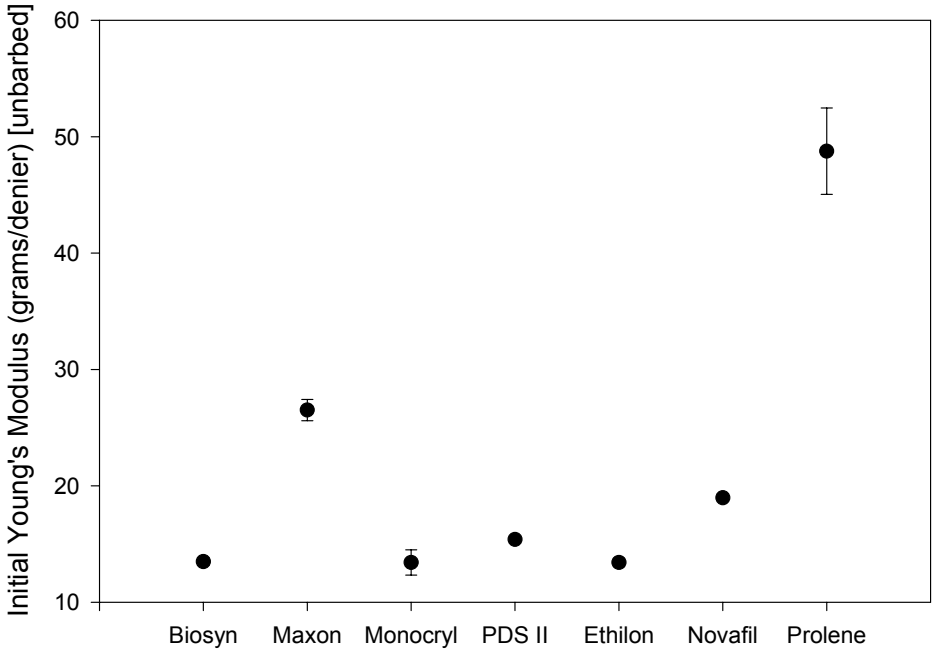

Figure 4. 15: Initial Young's modulus for sutures.

The t-test results show that the values for the initial Young's modulus were significantly different from each other at p=0.05, except for three cases. There was no significant difference between the initial modulus between the sutures: Biosyn & Monocryl; Monocryl & PDS II; and Monocryl & Ethilon.

4.1.5.4 Calculated bending rigidity

Table 4.14 and Figure 4.16 shows the results for the bending rigidity.

Table 4. 14: Calculated bending rigidity of unbarbed sutures.

	Unbarbed Tensile Modulus (grams/denier)	Bending / Flexural Rigidity X 10^{-5} (gf.cm^2)
Biosyn	13.48	0.0442
Maxon	26.51	0.0945
Monocryl	13.41	0.0461
PDS II	15.38	0.0483
Ethilon	13.41	0.0386
Novafil	18.96	0.0321
Prolene	48.75	0.1306

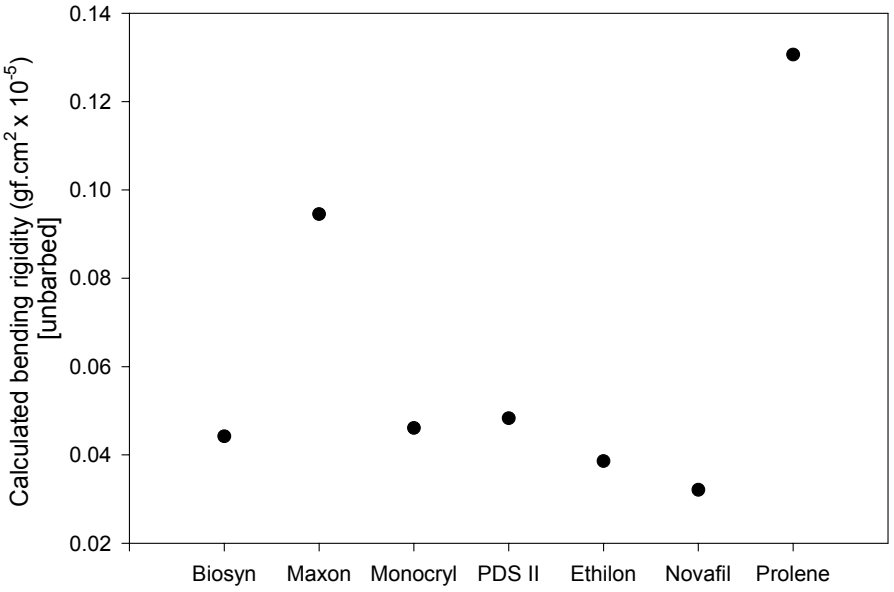

Figure 4. 16: Calculated bending rigidity for different polymers.

4.1.6 Suture Toughness

Suture toughness is the area under the load elongation curve when the specimen is loaded axially on a tensile testing machine at constant rate of elongation. This is also called the energy to break and is expressed in joules, Table 4.15 – 4.16.

Table 4. 15: Barbed suture toughness (joules)

Sr #	Biosyn	Maxon	Monocryl	PDS II	Ethilon	Novafil	Prolene
1	0.36	0.59	0.43	0.61	0.36	0.25	0.19
2	0.32	0.53	0.44	0.54	0.38	0.25	0.14
3	0.35	0.50	0.43	0.59	0.33	0.26	0.14
4	0.37	0.57	0.44	0.63	0.37	0.24	0.15
5	0.37	0.57	0.46	0.61	0.41	0.24	0.14
6	0.34	0.37	0.48	0.59	0.37	0.23	0.12
7	0.33	0.63	0.38	0.63	0.38	0.26	0.13
8	0.34	0.60	0.43	0.53	0.39	0.24	0.17
9	0.35	0.53	0.46	0.56	0.38	0.25	0.17
10	0.42	0.54	0.40	0.59	0.38	0.24	0.16
Mean	**0.36**	**0.54**	**0.44**	**0.59**	**0.38**	**0.25**	**0.15**
SD	**0.03**	**0.07**	**0.03**	**0.03**	**0.02**	**0.01**	**0.02**
CV%	**7.88**	**13.25**	**6.70**	**5.93**	**5.52**	**3.93**	**14.12**
variance	**0.00**	**0.01**	**0.00**	**0.00**	**0.00**	**0.00**	**0.00**
SE	**0.01**	**0.02**	**0.01**	**0.01**	**0.01**	**0.00**	**0.01**

The t-test values show significant difference between sutures for suture toughness at p=0.05, except for two cases. There was no significant difference between the values for suture toughness between sutures: Biosyn & Ethilon; and Maxon & PDS II.

Table 4. 16: Unbarbed suture toughness (joules)

Sr #	Biosyn	Maxon	Monocryl	PDS II	Ethilon	Novafil	Prolene
1	2.49	2.50	3.30	2.75	2.73	1.23	2.74
2	2.54	2.83	3.23	2.80	2.84	1.23	3.11
3	1.96	2.13	3.19	3.39	2.94	1.30	0.38
4	2.53	2.43	2.86	4.09	2.82	1.22	3.55
5	2.47	2.39	2.67	3.90	2.76	1.24	2.89
6	1.96	2.67	3.10	3.56	2.69	1.28	3.11
7	2.42	2.04	3.08	3.92	2.75	1.27	3.29
8	2.54	2.55	2.87	2.66	2.99	1.21	3.18
Mean	**2.36**	**2.44**	**3.04**	**3.38**	**2.82**	**1.25**	**2.78**
SD	**0.25**	**0.26**	**0.22**	**0.58**	**0.10**	**0.03**	**1.00**
CV%	**10.68**	**10.71**	**7.14**	**17.12**	**3.73**	**2.56**	**35.97**
variance	**0.06**	**0.07**	**0.05**	**0.34**	**0.01**	**0.00**	**1.00**
SE	**0.09**	**0.08**	**0.07**	**0.18**	**0.03**	**0.01**	**0.32**
(literature)>>	-	2.67[59]	-	-	2.36[59]	0.80[59]	1.22[59]

The t-test results show that there was significant difference between the values for suture toughness in the unbarbed sutures at p=0.05 except in four cases. There was no significant difference between the suture toughness values between the sutures: Biosyn & Maxon; Monocryl & PDS II; Monocryl & Prolene; and PDS II & Prolene at p=0.05, Figure 4.17. The higher reading in the present study may be due to the use of capstan clamp, because the literature values were sought by using studs/cleats.

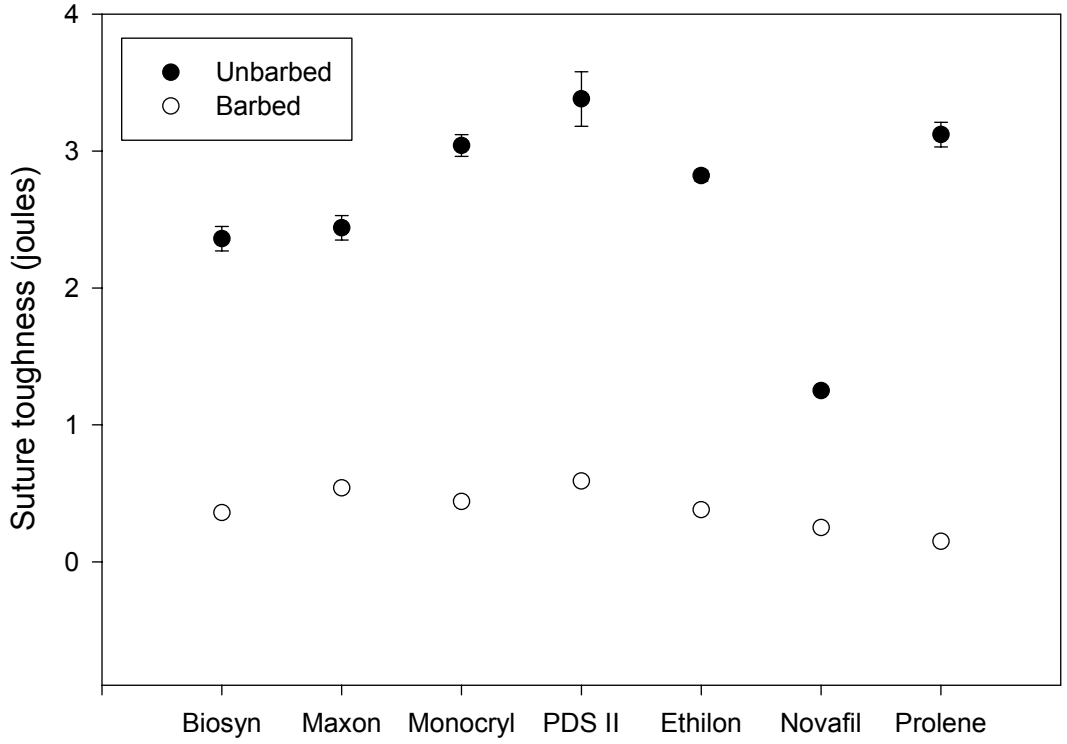

Figure 4. 17: Suture toughness for different sutures.

4.1.7 Suture/Tissue Pull-out force Values:

The results of the suture/ tissue pull out force test are shown in Table 4.17 & 4.18 and Figure 4.18. The values lie in the range of 1334 grams to 2135 grams for the non-resorbable suture polymers and in the range of 1419 grams to 1849 grams for the resorbable polymers. It can be seen that the values are higher for the non-resorbable sutures in spite of the tensile load of the barbed and the unbarbed sutures being lower as compared to the resorbable polymer type sutures. This can be explained in terms of the composition of the crystals of different sizes

which have a certain molecular orientation and degree of crystallinity. All the suture/tissue pull-out force test results were significant at p=0.05, by f-test, Table 4.17.

Table 4. 17: Suture/ Tissue Pull-out force (peak load in grams) for different barbed sutures

Sr #	Biosyn	Maxon	Monocryl	PDS II	Ethilon	Novafil	Prolene
1	1,397	2,017	1,038	1,683	2,124	1,113	1,608
2	1,703	2,091	1,531	1,839	2,247	1,564	1,556
3	1,279	1,919	1,294	1,536	2,041	1,619.74	1,378
4	1,342	1,653	1,466	1,459	1,847	1,035	1,724
5	1,872	1,742	1,259	1,909	1,926	1,314	1,575
6	1,283	1,870	1,727	1,778	2,405	1,192	1,518
7	1,405	1,882	1,253	2,017	2,719	1,352	1,759
8	1,084	2,032	1,592	1,425	1,863	1,345	1,975
9	1,387	1,659	1,749	1,436	2,386	1,442	1,785
10	1,439	1,625	1,793	1,474	1,791	1,360	1,638
Mean	**1,419**	**1,849**	**1,470**	**1,656**	**2,135**	**1,334**	**1,652**
SD	**222**	**170**	**253**	**219**	**302**	**184**	**166**
CV%	**15.66**	**9.23**	**17.21**	**13.24**	**14.13**	**13.83**	**10.06**
variance	**49,396**	**29,109**	**64,014**	**48,018**	**90,949**	**34,017**	**27,627**
SE	**70**	**53**	**80**	**69**	**95**	**58**	**52**

The t-test results indicate that the peak suture/tissue pull-out force was significantly different between all the sutures at p=0.05, except the six cases. No significant difference was found in the peak suture/tissue pull-out force between the sutures: Biosyn & Monocryl; Biosyn & Novafil; Monocryl & PDS II; Monocryl & Novafil; Monocryl & Prolene; and PDS II & Prolene.

Table 4. 18: Suture/tissue pull-out force (peak load in grams) for unbarbed sutures.

Sr #	Biosyn	Maxon	Monocryl	PDS II	Ethilon	Novafil	Prolene
1	34.9	44.8	16.0	6.3	34.9	11.5	51.9
2	32.3	29.4	38.2	39.6	32.3	39.8	39.2
3	61.8	19.2	51.0	56.4	61.8	51.9	42.1
Mean	**43.0**	**31.1**	**35.1**	**34.1**	**43.0**	**34.4**	**44.4**
SD	**16.3**	**12.9**	**17.7**	**25.5**	**16.3**	**20.8**	**6.7**
CV%	**37.98**	**41.40**	**50.50**	**74.78**	**37.98**	**60.36**	**14.99**
variance	**266.8**	**166.1**	**313.6**	**650.2**	**266.8**	**431**	**44.3**
SE	**9.4**	**7.4**	**10.2**	**14.7**	**9.4**	**12.0**	**3.8**

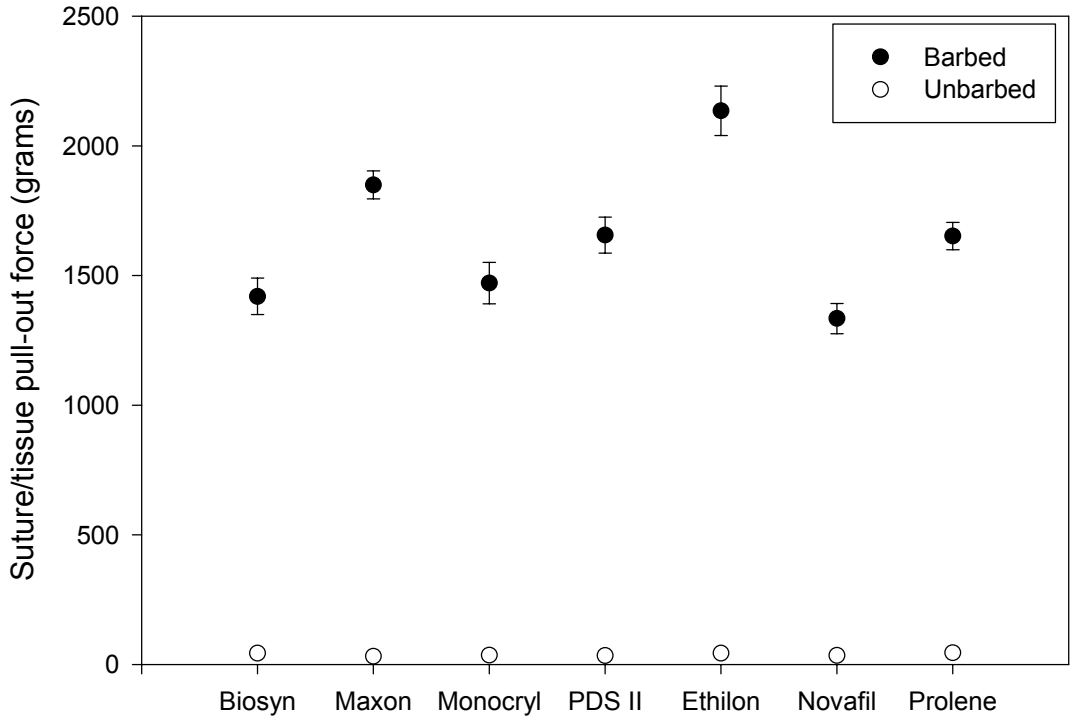

Figure 4. 18: Suture/tissue pull-out force for barbed and unbarbed.

The t-test showed that there was no significant difference in the suture/tissue pull-out force values for the unbarbed sutures at p=0.05, Table 4.18 and Figure 4.18.

4.1.7.1 Length of suture pulled out of tissue simulant

Table 4. 19: Length of suture pulled out of tissue simulant (with curve length of 40.82 mm).

Polymer	# of barbs	DBB (mm)	Pull-out Length (mm)	Remaining length in tissue (mm)
Biosyn	15.00	**0.9728**	13.62	27.21
Maxon	6.60	**0.9472**	5.30	35.53
Monocryl	16.20	**0.9167**	13.93	26.90
PDS II	15.80	**0.9357**	13.85	26.98
Ethilon	9.40	**0.9494**	7.98	32.85
Novafil	13.40	**0.9282**	11.51	29.32
Prolene	6.40	**1.4969**	8.08	32.75

The pull-out length can be classified into four classes as shown in the figure below, depending upon the length of the suture remaining inside the tissue simulant after the pull-out has occurred.

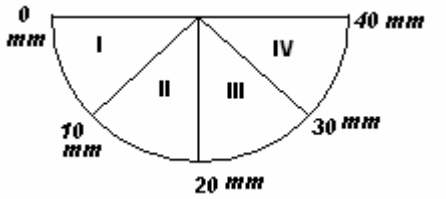

Figure 4. 19: Classification of pull-out lengths.

Figure 4.19 shows four classes, I, II, III and IV, which are the four quadrants which divide the curve length of approximately 40mm into four equal parts. In the present study most of the breaks occurred in the region III and IV. This means that there was almost half of the suture still remaining inside the tissue.

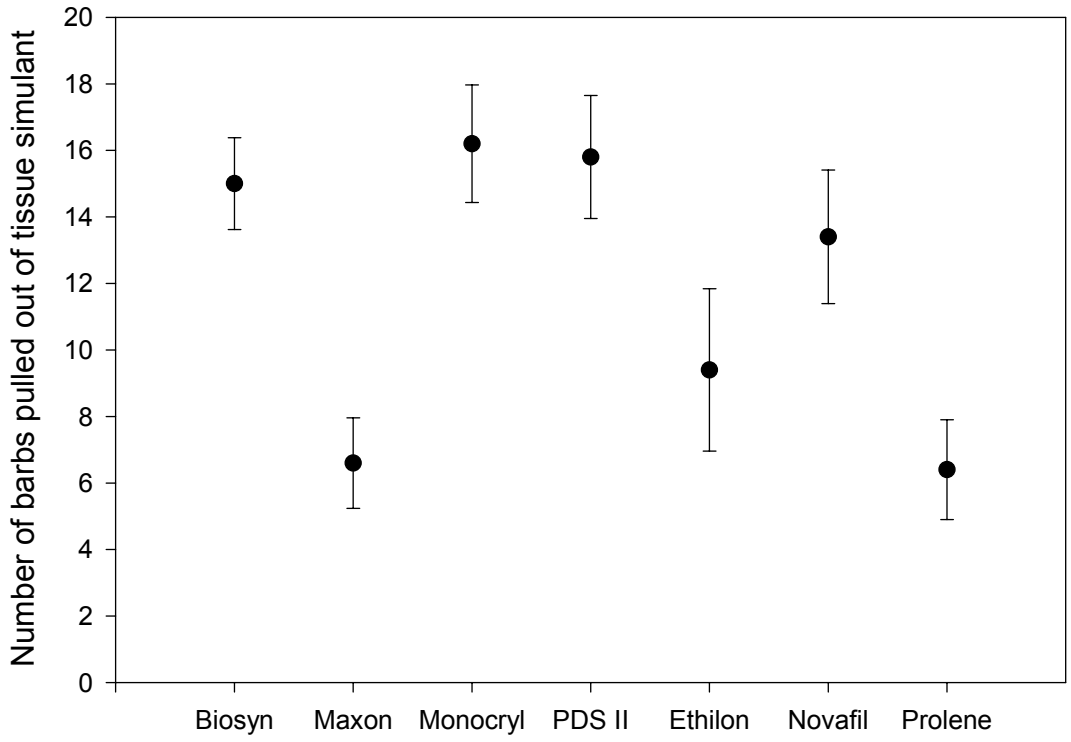

Figure 4. 20: Number of barbs pulled out of tissue simulant.

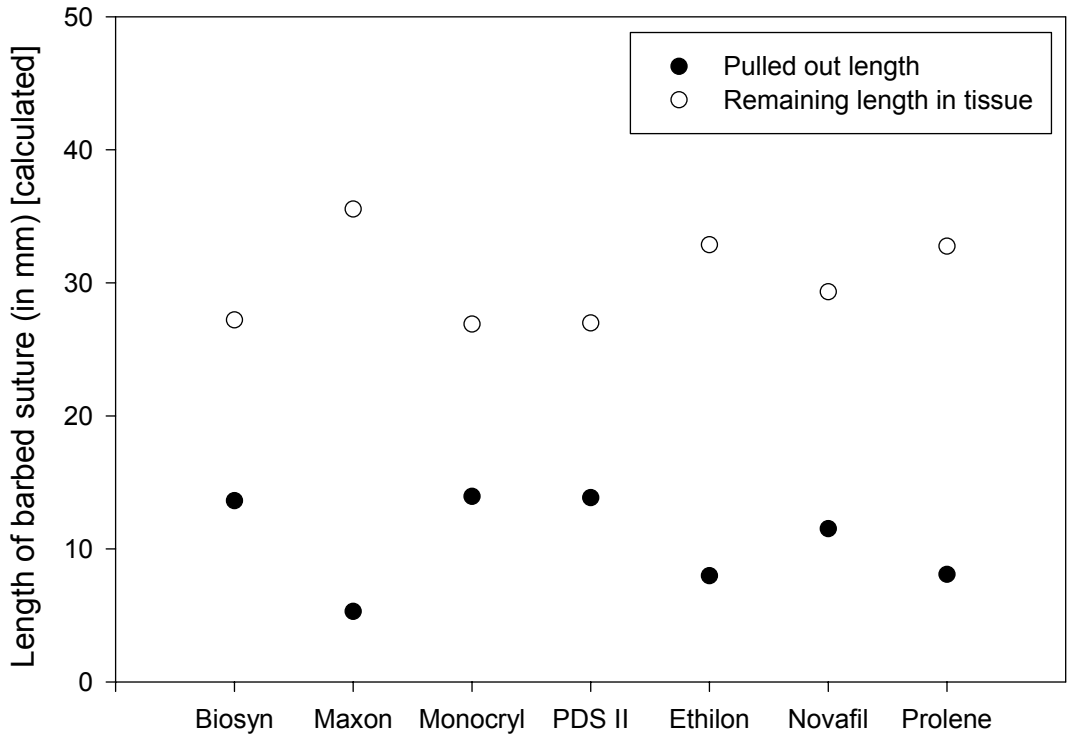

Figure 4. 21: Calculated length of suture pulled out of tissue simulant.

The t-test was applied to the actual measurement of the number of barbs pulled out of the tissue simulant in a suture/tissue pull-out test, Figure 4.20. It was found that there were significant differences in the number of barbs pulled out at p=0.05, for only these pairs of sutures: Biosyn & Maxon; Biosyn & Prolene; Maxon & Monocryl; Maxon & PDS II, Maxon & Novafil; Monocryl & Prolene; PDS & Prolene; Novafil & Prolene. All other values were insignificant at p=0.05. The same relation of significance can be considered for the length of suture pulled out of the tissue simulant, since these values are calculated from the same number of barbs pulled out, Figure 4.21.

4.2 Discussion

This section of the chapter will give explanations for the phenomena observed by the different types of testing. Attempts will be made by statistical correlation analysis to determine the degree of association between the dependent and independent variables.

4.2.1 Dependent Variables:

4.2.1.1 Number of barbs pulled out vs. Suture/ tissue pull-out load

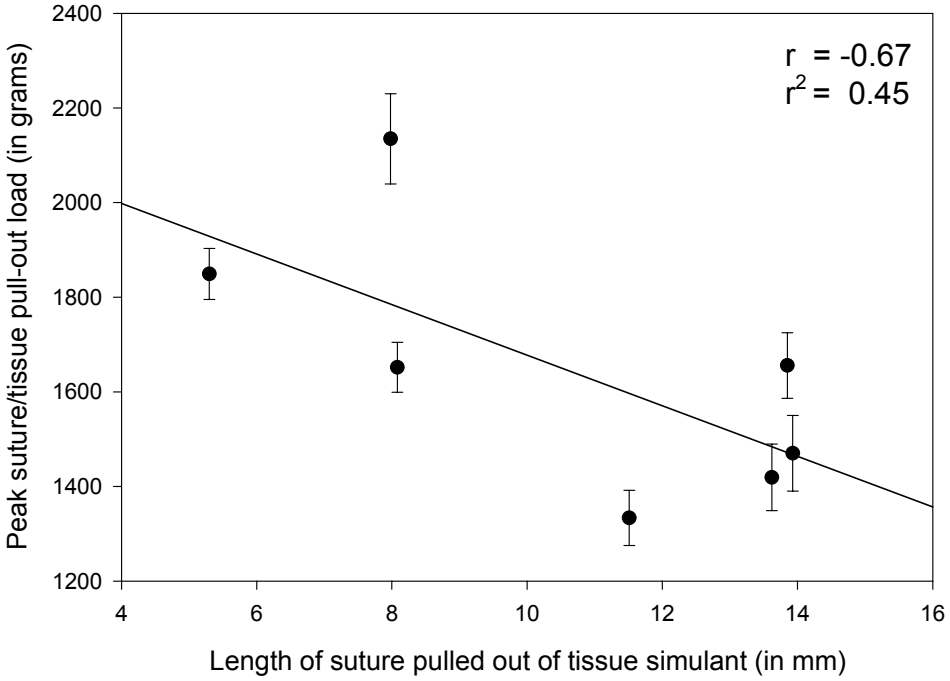

Figure 4. 22: Effect of number of barbs pulled out on the suture/ tissue pull-out load.

A moderately strong correlation, r = -0.67, was seen between the association of the number of barbs pulled out from the tissue simulant in the suture/tissue pullout test and the peak load recorded during the test. The negative sign indicates that if more barbs are pulled out of the tissue, then the suture/tissue pullout load for that suture becomes less, Figure 4.22.

This can be explained by the fact that when a barb fixed inside the tissue is pulled in the direction such that the barb offers a higher resistance, a stronger barb will not bend at a lower load. It will stay in the same position without

bending. However a weaker barb will tend to bend backwards. After bending backwards, this barb will tend to pull out of the tissue and curl. Once it is dislodged from the anchored position in the tissue, there is no further anchoring of this barb. Hence the force required to pull such a barb is lower.

Thus we can say that the higher the number of barbs that were pulled out of the tissue simulant under identical test conditions indicates that the barbs were providing a lower resistance to the pulling force. This may be due to either lower barb stiffness that causes the barb to curl, or due to lower barb force which causes the barb to be peeled off at its base. In either case a lower resistance to pull will give a lower suture/tissue pull out force. This is evident from Figure 4.22.

4.2.2 Independent Variables

4.2.2.1 Length of suture pulled out of tissue simulant vs. crystal size

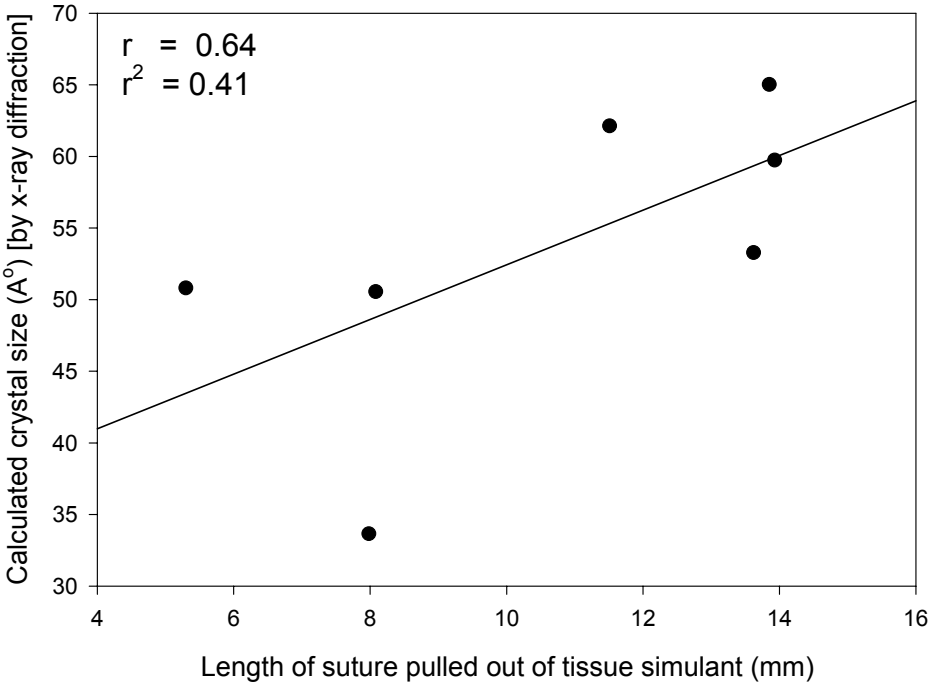

Figure 4. 23: Effect of crystal size on the number of barbs pulled out of the tissue simulant in a suture/ tissue pull out force test.

The value of r=0.64 suggests a moderately strong correlation, and the positive value indicates that if the number of barbs pulled out in a suture/tissue pullout test increases, then the crystal size is higher, Fig. 4.23. In other words, the lower

the crystal size the fewer the number of barbs pulled out, which on the other hand means that a higher load is required to pull the barbed suture which is composed of smaller crystals.

This means that a monofilament with smaller crystals may be able to make stiffer barbs. Hence a barb cut on such a filament will be stiffer. This is possible when these small crystals are arranged in a compact way inside the amorphous molecular matrix. The polymer matrix can be considered to be a composite structure made up of crystals dispersed in the amorphous molecular matrix. If such a composite structure was to become stiffer, these small crystals have to be arranged compactly in the structure. Thus the stiffer the barb, the higher is the pulling resistance and a fewer number of barbs are completely pulled out of the tissue.

4.2.2.2 Correlation between suture/tissue pull-out force and different independent variables

Following statistical analysis by ANOVA, linear regression analysis was performed the correlation coefficients of suture/tissue pull-out force against various independent variables are listed below in Table 4.20.

Table 4. 20: Correlation coefficients for various suture/tissue pull-out force parameters

Independent Variables	Correlation coefficient	
	r	r^2
Crystal size	-0.80	0.64
Unbarbed peak tensile elongation	0.69	0.48
Unbarbed toughness	0.42	0.18
Unbarbed peak tensile load	-0.35	0.12
Degree of crystallinity	0.18	0.03
Unbarbed bending rigidity	0.15	0.02
Herman's Orientation Factor	0.08	0.01
Unbarbed tensile modulus	0.06	0.00

It was discovered that the pull-out force had a strong correlation with the crystal size of the suture monofilaments Figure 4.24.

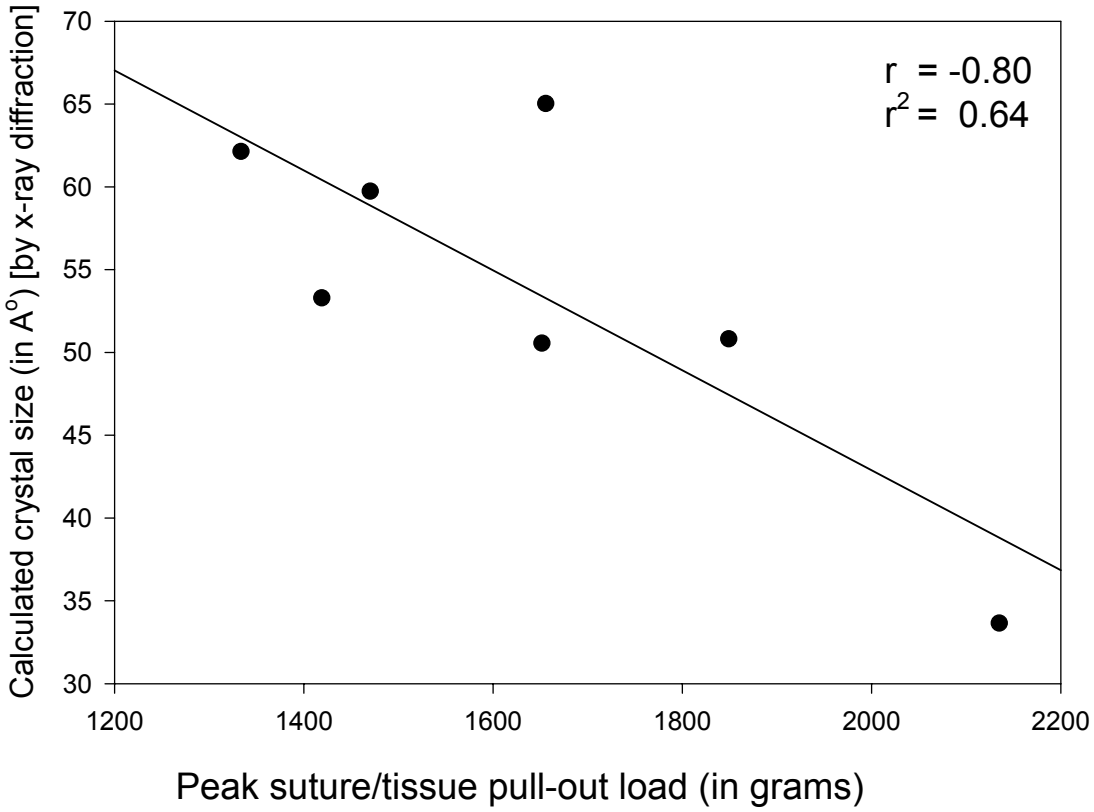

Figure 4. 24: Correlation between crystal size and suture/ tissue pull-out force.

It appears that it is the size and the composition of these crystals which increases the tissue holding capacity. The barb tissue holding capacity (measured by suture/tissue pull-out force) was found to be higher if the monofilament contains small size crystals which are compactly arranged instead of having randomly spaced big crystals.

Table 4. 21: Effect of crystal size on suture/tissue pull-out force

	Crystal size (A°)	Barbed suture/ tissue pull-out force (grams)
Biosyn	53	1,419 ± 70
Maxon	51	1,849. ± 54
Monocryl	60	1,470 ± 80
PDS II	65	1,656 ± 69
Ethilon	34	2,135 ± 95
Novafil	62	1,334 ± 58
Prolene	51	1,652 ± 53

Ethilon, with the smallest crystal size, was found to have the highest tissue holding capacity which is significant at p=0.05. A general trend can be observed that by increasing the size of the crystals, suture the tissue holding capacity of the barbed sutures falls, Table 4.21.

A low correlation coefficient was found between the suture/tissue holding capacity and the monofilament peak tensile load and the tensile modulus. These properties appear to have little influence on the force and performance of the barbs.

4.2.2.3 Correlation between length of suture pulled out of the tissue simulant in a suture/tissue pull-out test

The length pulled out of the tissue simulant gives an idea of how much resistance the barbs had to withstand the pulling force. If the barbs are weak, then they will fail easily, with least resistance to the pulling force. Thus the length of the suture being pulled out in this case will be more. Hence if there is less length pulled out, it means that there was a greater resistance offered by the barbs to the pulling force. This is also a desirable quality of a 'good' barb. In contrast to the pulled out length, the remaining length of the suture remains inside the tissue.

Table 4.22 shows the values for the correlation coefficient for relating the length of suture pulled out of the tissue simulant to various independent parameters. There was low correlation of the length pulled out to all the parameters. However it can be seen that among the given parameters the crystal size showed a highest correlation of r = 0.64. The positive sign indicates that the length pulled out is directly proportional to the crystal size. It means that the greater the size of the crystal, more will be the length of the suture pulled out length because of less rigid barbs. This can also be seen from the negative value for the correlation coefficient, r = -0.55, which indicates that the suture pull out length is inversely proportional to the bending rigidity of the suture polymer. In other words, the suture pull out length will be less when the barbs are more rigid, since they will offer a higher resistance to the pulling force.

Table 4. 22: Correlation of length of suture pulled out of tissue simulant

Independent Variables	Correlation coefficient r	r^2
Unbarbed bending rigidity	-0.65	0.43
Crystal size	0.64	0.41
Unbarbed tensile modulus	-0.54	0.29
Herman's Orientation Factor	-0.38	0.14
Unbarbed peak tensile load	0.36	0.13
Degree of crystallinity	-0.30	0.09
Unbarbed toughness	0.13	0.02
Unbarbed peak tensile elongation	-0.03	0.00

Table 4.22 also shows that the suture pull out length is very weakly correlated to the suture tensile properties.

4.2.3 Effect of microstructure on barb performance

In section 1.1, Problem Statement, it is explained that certain types of sutures and polymers, such as PDS II, Prolene, Ethilon and Maxon produce stiff barbs that stand out and mechanically engage the surrounding tissue, whereas other sutures and polymers, such as Biosyn, Monocryl and Novafil, form limp barbs that do not perform as well. The results of suture/tissue pull-out testing presented in Figure 4.18 clearly demonstrate the difference in barb performance between those sutures with “stiff” barbs (which give mean peak pull-out loads greater than 1,500 grams) and those with “limp” barbs or inferior barb performance, that is mean peak pull-out loads below 1,500 grams.

Attempts to explain this difference in barb performance in terms of the sutures mechanical properties, such as tenacity, toughness and bending rigidity, have provided no clear explanation of this phenomenon. We now review whether the microstructure characteristics of the polymers as elucidated by x-ray diffraction spectrometry and differential scanning calorimetry, may provide an explanation.

The polypropylene polymer (Prolene) has a higher degree of orientation and a higher degree of crystallinity compared to Monocryl, though the unbarbed peak tensile load of the Prolene suture is lower. However Prolene performs better than Monocryl in the suture/ tissue pull-out force test because of the higher

rigidity of Prolene (see Table 4.14). This higher rigidity is due to its highly oriented crystalline structure.

4.2.4 Barb and Filament Failure

4.2.4.1 Unbarbed Sutures from Tensile Load Test:

The images of unbarbed sutures after failure during tensile loading are shown below.

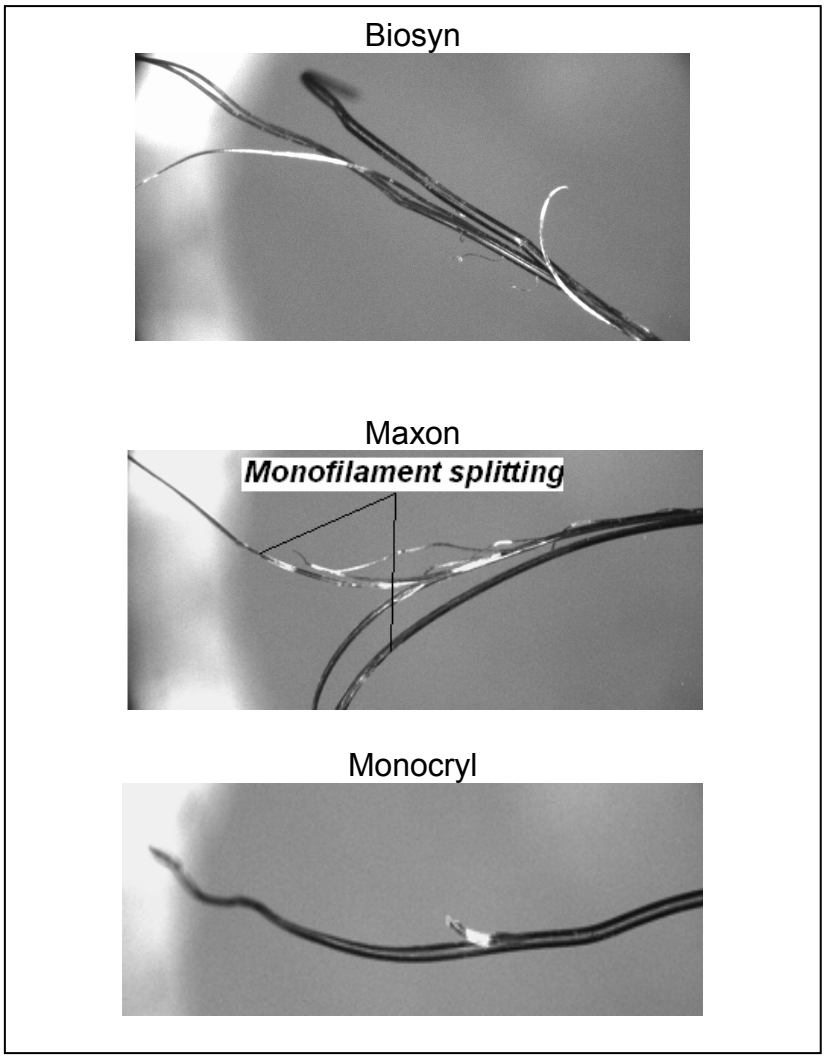

Figure 4. 25: Images of the ruptured unbarbed sutures after tensile loading

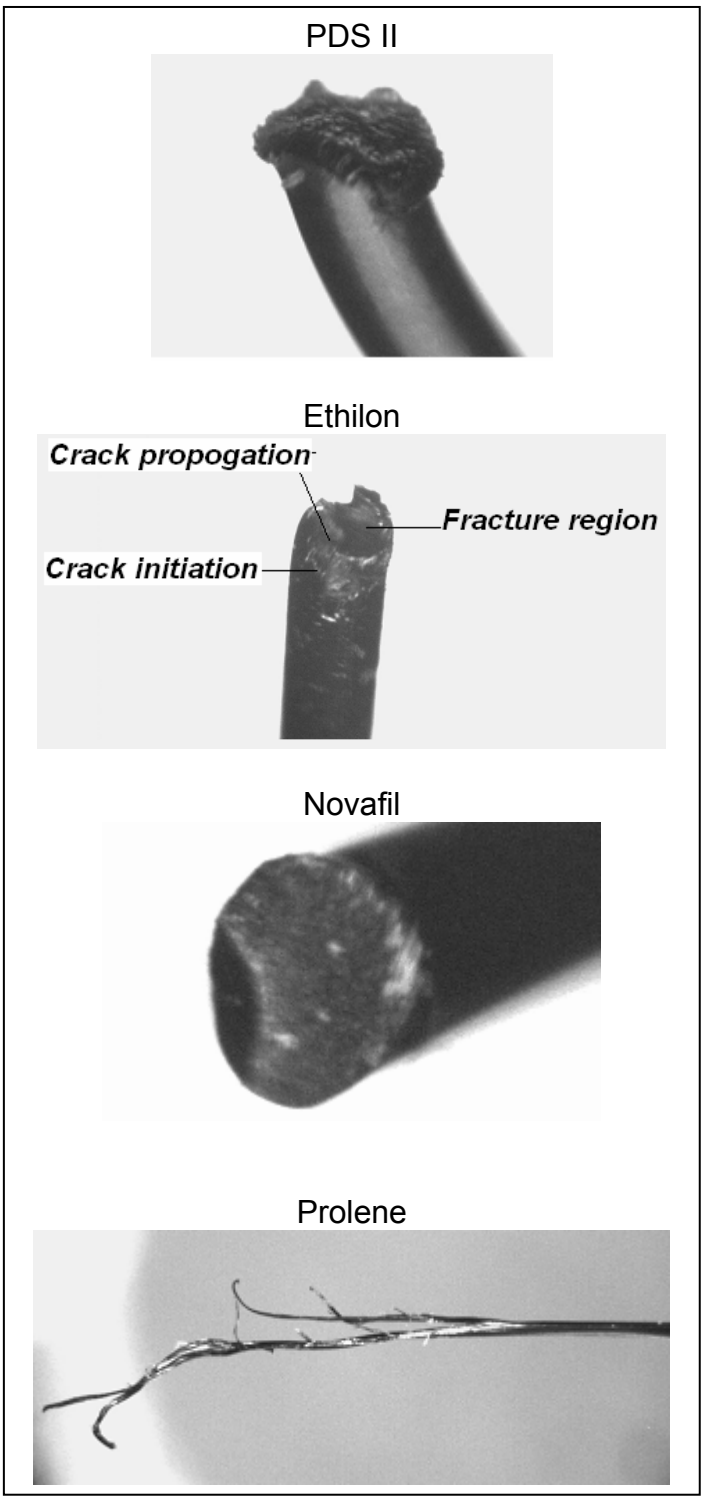

Figure 4. 26: Images of the ruptured unbarbed sutures after tensile loading

It can be seen from Figure 4.25 and 4.26, that the Maxon and Prolene polymers show a tendency to split into fibrils at the point of failure. Monocryl breaks

following thinning of the monofilament until the point is reached when it can no longer sustain the load. The cross-section of the PDS II monofilament after the break is circular.

4.2.4.2 Barbed Sutures from Tensile Load Test:

Images of the barbed failed suture fragments after tensile load testing are shown below.

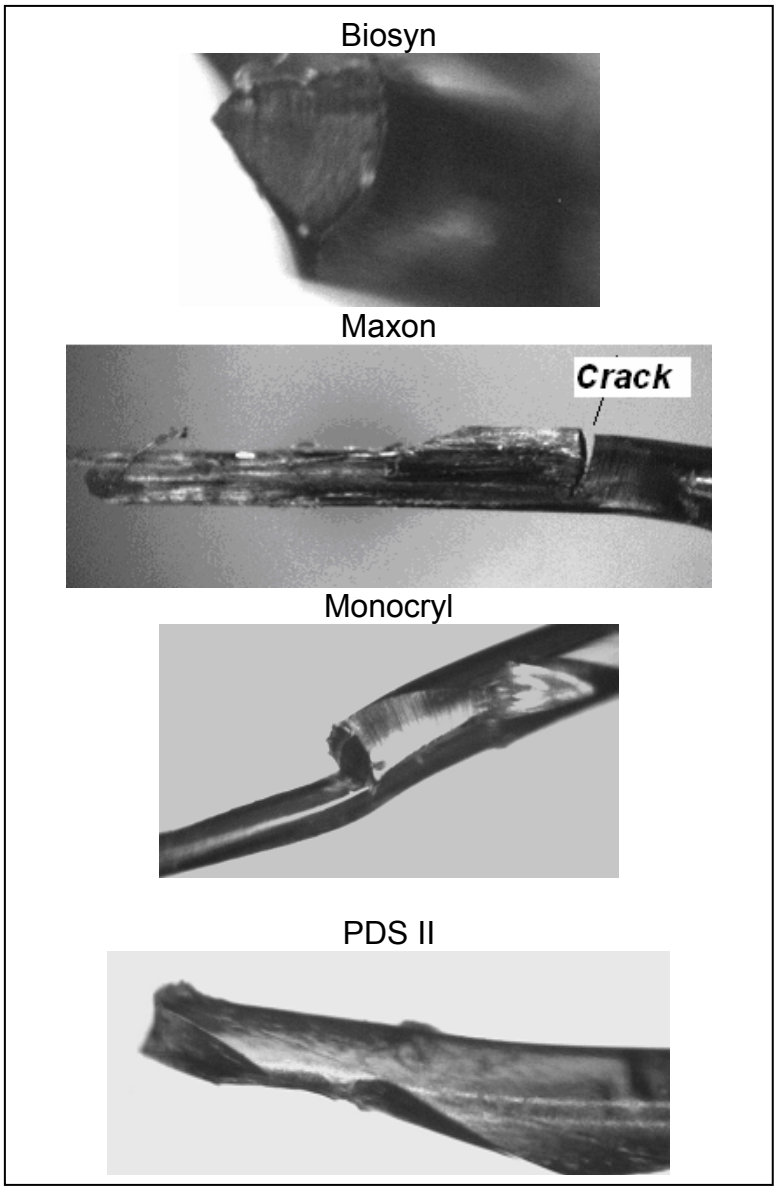

Figure 4. 27: Images of ruptured barbed sutures after tensile loading

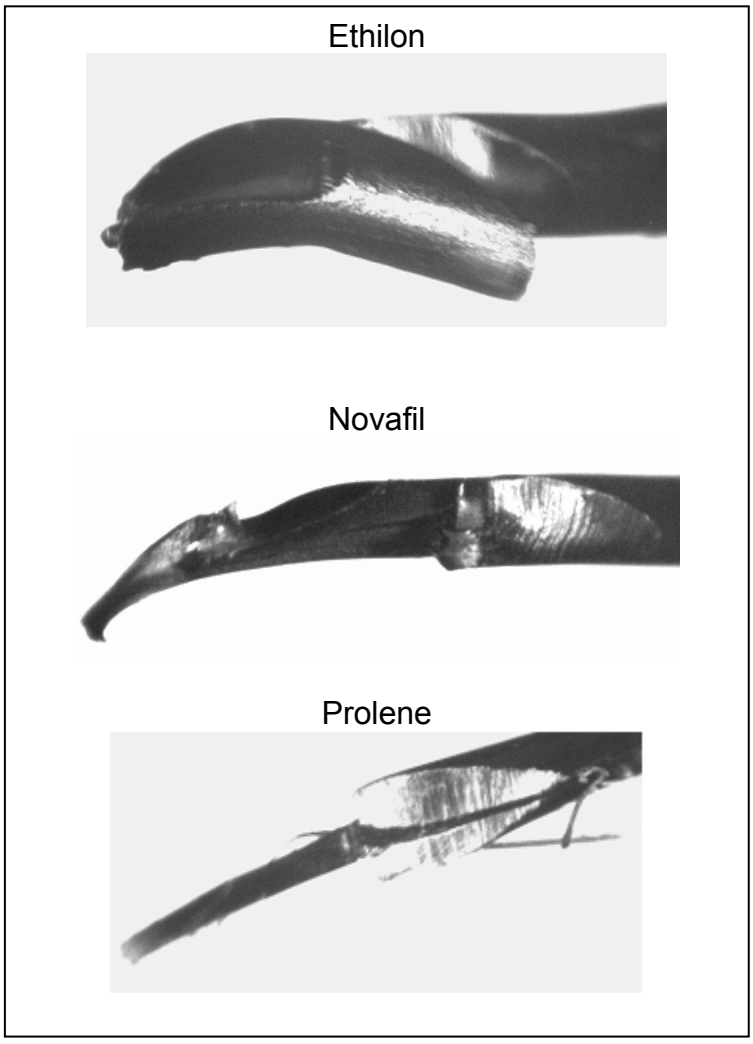

Figure 4. 28: Images of ruptured barbed sutures after tensile loading

In the case of all seven suture polymers the break is initiated at the end of the cut notch, Figure 4.27 and 4.28. Creating the barb has in itself generated a crack in the monofilament, which is a potential weak point. When stressed the crack then proceeds to peel along the filament length at a slight angle. The monofilament eventually ruptures when this crack passes through the entire diameter.

It can be seen from the images that Maxon shows distinct crack formation at the base of the barb when the suture monofilament is loaded axially. Monocryl and Prolene have a barb tail left behind after the monofilament ruptures. PDS II and Ethilon have a straight fracture plane across the filament diameter, and no tail formation is seen.

4.2.4.3 Suture/ Tissue Pull-out Force Test:

This section depicts the images of the barbed suture tips as viewed under a light microscope after the suture/tissue pull-out force tests. It was believed that views of the failed fracture planes would provide information about the failure mechanism of the barbed sutures and assist in explaining the relative performance of the different types of sutures.

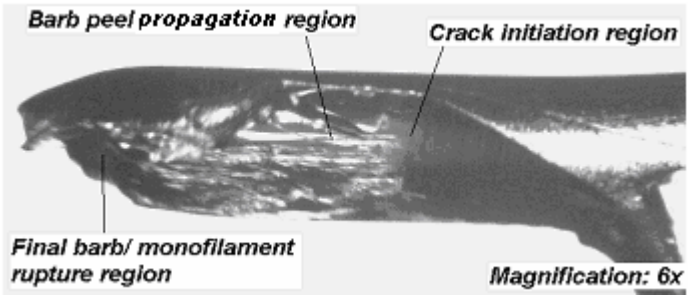

Figure 4. 29: Image of a failed suture, Ethilon.

The Figure 4.29 shows the image of fractured specimens after a suture/ tissue pull out force test. Failure usually starts at the base of the barb crack as the barb is bent back on itself and peeling and elongation of the barb takes place. It can be seen that striations are formed in the barb peeling path in the case of all seven polymers. The peeling path is the length over which a barb keeps peeling from the monofilament surface, even after the barb base has been detached from the monofilament. Eventually a point is reached where the barb along with its tail is completely detached from the monofilament. No brittle fracture was observed with any of these suture polymers.

4.2.5 Process of suture failure in a suture/tissue pull-out test:

The images below depict the process of barb failure in eight sequential steps. When a barbed suture is sutured inside the tissue, the barbs that stand out penetrate the tissue surrounding it. At this time the barb is acted upon by the forces of the tissue, that try to pull it backwards. When a forward force is applied to such an anchored suture, the part of the barb anchored inside the tissue acts as a fixed point. This can be considered to be shown in the inset 1 of Figure 4.30. This barb begins to curl back and peel off from the monofilament. Inset 2 shows the top view of the barb that has been peeled through a small distance from the cut point. Inset 3 shows the adjacent barb being acted upon by the tissue. By the time the second barb is about to begin to be peeled, the first barb has already being peeled through the between-barb distance. Inset 5 shows that the barbs continue their peeling path in a spiral towards the other side of the monofilament. Inset 6 shows that a barb can also peel into the cut area of the previous barb.

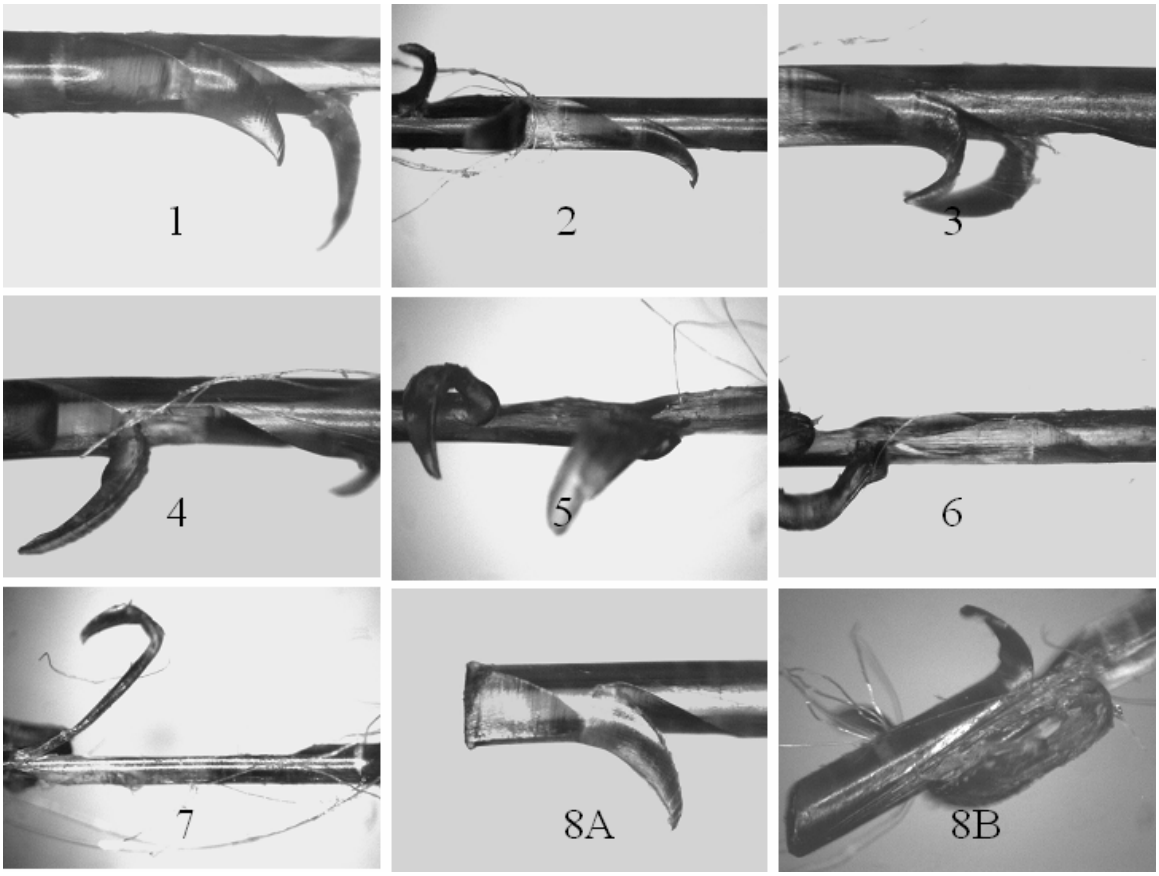

Figure 4. 30: Barb rupture process in a suture/tissue pull-out test, PDS.

The final peeling point is reached near the surface of the monofilament. With further increases in the applied force, the barb is completely detached from the monofilament surface, as shown in Inset 7. The cross-sections of the monofilament after the barb detaches completely are shown in Insets 8A & 8B. The two types of failure mechanisms involve either a curling or bending back of the barbs, or an extended peeling path towards the surface of the monofilament.

4.2.6 Barb Failure Modes:

The barb failure modes can be classified into two types:

1. Peeling
2. Curling

1. Peeling Failure:

Figure 4.31 shows two images of peeling failure. The left hand image shows that the peeling of a barb has reached the final point of detachment from the monofilament. In the right hand image the bar is peeled through an adjacent barbed region which has already been peeled off.

Figure 4. 31: Barb failure: Peeling

2. Curling Failure:

A barb created on a less stiff monofilament suture polymer tends to curl back when stressed. This occurs after the barb is dislodged from the tissue and is dragged from inside the tissue, Figure 4.32.

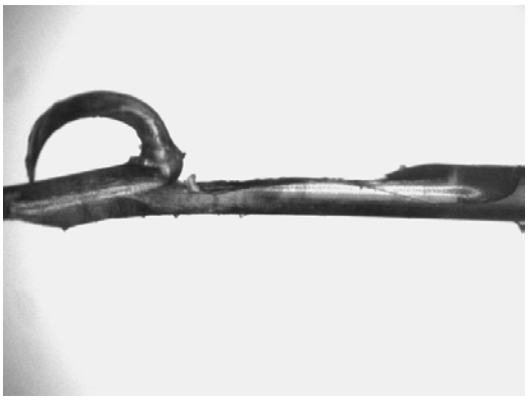

Figure 4. 32: A curled barb.

4.2.7 Finite Element Analysis:

The flow of stresses in the x-axis and y-axis directions can be observed in Figure 4.33 and 4.36 respectively. Since a truly visco-elastic model was not used, the quantitative data of the simulation results may not be reliable. However the flow of stresses can be seen in the barb region. In Figure 4.34 we can see that the upper region of the barb is under compression and the inner surface of the barb is under extension. The concentration of the stress is above the cut point of the barbed suture. The stress level in the barb decreases at we move from the inner side of the barb towards the outer surface. This stress flows all the way behind the barb region, which in turn will affect the adjacent barbs.

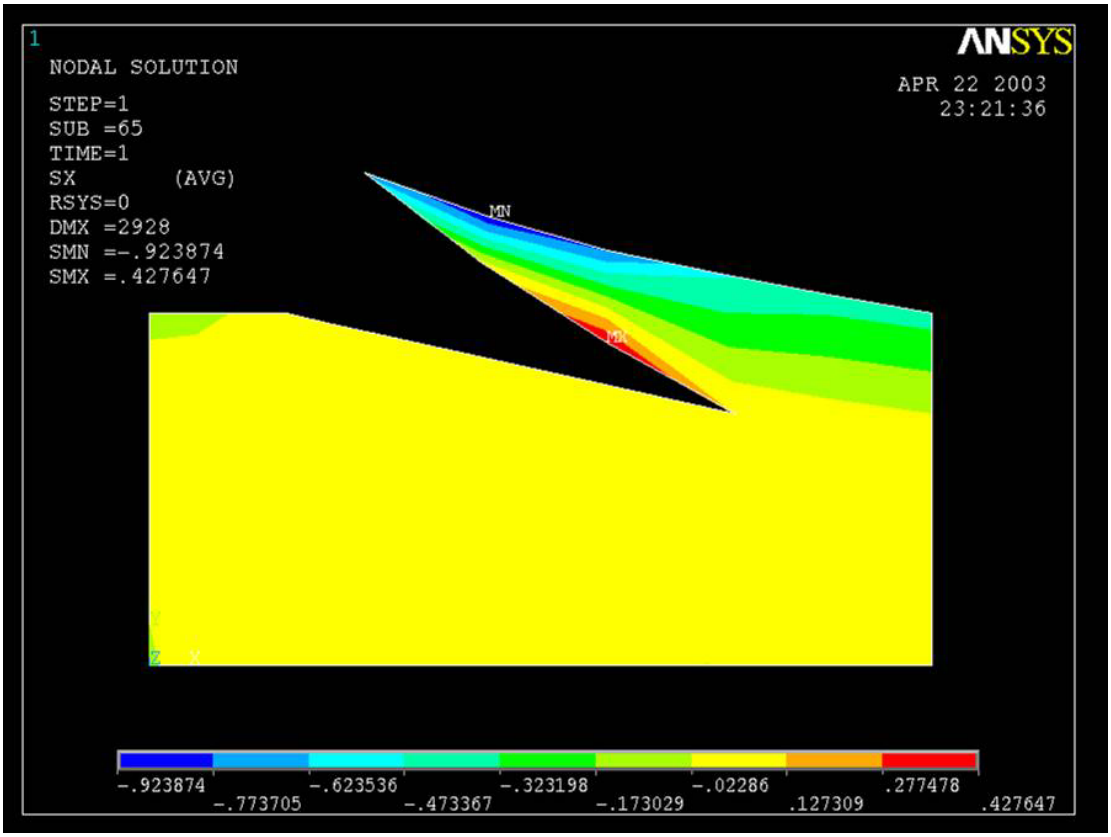

Figure 4. 33: Nodal stresses in x-direction in barb.

Image analysis of such a deformed barb confirmed the above observations. The effect of this stress concentration can be observed in the Fig. 4.34.

Figure 4. 34: Barb deformed at the place of maximum stress.

The Fig. 4.35 shows the effect of flow of the stresses into an adjacent barbed region. This is the result of barb peeling. Thus we can confirm the peeling behavior predicted reasons from the simulations by making observations of the ruptured barbs by image analysis.

Figure 4. 35:Flow of stresses in adjacent barb

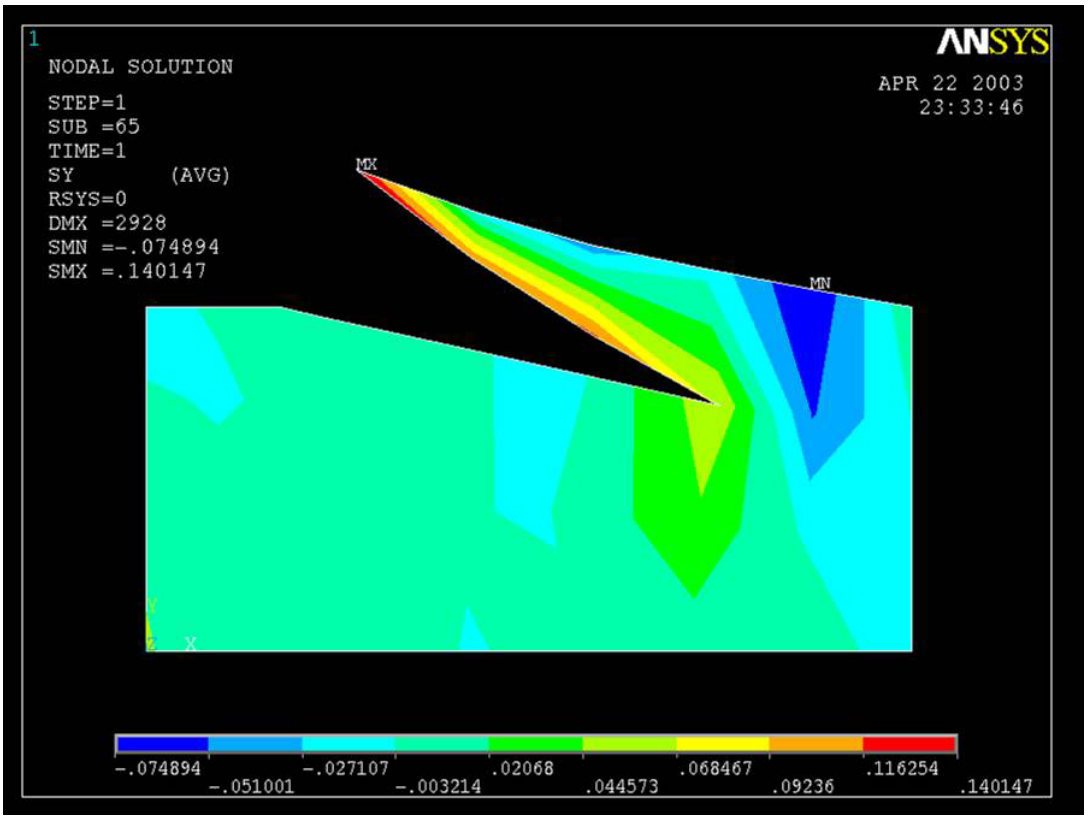

Figure 4. 36: Nodal stresses in y-direction in barb.

Similarly from Fig. 4.36 we can see the flow of stresses in the y-direction. There appears to be an area of high compressive stress just behind the barb. This compressive stress penetrates the filament to a depth equivalent to the cut depth. After it reaches the cut depth it then lessens in intensity. However the stress concentration in the region surrounding the cut point is of the extension type and it flows beyond the diameter of the monofilament.

Hence we can say that the initiation of the barb peeling process takes place due a concentration of compressive forces above the barb region and extensional forces at the cut point. These forces detach the barb from its base. This fracture plane becomes enlarged depending upon the magnitude of forces in the x and y directions. Now, a majority of the molecular chains are arranged parallel to the monofilament axis which results in the alignment of strong covalent bonds parallel to the fiber axis. As a result, the bonds inter-connecting two such

molecular chains become aligned perpendicular to the monofilament axis. Such bonds interlinking two parallel molecular chains are unlikely to be strong covalent bonds, and are largely supported by secondary bonds. Thus it is easier to break the bonds that are perpendicular to the monofilament axis. Hence we can say that the forces along the x-axis direction are primarily responsible for initiating and continuing the peeling process.

5 Conclusions & Further Work

5.1 Conclusions

1. The suture/tissue pull-out test method developed during the study was successful in distinguishing between barbed sutures that give superior and inferior tissue holding capacities
2. The resorbable polymer sutures have a higher peak tensile load as compared to the non-resorbable polymers sutures.
3. Among all the sutures, Ethilon had the highest suture/tissue pull-out force, followed by Maxon, PDS II & Prolene. Monocryl, Biosyn and Novafil had the lowest suture/tissue pull-out forces. PDS II & Prolene had no significant difference in their pull-out force. Similarly, there was no significant difference in the pull-out force of Monocryl, Biosyn and Novafil sutures.
4. The suture/tissue pull-out force of the barbed sutures was significantly higher than that for the unbarbed sutures.
5. Of all the microstructural characteristics of the suture polymer as measured by x-ray diffraction and DSC, crystal size was found to be the most important single variable in predicting the barb performance.
6. Those suture polymers with small crystal size were found to give superior barb performances.
7. Among the mechanical properties measured on the suture polymers, the peak tensile elongation of the unbarbed suture was found to be correlated with the tissue holding capacity of the barbs.
8. The mechanism of barb failure proceeds either through curling or peeling. Peeling always starts at cut notch under the barb and continues in the axial direction of the suture.
9. Finite element analysis has demonstrated that when mechanically stressed the upper surface of the barb is under compressive loading while the under surface of the barb experiences tension.

5.2 Further Work

A series of crystalline compositions with different crystal sizes, degrees of crystallinity and amount of orientation could be prepared for desired levels of barb performance, depending on the end use in a particular type of tissue. Thus there will be a specific composition for each type of tissue in the body.

When cutting the barbs, the shape of the region at the cut point could be varied such as made into a circular shape, which might increase the barb resistance to peeling and increase suture/tissue pull-out.

The effect of diameter on the propagation of the crack could be studied with and without the factor of crystallinity.

Three dimensional finite element analysis could be performed to evaluate different mechanical factors, such as the effect of change in diameter, change in barb geometry, change in physical properties of the polymer, such as tensile elongation, and change in crystal size. Changing the shape of the cut point to see the change in barb performance could also be considered. Also, the distance between barbs and the angle of spirality could be optimized. In addition, all these factors could be optimized for different tissues such as dermal, tendon, ligament and bone. Thus a code could be written, where we input the tissue properties and retrieve the required polymer characteristics and barb geometry from the computer simulations. It is believed that this approach could lead to the optimization of barb performance for a range of different suture polymers.

6 References

1. Dattilo DP, King MW, Leung JC. Tissue holding performance of knotless absorbable sutures. Annual Conference of Society for Biomaterials April 2003.
2. Cox WA. Method and apparatus for grinding and polishing ligatures. United States Patent # 2,355,907; August 15, 1944.
3. Buncke HJ. Surgical methods using one-way suture. United States Patent # 5,931,855; August 3, 1999.
4. Kaplan A, Ruff GL, Megaro MA. Suture Method. United States Patent Application # 2003/0074023; April 17, 2003.
5. Brotz GR. Suture Assembly. United States Patent # 5,584,859; December 17, 1996.
6. Wilk PJ, Sekons D. Suture Device. United States Patent # 5,123,913; June 23, 1992.
7. Aklyama T. Surgical thread and cutting apparatus for the same. United States Patent # 4,069,825; January 24, 1978.
8. Yoon I. Suture devices particularly useful in endoscopic surgery. United States Patent # 5,222,976; June 29, 1993.
9. Lemole GM. Suture apparatus and method. United States Patent # 3,570,497; March 16, 1971.
10. Matlin NA. Wool-like artificial fibers. United States Patent # 2,866,256; December 30, 1958.
11. Alcamo JH. Surgical suture. United States Patent # 3,123,077; March 3, 1964.
12. Sullivan CJP. Suture provided with radiopaque free methal
13. Williams RC, Jewett W, Genova P. Method of forming barbs ona suture and apparatus for performing same. United States Patent Application # 2003041426; March 6, 2003.
14. Private conversation with Buchanan DR in August 2003 at College of Textiles, North Carolina State University, Raleigh, NC 27695.

15. Logan DL. A first course in finite element analysis. Second Edition, PWS Publishing Company, 1993.
16. Moaveni S. Finite element analysis: Theory and applications with Ansys. Prentice Hall, Upper Saddle River, New Jersey 07458.
17. Brandrup J, Immergut EH, Grulke EA. Polymer Handbook, Fourth Edition. John Wiley & Sons, Inc. 1999.
18. Ansys help manual.
19. KimYH. An overview on biodegradable polymers in biomedical application. ICS-UNIDO EDP EGM, September 2002, Trieste, Italy.
20. Sabino MA, Feijoo JL, Muller AJ. Crystallization and morphology of poly(p-dioxanone). Macromolecular Chemistry Physics, `2687-2698, 201, 2000.
21. X-ray diffraction laboratory, Safety and operating procedure. College of Textiles, North Carolina State University, Raleigh, NC 27606.
22. Dumbelton JH, Buchanan DR, Bowles BB. Characterization of Nylon 66 structure from x-ray diffraction. Journal of Applied Polymer Science, vol. 12, 2067-2078, 1968.
23. Bernakiewicz M, Viceconti A T. Investigation of the influence of periprosthetic fibrous tissue on the primary stability of uncemented hip prostheses. Laboratorio di technologia medica, Instituti Ortopedici Rizzoli, Bologna. Science and Supercomputing at CINECA – Report 2001.
24. Private conversation with Dr. Hamouda H in College of Textiles, North Carolina State University, Raleigh, NC during Spring 2003.
25. Feng Si-Shen. On lipid monolayer-bilayer correspondence a theoretical molecular biomechanics of biomembranes. BED-Vol. 50, 2001 Bioengineering Conference, ASME 2001.
26. Aurich M, Mollenhauer J, Irving TC. X-ray diffraction studies of the molecular substructure of human articular cartilage. Department of Biochemistry, Rush Medical College, Chicago, IL 60612; Bio-CAT, Dept. BCPS, Illinois Institute of Technology, Chicago, IL 60616.(other details unknown).

27. Williams DF, Chu CC, Dwyer J. Effects of enzymes and gamma irradiation on the tensile load and morphology of Poly(p-dioxanone) fibers. Journal of Applied Polymer Science, Vol. 29, 1865-1877, 1984
28. Vallejo B, Selgas C, Mahar A, Impelluso T. Using model analysis to determine failure characteristics of remodeled bone in a fractured femur model. Department of Mechanical Engineering, San Diego State University, San Diego, CA, USA; Orthopedic Biomechanics Research Center, Children's Hospital San Diego, CA, USA.
29. Proceedings of FEM Workshop 2002: The finite element method in biomedical engineering, biomechanics and related fields. University of Ulm, July 2002.
30. Tsap LV, Goldgof DB, Sarkar S. Efficient nonlinear finite element modeling of nonrigid objects via optimization of mesh models. Computer Vision and Image Understanding, Vol. 69, No. 3, March 1998.
31. Smith ADC, Hartkens T, Schnabel JA, Hose R, Liu H, Hall W, Truwit C, Hawkes DJ, Hill DLG. A registration based mesh construction technique for finite element models of brains. Computational Imaging Sciences Group, Radiological Sciences, Kings College, Guy's Hospital, London SE1 9RT, UK; Medical Physics Department, Clinical Engineering, Clinical Sciences Division, University of Sheffield, UK; Dept. of Neurosurgery, University of Minnesota, Minneapolis, MN, USA. (other details unknown).
32. Spring 2003. Ansys Tutorials: Solid Modeling. University of Alberta. [On-line], Available: www.mece.ualberta.ca/tutorials/ansys/ .
33. Hearle JWS, Peters RH. Fiber Structure. Published by: The Textile Institute Butterworths, 1963.
34. Spring 2003. Stiffness and Bending. [On-line], Available: http://pergatory.mit.edu/2.007/handouts/bending/bending.html
35. Chu CC. Hydrolytic degradation of polyglycolic acid: Tensile load and crystallinity study. Journal of Applied Polymer Science, vol. 26, 1727-1734, 1981.

36. Spring 2003. Macrogalleria [On-line], Available: www.psrc.usm.edu/macrog/.
37. Spring 2003. Differential Scanning Calorimetry [On-line], Available: http://www.psrc.usm.edu/macrog/dsc.htm in July 2003.
38. Spring 2003. Polyester [On-line]. Available: www.pslc.ws/macrog/pet.htm
39. Spring 2003. Moment of Inertia [On-line]. Available: http://www.ac.wwu.edu/~vawter/PhysicsNet/Topics/RotationalKinematics/MomentInertia.html .
40. Snedecor G, Cochran W. Book: Statistical Methods, Sixth Edition. Published by: The Iowa State University Press. 1973
41. Ooi CP, Cameron RE. The hydrolytic degradation of polydioxanone (PDSII) sutures. Part I: Morphological aspects. Journal of Biomedical Materials Research, Vol. 63, Issue 3, 2002, pages: 280-290.
42. Stone IK, Masterson BJ, Fraunhofer Von JA. Knot stability and tensile load of an absorbable suture material. Surface and Coatings Technology, 27 (1996) 287-293.
43. Gee DR, Melia TP. Thermal properties of melt and solution crystallized Isotactic polypropylene. Die Makromolekulare Chemie 132 (1970), 195-201.
44. Avramova N, Fakirov S. Melting behaviour of drawn and undrawn annealed nylon 6. Acta Polymerica, 32 (1981), Heft 6, 381-322.
45. Lee KH, Chu CC. The role of superoxide ions in the degradation of synthetic absorbable sutures. Journal of Biomedical Materials Research, 49, 25-35, 2000.
46. Krigbaum WR. Uematsu I. Heat of entropy of fusion of Isotactic polypropylene. Journal of Polymer Science. Part A, Vol. 3, pp. 767-776(1965).
47. Quynn RG, Riley JL, Young DA, Noether HD. Density, crystallinity, and heptane insolubility in Isotactic polypropylene. Journal of Applied Polymer Science, Vol. II, Issue no. 5, pp. 166-173 (1959).

48. Jacoby P, Bersted BH, Kissel WJ, Smith. Studies of the β-crystalline form of Isotactic polypropylene. Journal of Polymer Science: Part B: Polymer Physics, Vol. 24, 461-491 (1986).
49. Chu CC, Zhang L, Coyne LD. Effect of gamma irradiation and irradiation temperatures on hydrolytic degradation of synthetic absorbable sutures. Journal of Applied Polymer Science, Vol. 56, 1275-1294 (1995).
50. Tomihata K, Suzuki M, Ikada Y. The pH dependence of monofilament sutures on hydrolyti degradation. Journal of Biomedical Materials Research (Applied Biomaterials), 58: 511-518, 2001.
51. Makela P, Pohjonen T, Tormala P, Waris T, Ashammakhi N. Force retention properties of self-reinforced poly L-lactide (SR-PLLA) sutures compared with polyglyconate (MaxonR) and polydioxanone (PDS) sutures. An in vitro study. Biomaterials, 23, (2002), pp. 2587-2592.
52. Khanna YP, Kuhn WP. Measurement of crystalline index in nylons by DSC: Complexities and Recommendations. Journal of Polymer Science B: Polymer Physics 35: 2219-2231, 1997.
53. Griesser HJ, Chatelier RC, Martin C, Vasic ZR, Gengenbach GJ. Elimination of stick-slip of elastomeric sutures by radiofrequency glow discharge deposited coatings. Journal of Biomedical Materials Research (Applied Biomaterials) 53: 235-243, 2000.
54. Sabino M, Gonzalez S, Marquez L, Feijoo JL Study of the hydrolytic degradation of polydioxanone PPDX. Polymer Degradation and Stability, 69 (2000), 209-216.
55. Metz SA, Chegini N, Masterson B. In vivo and in vitro degradation of monofilament absorbable sutures, PDS and Maxon. Biomaterials, Vol. 11, Jan-1990.
56. S. Lima MF, Vasconcellos MAZ, Samios D. Crystallinity changes in plastically deformed Isotactic polypropylene evaluated by X-ray diffraction and differential scanning calorimetry methods. Journal of Polymer Science Part B: Polymer Physics, 40: 896-903, 2002.

57. Isasi JR, Mandelkern L, Galante MJ, Alamo RG. The degree of crystallinity of monoclinic Isotactic poly(propylene). Journal of Polymer Science B: Polymer Physics, 37: 323-334, 1999.
58. Nunn DB, Letort M, Maini R. Problems resulting from interaction of fabric and stent components of endografts: Can they be prevented?. Combined Session: Vascular Surgery and Interventional Radiology. (complete reference not available).
59. Fraunhofer JA, Storey RJ, Masterson BJ. Tensile properties of suture materials. Biomaterials. Vol. 9, July 1988.
60. Wada A, Kubota H, Taketa M, Miura H, Iwamoto Y. Comparison of the mechanical properties of polyglycolide-trimethylene carbonate (Maxon) and polydioxanone sutures (PDS 2) used for flexor tendon repair and active mobilization. Journal of Hand Surgery (British and Europena Volume, 2002) 27B: 4: 329-332.
61. Fraunhofer JA, Sichina WJ. Characterization of surgical suture materials using dynamic mechanical analysis. Biomaterials. Vol. 13, no. 10, 1992.
62. King E, Cameron RE. Effect of hydrolytic degradation on the microstructure of polyglycolic acid: An x-ray scattering and ultraviolet spectrophotometry study of wet samples ultraviolet. Journal of Applied Polymer Science. Vol. 66, 1997, 1681-1690.
63. Akieda H, Shioya Y, Kajita M, Kazuhiro O. Method of producing poly(p-dioxanone), poly(p-dioxanone) monofilaments and method for producing the same. US Patent # 6,448,367, September 10, 2002.
64. Psarki M, Pracella M, Galeski A. Crystal phase and crystallinity of polyamide 6/functionalized polyolefin blends. Polymer, 41, 2000, 4923-4932.
65. Wlochowicz A, Jeziorny A. Evaluation of the crystallinity of copolyamide fibers. Journal of Polymer Science: Polymer Chemistry Edition, Vol. 11, 2719-2725, 1973.

7 Appendix

7.1 X-ray Diffraction Calculations:

A standard curve was plotted by Buchanan *et.al.* which can be calculated from the formula for $<\cos^2\phi>$ (explained earlier in Chapter 3):

$$\cos^2\phi = \frac{\int_0^{\pi/2} I(\phi)\cos^2\phi\sin\phi\,d\phi}{\int_0^{\pi/2} I(\phi)\sin\phi\,d\phi}$$

phi(1/2)	cos^2<phi>= A/B
0	1.0000
10	0.9575
20	0.8476
30	0.7101
40	0.5901
50	0.5081
60	0.4563
70	0.4232
80	0.4011
90	0.3858
100	0.3748
110	0.3662
120	0.3604
130	0.3556
140	0.3517

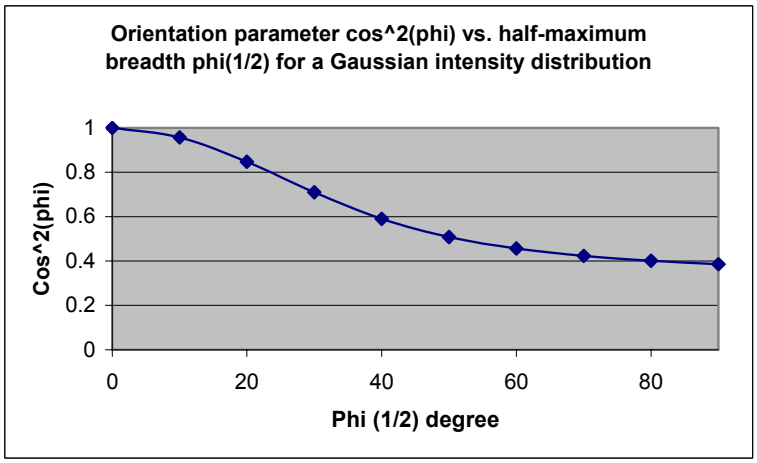

Figure 7. 1: $<\cos^2\phi>$ **curve**

The following are the values calculated for the polymers:

Table 7. 1: Biosyn

Polymer: Biosyn

Phi (1/2)= **17** (degree, as measured from x-ray image)

Phi (1/2)= 0.29655556 (radians)

h = 2.80891720

Phi (degrees)	Phi (Radians)	I(phi)	cos^2(phi)	sin(phi)	A	B
0	0.00000000	1.58516368	1.00000000	0.00000000	0.00000000	0.00000000
2	0.03488889	1.57001254	0.99878326	0.03488181	0.05469825	0.05476488
4	0.06977778	1.52542249	0.99513896	0.06972117	0.10583724	0.10635424
6	0.10466667	1.45390217	0.98908484	0.10447567	0.15023941	0.15189740
8	0.13955556	1.35937175	0.98065035	0.13910300	0.18543382	0.18909269
10	0.17444444	1.24680723	0.96987657	0.17356104	0.20987853	0.21639716
12	0.20933333	1.12180765	0.95681590	0.20780783	0.22305332	0.23312042
14	0.24422222	0.99013748	0.94153194	0.24180170	0.22541868	0.23941693
16	0.27911111	0.85729565	0.92409905	0.27550127	0.21825929	0.23618604
18	0.31400000	0.72815486	0.90460209	0.30886552	0.20344676	0.22490193
20	0.34888889	0.60670127	0.88313595	0.34185385	0.18316519	0.20740316
22	0.38377778	0.49588854	0.85980509	0.37442610	0.15964312	0.18567361
24	0.41866667	0.39760446	0.83472308	0.40654264	0.13492728	0.16164317
26	0.45355556	0.31273497	0.80801199	0.43816437	0.11072133	0.13702932
28	0.48844444	0.24130130	0.77980181	0.46925280	0.08829798	0.11323131
30	0.52333333	0.18264210	0.75022984	0.49977010	0.06848028	0.09127906
32	0.55822222	0.13561263	0.71944002	0.52967913	0.05167823	0.07183118
34	0.59311111	0.09877736	0.68758219	0.55894348	0.03796207	0.05521096
36	0.62800000	0.07057854	0.65481141	0.58752753	0.02715296	0.04146684
38	0.66288889	0.04947046	0.62128716	0.61539649	0.01891443	0.03044395
40	0.69777778	0.03401553	0.58717261	0.64251645	0.01283297	0.02185554
42	0.73266667	0.02294387	0.55263380	0.66885439	0.00848078	0.01534611
44	0.76755556	0.01518147	0.51783882	0.69437827	0.00545889	0.01054169
46	0.80244444	0.00985415	0.48295702	0.71905701	0.00342209	0.00708570
48	0.83733333	0.00627455	0.44815817	0.74286057	0.00208892	0.00466112
50	0.87222222	0.00391926	0.41361163	0.76576000	0.00124134	0.00300121
52	0.90711111	0.00240150	0.37948554	0.78772740	0.00071788	0.00189173
54	0.94200000	0.00144351	0.34594598	0.80873606	0.00040386	0.00116742
56	0.97688889	0.00085117	0.31315621	0.82876040	0.00022091	0.00070542
58	1.01177778	0.00049235	0.28127579	0.84777604	0.00011740	0.00041740
60	1.04666667	0.00027937	0.25045990	0.86575984	0.00006058	0.00024187
62	1.08155556	0.00015551	0.22085851	0.88268992	0.00003032	0.00013726
64	1.11644444	0.00008491	0.19261569	0.89854566	0.00001470	0.00007630
66	1.15133333	0.00004548	0.16586890	0.91330778	0.00000689	0.00004154
68	1.18622222	0.00002390	0.14074831	0.92695830	0.00000312	0.00002215
70	1.22111111	0.00001232	0.11737619	0.93948061	0.00000136	0.00001157
72	1.25600000	0.00000623	0.09586629	0.95085946	0.00000057	0.00000592
74	1.29088889	0.00000309	0.07632328	0.96108101	0.00000023	0.00000297
76	1.32577778	0.00000150	0.05884230	0.97013283	0.00000009	0.00000146
78	1.36066667	0.00000072	0.04350842	0.97800388	0.00000003	0.00000070
80	1.39555556	0.00000034	0.03039626	0.98468459	0.00000001	0.00000033
82	1.43044444	0.00000015	0.01956964	0.99016683	0.00000000	0.00000015
84	1.46533333	0.00000007	0.01108127	0.99444393	0.00000000	0.00000007
86	1.50022222	0.00000003	0.00497244	0.99751068	0.00000000	0.00000003
88	1.53511111	0.00000001	0.00127289	0.99936335	0.00000000	0.00000001
90	1.57000000	0.00000001	0.00000063	0.99999968	0.00000000	0.00000001
				Total	2.49231111	2.81455993

cos^2 <phi> = A/B

= **0.88550650**

Table 7. 2: Monocryl:

Polymer Type: Monocryl

Phi (1/2)= **19.5** (degree, as measured from x-ray image)

Phi (1/2)= 0.340166667 (radians)

h = 2.448799608

Phi (degrees)	Phi (Radians)	I(phi)	cos^2(phi)	sin(phi)	A	B
0	0.00000000	1.38193757	1.00000000	0.00000000	0.00000000	0.00000000
2	0.03488889	1.37188706	0.99878326	0.03488181	0.04779568	0.04785391
4	0.06977778	1.34217198	0.99513896	0.06972117	0.09312291	0.09357780
6	0.10466667	1.29407024	0.98908484	0.10447567	0.13372313	0.13519885
8	0.13955556	1.22961005	0.98065035	0.13910300	0.16773284	0.17104245
10	0.17444444	1.15142812	0.96987657	0.17356104	0.19382310	0.19984306
12	0.20933333	1.06259099	0.95681590	0.20780783	0.21127905	0.22081473
14	0.24422222	0.96639640	0.94153194	0.24180170	0.22001369	0.23367629
16	0.27911111	0.86617241	0.92409905	0.27550127	0.22051923	0.23863160
18	0.31400000	0.76509130	0.90460209	0.30886552	0.21376681	0.23631032
20	0.34888889	0.66601200	0.88313595	0.34185385	0.20107130	0.22767877
22	0.38377778	0.57136116	0.85980509	0.37442610	0.18394028	0.21393253
24	0.41866667	0.48305797	0.83472308	0.40654264	0.16392598	0.19638366
26	0.45355556	0.40248311	0.80801199	0.43816437	0.14249595	0.17635376
28	0.48844444	0.33048819	0.77980181	0.46925280	0.12093362	0.15508251
30	0.52333333	0.26743860	0.75022984	0.49977010	0.10027408	0.13365782
32	0.55822222	0.21328098	0.71944002	0.52967913	0.08127549	0.11297048
34	0.59311111	0.16762547	0.68758219	0.55894348	0.06442175	0.09369317
36	0.62800000	0.12983381	0.65481141	0.58752753	0.04994963	0.07628094
38	0.66288889	0.09910497	0.62128716	0.61539649	0.03789159	0.06098885
40	0.69777778	0.07455263	0.58717261	0.64251645	0.02812633	0.04790129
42	0.73266667	0.05527011	0.55263380	0.66885439	0.02042958	0.03696766
44	0.76755556	0.04038105	0.51783882	0.69437827	0.01452006	0.02803972
46	0.80244444	0.02907534	0.48295702	0.71905701	0.01009710	0.02090682
48	0.83733333	0.02063154	0.44815817	0.74286057	0.00686863	0.01532636
50	0.87222222	0.01442775	0.41361163	0.76576000	0.00456966	0.01104819
52	0.90711111	0.00994318	0.37948554	0.78772740	0.00297233	0.00783252
54	0.94200000	0.00675324	0.34594598	0.80873606	0.00188941	0.00546159
56	0.97688889	0.00452021	0.31315621	0.82876040	0.00117314	0.00374617
58	1.01177778	0.00298171	0.28127579	0.84777604	0.00071101	0.00252782
60	1.04666667	0.00193835	0.25045990	0.86575984	0.00042031	0.00167814
62	1.08155556	0.00124182	0.22085851	0.88268992	0.00024209	0.00109614
64	1.11644444	0.00078405	0.19261569	0.89854566	0.00013570	0.00070450
66	1.15133333	0.00048785	0.16586890	0.91330778	0.00007390	0.00044556
68	1.18622222	0.00029915	0.14074831	0.92695830	0.00003903	0.00027730
70	1.22111111	0.00018078	0.11737619	0.93948061	0.00001994	0.00016984
72	1.25600000	0.00010767	0.09586629	0.95085946	0.00000981	0.00010238
74	1.29088889	0.00006319	0.07632328	0.96108101	0.00000464	0.00006073
76	1.32577778	0.00003655	0.05884230	0.97013283	0.00000209	0.00003546
78	1.36066667	0.00002084	0.04350842	0.97800388	0.00000089	0.00002038
80	1.39555556	0.00001171	0.03039626	0.98468459	0.00000035	0.00001153
82	1.43044444	0.00000648	0.01956964	0.99016683	0.00000013	0.00000642
84	1.46533333	0.00000354	0.01108127	0.99444393	0.00000004	0.00000352
86	1.50022222	0.00000190	0.00497244	0.99751068	0.00000001	0.00000190
88	1.53511111	0.00000101	0.00127289	0.99936335	0.00000000	0.00000101
90	1.57000000	0.00000053	0.00000063	0.99999968	0.00000000	0.00000053
					2.74026228	3.20834496
					cos^2 <phi> = A/B =	**0.85410463**

Table 7. 3: Maxon

Polymer Type: Maxon

Phi (1/2)= **17** (degree, as measured from x-ray image)

Phi (1/2)= 0.296555556 (radians)

h = 2.808917197

Phi (degrees)	Phi (Radians)	I(phi)	cos^2(phi)	sin(phi)	A	B
0	0.00000000	1.58516368	1.00000000	0.00000000	0.00000000	0.00000000
2	0.03488889	1.57001254	0.99878326	0.03488181	0.05469825	0.05476488
4	0.06977778	1.52542249	0.99513896	0.06972117	0.10583724	0.10635424
6	0.10466667	1.45390217	0.98908484	0.10447567	0.15023941	0.15189740
8	0.13955556	1.35937175	0.98065035	0.13910300	0.18543382	0.18909269
10	0.17444444	1.24680723	0.96987657	0.17356104	0.20987853	0.21639716
12	0.20933333	1.12180765	0.95681590	0.20780783	0.22305332	0.23312042
14	0.24422222	0.99013748	0.94153194	0.24180170	0.22541868	0.23941693
16	0.27911111	0.85729565	0.92409905	0.27550127	0.21825929	0.23618604
18	0.31400000	0.72815486	0.90460209	0.30886552	0.20344676	0.22490193
20	0.34888889	0.60670127	0.88313595	0.34185385	0.18316519	0.20740316
22	0.38377778	0.49588854	0.85980509	0.37442610	0.15964312	0.18567361
24	0.41866667	0.39760446	0.83472308	0.40654264	0.13492728	0.16164317
26	0.45355556	0.31273497	0.80801199	0.43816437	0.11072133	0.13702932
28	0.48844444	0.24130130	0.77980181	0.46925280	0.08829798	0.11323131
30	0.52333333	0.18264210	0.75022984	0.49977010	0.06848028	0.09127906
32	0.55822222	0.13561263	0.71944002	0.52967913	0.05167823	0.07183118
34	0.59311111	0.09877736	0.68758219	0.55894348	0.03796207	0.05521096
36	0.62800000	0.07057854	0.65481141	0.58752753	0.02715296	0.04146684
38	0.66288889	0.04947046	0.62128716	0.61539649	0.01891443	0.03044395
40	0.69777778	0.03401553	0.58717261	0.64251645	0.01283297	0.02185554
42	0.73266667	0.02294387	0.55263380	0.66885439	0.00848078	0.01534611
44	0.76755556	0.01518147	0.51783882	0.69437827	0.00545889	0.01054169
46	0.80244444	0.00985415	0.48295702	0.71905701	0.00342209	0.00708570
48	0.83733333	0.00627455	0.44815817	0.74286057	0.00208892	0.00466112
50	0.87222222	0.00391926	0.41361163	0.76576000	0.00124134	0.00300121
52	0.90711111	0.00240150	0.37948554	0.78772740	0.00071788	0.00189173
54	0.94200000	0.00144351	0.34594598	0.80873606	0.00040386	0.00116742
56	0.97688889	0.00085117	0.31315621	0.82876040	0.00022091	0.00070542
58	1.01177778	0.00049235	0.28127579	0.84777604	0.00011740	0.00041740
60	1.04666667	0.00027937	0.25045990	0.86575984	0.00006058	0.00024187
62	1.08155556	0.00015551	0.22085851	0.88268992	0.00003032	0.00013726
64	1.11644444	0.00008491	0.19261569	0.89854566	0.00001470	0.00007630
66	1.15133333	0.00004548	0.16586890	0.91330778	0.00000689	0.00004154
68	1.18622222	0.00002390	0.14074831	0.92695830	0.00000312	0.00002215
70	1.22111111	0.00001232	0.11737619	0.93948061	0.00000136	0.00001157
72	1.25600000	0.00000623	0.09586629	0.95085946	0.00000057	0.00000592
74	1.29088889	0.00000309	0.07632328	0.96108101	0.00000023	0.00000297
76	1.32577778	0.00000150	0.05884230	0.97013283	0.00000009	0.00000146
78	1.36066667	0.00000072	0.04350842	0.97800388	0.00000003	0.00000070
80	1.39555556	0.00000034	0.03039626	0.98468459	0.00000001	0.00000033
82	1.43044444	0.00000015	0.01956964	0.99016683	0.00000000	0.00000015
84	1.46533333	0.00000007	0.01108127	0.99444393	0.00000000	0.00000007
86	1.50022222	0.00000003	0.00497244	0.99751068	0.00000000	0.00000003
88	1.53511111	0.00000001	0.00127289	0.99936335	0.00000000	0.00000001
90	1.57000000	0.00000001	0.00000063	0.99999968	0.00000000	0.00000001
					2.49231111	2.81455993

cos^2<phi> = A/B = **0.8855**

Table 7. 4: PDS II

Polymer Type:	PDS II					
Phi (1/2)=	**17.5**	(degree)				
Phi (1/2)=	0.30527777					
h =	2.72866242					
Phi (degrees)	**Phi (Radians)**	**I(phi)**	**cos^2(phi)**	**sin(phi)**	**A**	**B**
0	0.00000000	1.53987329	1.00000000	0.00000000	0.00000000	0.00000000
2	0.03488889	1.52598031	0.99878326	0.03488181	0.05316419	0.05322896
4	0.06977778	1.48504894	0.99513896	0.06972117	0.10303604	0.10353935
6	0.10466667	1.41925520	0.98908484	0.10447567	0.14665916	0.14827763
8	0.13955556	1.33201192	0.98065035	0.13910300	0.18170163	0.18528686
10	0.17444444	1.22767559	0.96987657	0.17356104	0.20665805	0.21307665
12	0.20933333	1.11118667	0.95681590	0.20780783	0.22094151	0.23091329
14	0.24422222	0.98768467	0.94153194	0.24180170	0.22486027	0.23882383
16	0.27911111	0.86213940	0.92409905	0.27550127	0.21949247	0.23752050
18	0.31400000	0.73903425	0.90460209	0.30886552	0.20648646	0.22826220
20	0.34888889	0.62212769	0.88313595	0.34185385	0.18782248	0.21267674
22	0.38377778	0.51430694	0.85980509	0.37442610	0.16557262	0.19256994
24	0.41866667	0.41753523	0.83472308	0.40654264	0.14169080	0.16974587
26	0.45355556	0.33288311	0.80801199	0.43816437	0.11785462	0.14585752
28	0.48844444	0.26062633	0.77980181	0.46925280	0.09536948	0.12229964
30	0.52333333	0.20038846	0.75022984	0.49977010	0.07513414	0.10014816
32	0.55822222	0.15130560	0.71944002	0.52967913	0.05765838	0.08014342
34	0.59311111	0.11219286	0.68758219	0.55894348	0.04311791	0.06270947
36	0.62800000	0.08169647	0.65481141	0.58752753	0.03143024	0.04799893
38	0.66288889	0.05842104	0.62128716	0.61539649	0.02233658	0.03595210
40	0.69777778	0.04102638	0.58717261	0.64251645	0.01547794	0.02636012
42	0.73266667	0.02829339	0.55263380	0.66885439	0.01045813	0.01892416
44	0.76755556	0.01916172	0.51783882	0.69437827	0.00689010	0.01330548
46	0.80244444	0.01274419	0.48295702	0.71905701	0.00442572	0.00916380
48	0.83733333	0.00832372	0.44815817	0.74286057	0.00277113	0.00618336
50	0.87222222	0.00533889	0.41361163	0.76576000	0.00169097	0.00408831
52	0.90711111	0.00336289	0.37948554	0.78772740	0.00100527	0.00264904
54	0.94200000	0.00208018	0.34594598	0.80873606	0.00058199	0.00168232
56	0.97688889	0.00126362	0.31315621	0.82876040	0.00032795	0.00104724
58	1.01177778	0.00075381	0.28127579	0.84777604	0.00017975	0.00063906
60	1.04666667	0.00044161	0.25045990	0.86575984	0.00009576	0.00038233
62	1.08155556	0.00025406	0.22085851	0.88268992	0.00004953	0.00022426
64	1.11644444	0.00014354	0.19261569	0.89854566	0.00002484	0.00012897
66	1.15133333	0.00007964	0.16586890	0.91330778	0.00001206	0.00007273
68	1.18622222	0.00004339	0.14074831	0.92695830	0.00000566	0.00004022
70	1.22111111	0.00002322	0.11737619	0.93948061	0.00000256	0.00002181
72	1.25600000	0.00001220	0.09586629	0.95085946	0.00000111	0.00001160
74	1.29088889	0.00000630	0.07632328	0.96108101	0.00000046	0.00000605
76	1.32577778	0.00000319	0.05884230	0.97013283	0.00000018	0.00000309
78	1.36066667	0.00000159	0.04350842	0.97800388	0.00000007	0.00000155
80	1.39555556	0.00000078	0.03039626	0.98468459	0.00000002	0.00000076
82	1.43044444	0.00000037	0.01956964	0.99016683	0.00000001	0.00000037
84	1.46533333	0.00000018	0.01108127	0.99444393	0.00000000	0.00000017
86	1.50022222	0.00000008	0.00497244	0.99751068	0.00000000	0.00000008
88	1.53511111	0.00000004	0.00127289	0.99936335	0.00000000	0.00000004
90	1.57000000	0.00000002	0.00000063	0.99999968	0.00000000	0.00000002
					2.54498824	2.89396802
				cos^2<phi>= A/B=		**0.87941132**

Table 7. 5: Ethilon

Polymer Type:	Ethilon					
Phi (1/2)=	**13**	(degree, as measured from x-ray image)				
Phi (1/2)=	0.22677778	(radians)				
h =	3.67319941					
Phi (degrees)	**Phi (Radians)**	**I(phi)**	**cos^2(phi)**	**sin(phi)**	**A**	**B**
0	0.00000000	2.07290635	1.00000000	0.00000000	0.00000000	0.00000000
2	0.03488889	2.03913998	0.99878326	0.03488181	0.07104235	0.07112890
4	0.06977778	1.94110536	0.99513896	0.06972117	0.13467826	0.13533613
6	0.10466667	1.78807566	0.98908484	0.10447567	0.18477133	0.18681040
8	0.13955556	1.59388649	0.98065035	0.13910300	0.21742431	0.22171440
10	0.17444444	1.37487622	0.96987657	0.17356104	0.23143674	0.23862495
12	0.20933333	1.14763695	0.95681590	0.20780783	0.22818906	0.23848795
14	0.24422222	0.92700091	0.94153194	0.24180170	0.21104476	0.22415040
16	0.27911111	0.72458696	0.92409905	0.27550127	0.18447293	0.19962463
18	0.31400000	0.54806943	0.90460209	0.30886552	0.15313081	0.16927975
20	0.34888889	0.40115791	0.88313595	0.34185385	0.12111094	0.13713737
22	0.38377778	0.28413834	0.85980509	0.37442610	0.09147364	0.10638881
24	0.41866667	0.19475071	0.83472308	0.40654264	0.06608876	0.07917447
26	0.45355556	0.12917039	0.80801199	0.43816437	0.04573175	0.05659786
28	0.48844444	0.08290517	0.77980181	0.46925280	0.03033701	0.03890348
30	0.52333333	0.05149143	0.75022984	0.49977010	0.01930632	0.02573388
32	0.55822222	0.03094732	0.71944002	0.52967913	0.01179317	0.01639215
34	0.59311111	0.01799889	0.68758219	0.55894348	0.00691733	0.01006036
36	0.62800000	0.01012986	0.65481141	0.58752753	0.00389716	0.00595157
38	0.66288889	0.00551690	0.62128716	0.61539649	0.00210932	0.00339508
40	0.69777778	0.00290752	0.58717261	0.64251645	0.00109691	0.00186813
42	0.73266667	0.00148280	0.55263380	0.66885439	0.00054809	0.00099178
44	0.76755556	0.00073178	0.51783882	0.69437827	0.00026313	0.00050813
46	0.80244444	0.00034947	0.48295702	0.71905701	0.00012136	0.00025129
48	0.83733333	0.00016150	0.44815817	0.74286057	0.00005377	0.00011997
50	0.87222222	0.00007222	0.41361163	0.76576000	0.00002288	0.00005531
52	0.90711111	0.00003125	0.37948554	0.78772740	0.00000934	0.00002462
54	0.94200000	0.00001309	0.34594598	0.80873606	0.00000366	0.00001058
56	0.97688889	0.00000530	0.31315621	0.82876040	0.00000138	0.00000440
58	1.01177778	0.00000208	0.28127579	0.84777604	0.00000050	0.00000176
60	1.04666667	0.00000079	0.25045990	0.86575984	0.00000017	0.00000068
62	1.08155556	0.00000029	0.22085851	0.88268992	0.00000006	0.00000026
64	1.11644444	0.00000010	0.19261569	0.89854566	0.00000002	0.00000009
66	1.15133333	0.00000004	0.16586890	0.91330778	0.00000001	0.00000003
68	1.18622222	0.00000001	0.14074831	0.92695830	0.00000000	0.00000001
70	1.22111111	0.00000000	0.11737619	0.93948061	0.00000000	0.00000000
72	1.25600000	0.00000000	0.09586629	0.95085946	0.00000000	0.00000000
74	1.29088889	0.00000000	0.07632328	0.96108101	0.00000000	0.00000000
76	1.32577778	0.00000000	0.05884230	0.97013283	0.00000000	0.00000000
78	1.36066667	0.00000000	0.04350842	0.97800388	0.00000000	0.00000000
80	1.39555556	0.00000000	0.03039626	0.98468459	0.00000000	0.00000000
82	1.43044444	0.00000000	0.01956964	0.99016683	0.00000000	0.00000000
84	1.46533333	0.00000000	0.01108127	0.99444393	0.00000000	0.00000000
86	1.50022222	0.00000000	0.00497244	0.99751068	0.00000000	0.00000000
88	1.53511111	0.00000000	0.00127289	0.99936335	0.00000000	0.00000000
90	1.57000000	0.00000000	0.00000063	0.99999968	0.00000000	0.00000000
					2.01707721	2.16872958
				cos^2<phi>= A/B =		**0.93007318**

Table 7. 6: Novafil

Polymer Type: Novafil

Phi (1/2)= **10** (degree, as measured from x-ray image)

Phi (1/2)= 0.174444444 (radians)

h = 4.775159236

Phi (degrees)	Phi (Radians)	I(phi)	cos^2(phi)	sin(phi)	A	B
0	0.00000000	2.69477826	1.00000000	0.00000000	0.00000000	0.00000000
2	0.03488889	2.62101114	0.99878326	0.03488181	0.09131437	0.09142562
4	0.06977778	2.41160606	0.99513896	0.06972117	0.16732265	0.16813999
6	0.10466667	2.09911161	0.98908484	0.10447567	0.21691232	0.21930608
8	0.13955556	1.72844817	0.98065035	0.13910300	0.23578005	0.24043233
10	0.17444444	1.34638373	0.96987657	0.17356104	0.22664052	0.23367976
12	0.20933333	0.99214013	0.95681590	0.20780783	0.19727103	0.20617449
14	0.24422222	0.69162207	0.94153194	0.24180170	0.15745746	0.16723539
16	0.27911111	0.45609608	0.92409905	0.27550127	0.11611771	0.12565505
18	0.31400000	0.28453487	0.90460209	0.30886552	0.07949916	0.08788301
20	0.34888889	0.16792151	0.88313595	0.34185385	0.05069608	0.05740461
22	0.38377778	0.09374947	0.85980509	0.37442610	0.03018109	0.03510225
24	0.41866667	0.04951342	0.83472308	0.40654264	0.01680241	0.02012932
26	0.45355556	0.02473824	0.80801199	0.43816437	0.00875838	0.01083942
28	0.48844444	0.01169247	0.77980181	0.46925280	0.00427856	0.00548672
30	0.52333333	0.00522800	0.75022984	0.49977010	0.00196020	0.00261280
32	0.55822222	0.00221134	0.71944002	0.52967913	0.00084268	0.00117130
34	0.59311111	0.00088485	0.68758219	0.55894348	0.00034006	0.00049458
36	0.62800000	0.00033494	0.65481141	0.58752753	0.00012886	0.00019679
38	0.66288889	0.00011994	0.62128716	0.61539649	0.00004586	0.00007381
40	0.69777778	0.00004063	0.58717261	0.64251645	0.00001533	0.00002611
42	0.73266667	0.00001302	0.55263380	0.66885439	0.00000481	0.00000871
44	0.76755556	0.00000395	0.51783882	0.69437827	0.00000142	0.00000274
46	0.80244444	0.00000113	0.48295702	0.71905701	0.00000039	0.00000081
48	0.83733333	0.00000031	0.44815817	0.74286057	0.00000010	0.00000023
50	0.87222222	0.00000008	0.41361163	0.76576000	0.00000002	0.00000006
52	0.90711111	0.00000002	0.37948554	0.78772740	0.00000001	0.00000002
54	0.94200000	0.00000000	0.34594598	0.80873606	0.00000000	0.00000000
56	0.97688889	0.00000000	0.31315621	0.82876040	0.00000000	0.00000000
58	1.01177778	0.00000000	0.28127579	0.84777604	0.00000000	0.00000000
60	1.04666667	0.00000000	0.25045990	0.86575984	0.00000000	0.00000000
62	1.08155556	0.00000000	0.22085851	0.88268992	0.00000000	0.00000000
64	1.11644444	0.00000000	0.19261569	0.89854566	0.00000000	0.00000000
66	1.15133333	0.00000000	0.16586890	0.91330778	0.00000000	0.00000000
68	1.18622222	0.00000000	0.14074831	0.92695830	0.00000000	0.00000000
70	1.22111111	0.00000000	0.11737619	0.93948061	0.00000000	0.00000000
72	1.25600000	0.00000000	0.09586629	0.95085946	0.00000000	0.00000000
74	1.29088889	0.00000000	0.07632328	0.96108101	0.00000000	0.00000000
76	1.32577778	0.00000000	0.05884230	0.97013283	0.00000000	0.00000000
78	1.36066667	0.00000000	0.04350842	0.97800388	0.00000000	0.00000000
80	1.39555556	0.00000000	0.03039626	0.98468459	0.00000000	0.00000000
82	1.43044444	0.00000000	0.01956964	0.99016683	0.00000000	0.00000000
84	1.46533333	0.00000000	0.01108127	0.99444393	0.00000000	0.00000000
86	1.50022222	0.00000000	0.00497244	0.99751068	0.00000000	0.00000000
88	1.53511111	0.00000000	0.00127289	0.99936335	0.00000000	0.00000000
90	1.57000000	0.00000000	0.00000063	0.99999968	0.00000000	0.00000000
					1.60237155	1.67348200
					cos^2<phi>= A/B =	**0.95750749**

Table 7. 7: Prolene

Polymer Type: Prolene

Phi (1/2)= **10** (degree, as measured from x-ray image)

Phi (1/2)= 0.174444444 (radians)

h = 4.775159236

phi		I(phi)	cos^2(phi)	sin(phi)	A	B
0	0.00000000	2.69477826	1.00000000	0.00000000	0.00000000	0.00000000
2	0.03488889	2.62101114	0.99878326	0.03488181	0.09131437	0.09142562
4	0.06977778	2.41160606	0.99513896	0.06972117	0.16732265	0.16813999
6	0.10466667	2.09911161	0.98908484	0.10447567	0.21691232	0.21930608
8	0.13955556	1.72844817	0.98065035	0.13910300	0.23578005	0.24043233
10	0.17444444	1.34638373	0.96987657	0.17356104	0.22664052	0.23367976
12	0.20933333	0.99214013	0.95681590	0.20780783	0.19727103	0.20617449
14	0.24422222	0.69162207	0.94153194	0.24180170	0.15745746	0.16723539
16	0.27911111	0.45609608	0.92409905	0.27550127	0.11611771	0.12565505
18	0.31400000	0.28453487	0.90460209	0.30886552	0.07949916	0.08788301
20	0.34888889	0.16792151	0.88313595	0.34185385	0.05069608	0.05740461
22	0.38377778	0.09374947	0.85980509	0.37442610	0.03018109	0.03510225
24	0.41866667	0.04951342	0.83472308	0.40654264	0.01680241	0.02012932
26	0.45355556	0.02473824	0.80801199	0.43816437	0.00875838	0.01083942
28	0.48844444	0.01169247	0.77980181	0.46925280	0.00427856	0.00548672
30	0.52333333	0.00522800	0.75022984	0.49977010	0.00196020	0.00261280
32	0.55822222	0.00221134	0.71944002	0.52967913	0.00084268	0.00117130
34	0.59311111	0.00088485	0.68758219	0.55894348	0.00034006	0.00049458
36	0.62800000	0.00033494	0.65481141	0.58752753	0.00012886	0.00019679
38	0.66288889	0.00011994	0.62128716	0.61539649	0.00004586	0.00007381
40	0.69777778	0.00004063	0.58717261	0.64251645	0.00001533	0.00002611
42	0.73266667	0.00001302	0.55263380	0.66885439	0.00000481	0.00000871
44	0.76755556	0.00000395	0.51783882	0.69437827	0.00000142	0.00000274
46	0.80244444	0.00000113	0.48295702	0.71905701	0.00000039	0.00000081
48	0.83733333	0.00000031	0.44815817	0.74286057	0.00000010	0.00000023
50	0.87222222	0.00000008	0.41361163	0.76576000	0.00000002	0.00000006
52	0.90711111	0.00000002	0.37948554	0.78772740	0.00000001	0.00000002
54	0.94200000	0.00000000	0.34594598	0.80873606	0.00000000	0.00000000
56	0.97688889	0.00000000	0.31315621	0.82876040	0.00000000	0.00000000
58	1.01177778	0.00000000	0.28127579	0.84777604	0.00000000	0.00000000
60	1.04666667	0.00000000	0.25045990	0.86575984	0.00000000	0.00000000
62	1.08155556	0.00000000	0.22085851	0.88268992	0.00000000	0.00000000
64	1.11644444	0.00000000	0.19261569	0.89854566	0.00000000	0.00000000
66	1.15133333	0.00000000	0.16586890	0.91330778	0.00000000	0.00000000
68	1.18622222	0.00000000	0.14074831	0.92695830	0.00000000	0.00000000
70	1.22111111	0.00000000	0.11737619	0.93948061	0.00000000	0.00000000
72	1.25600000	0.00000000	0.09586629	0.95085946	0.00000000	0.00000000
74	1.29088889	0.00000000	0.07632328	0.96108101	0.00000000	0.00000000
76	1.32577778	0.00000000	0.05884230	0.97013283	0.00000000	0.00000000
78	1.36066667	0.00000000	0.04350842	0.97800388	0.00000000	0.00000000
80	1.39555556	0.00000000	0.03039626	0.98468459	0.00000000	0.00000000
82	1.43044444	0.00000000	0.01956964	0.99016683	0.00000000	0.00000000
84	1.46533333	0.00000000	0.01108127	0.99444393	0.00000000	0.00000000
86	1.50022222	0.00000000	0.00497244	0.99751068	0.00000000	0.00000000
88	1.53511111	0.00000000	0.00127289	0.99936335	0.00000000	0.00000000
90	1.57000000	0.00000000	0.00000063	0.99999968	0.00000000	0.00000000
					1.60237155	1.67348200
				cos^2<phi>= A/B =		**0.95750749**

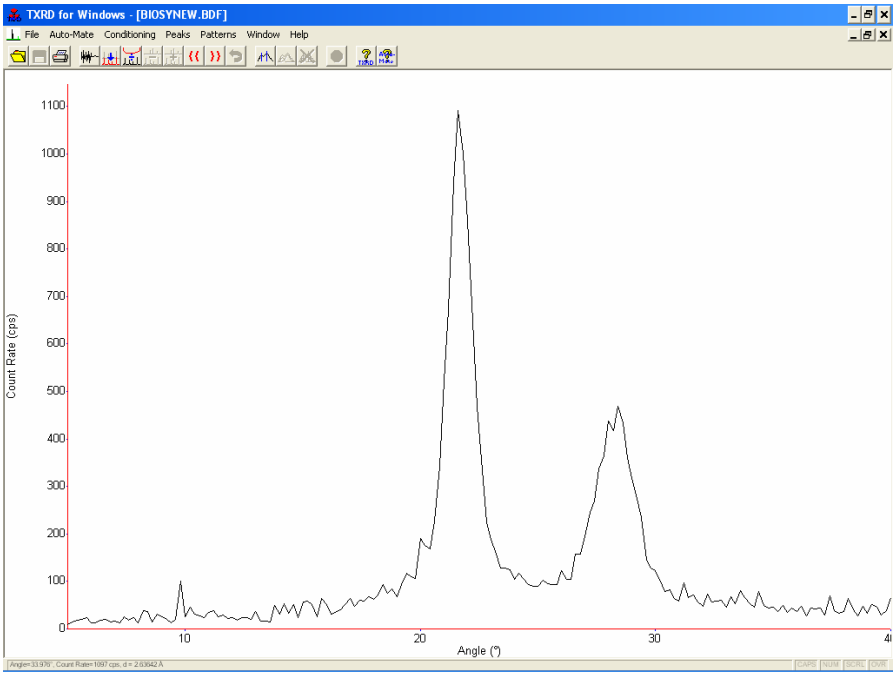

Figure 7. 2: X-ray diffraction curve for Biosyn

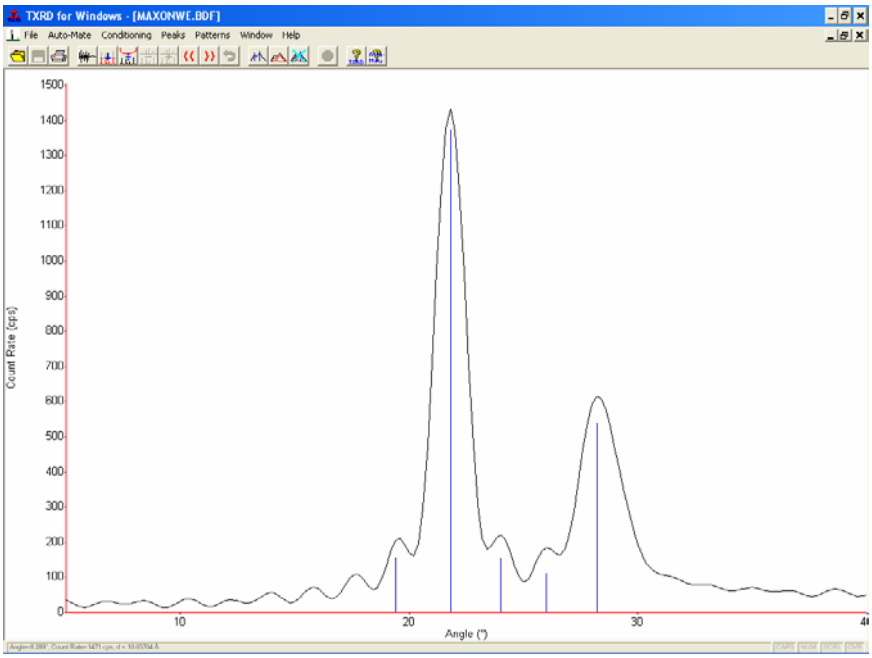

Figure 7. 3: X-ray diffraction curve for Maxon

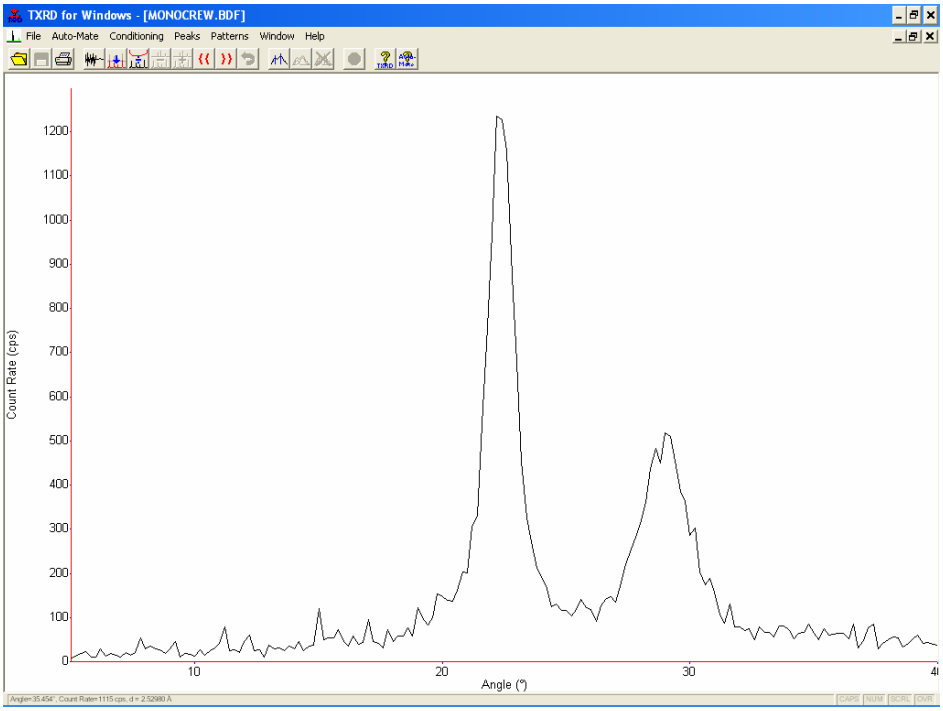

Figure 7. 4: X-ray diffraction curve for Monocryl

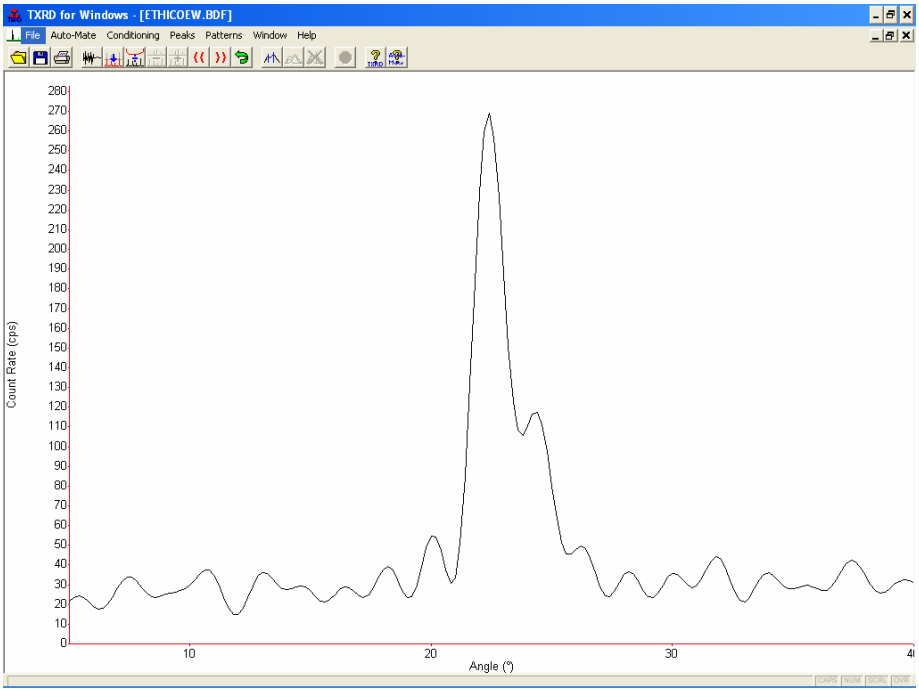

Figure 7. 5: X-ray diffraction curve fro PDS II.

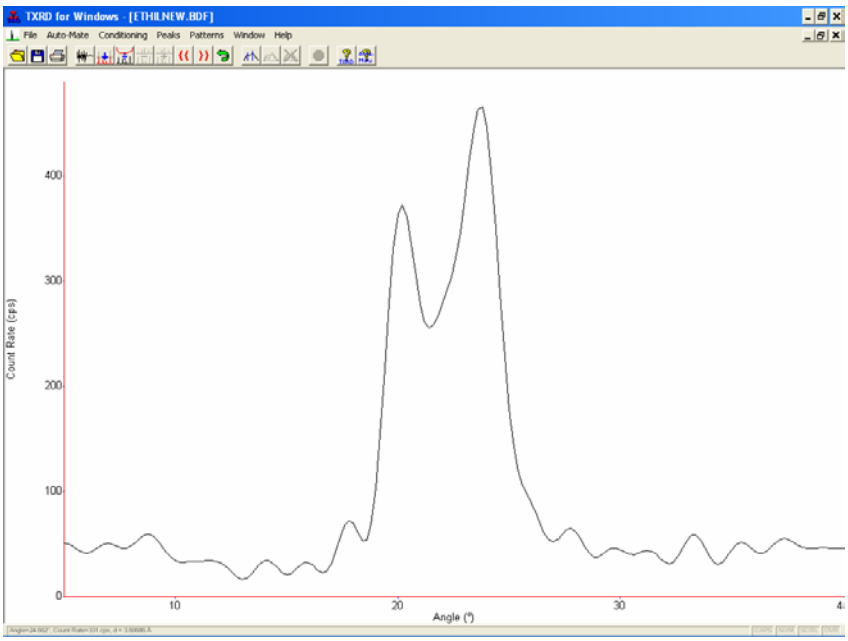

Figure 7. 6: X-ray diffraction curve for Ethilon.

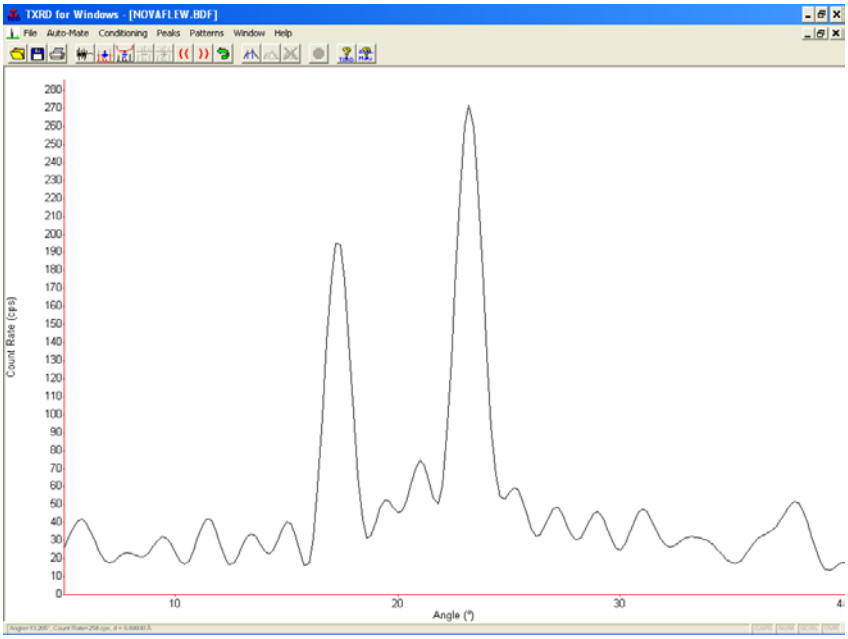

Figure 7. 7: X-ray diffraction curve for Novafil.

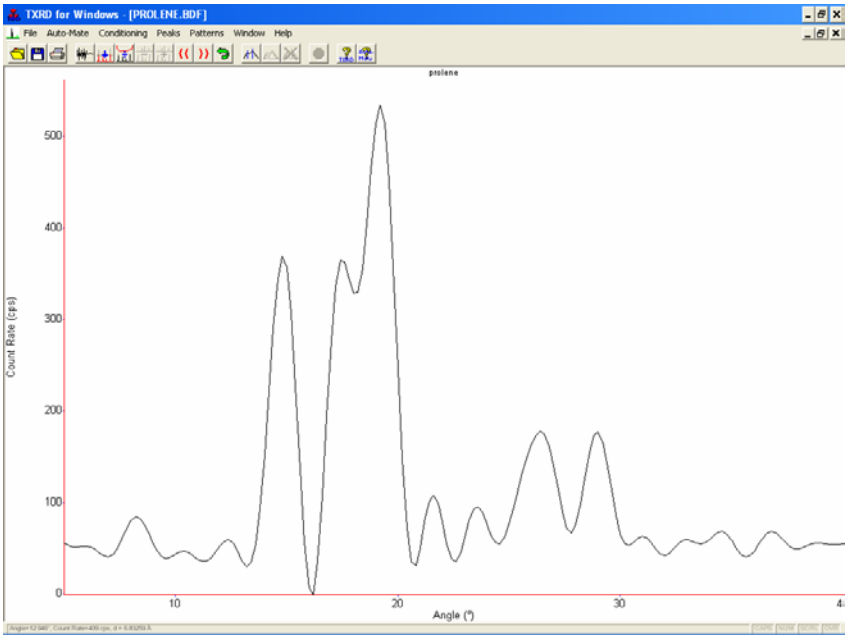

Figure 7. 8: X-ray diffraction curve for Prolene.

7.2 Differential Scanning Calorimetry Curves

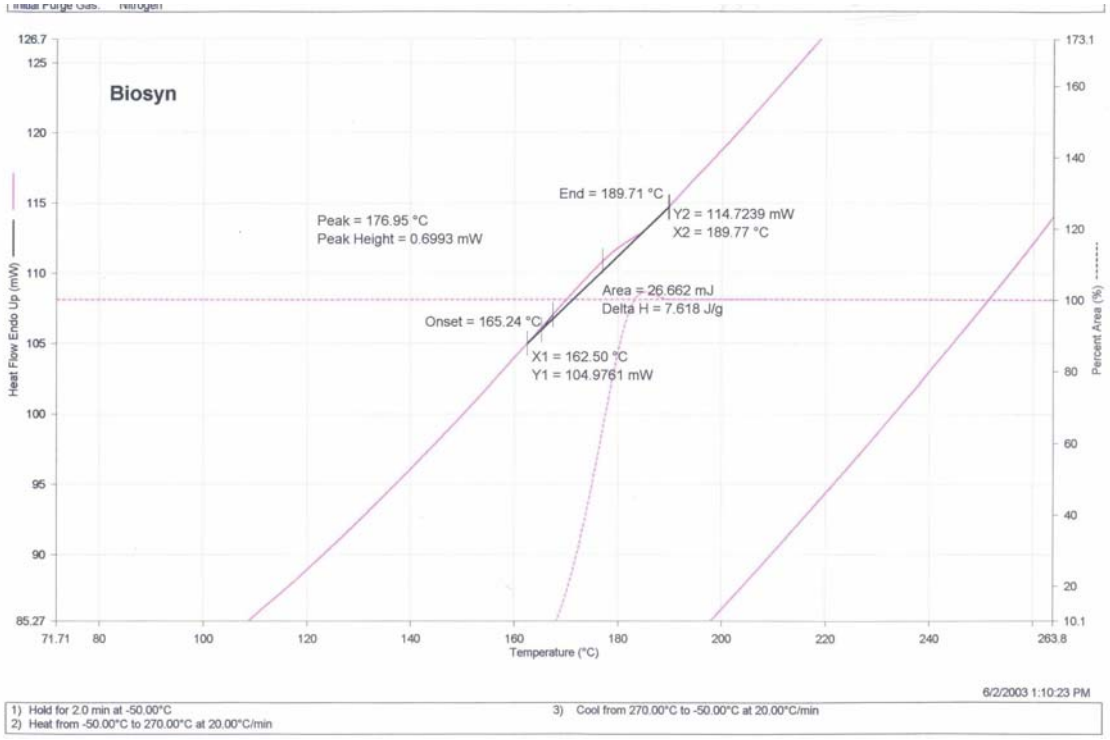

Figure 7. 9: DSC curve for Biosyn

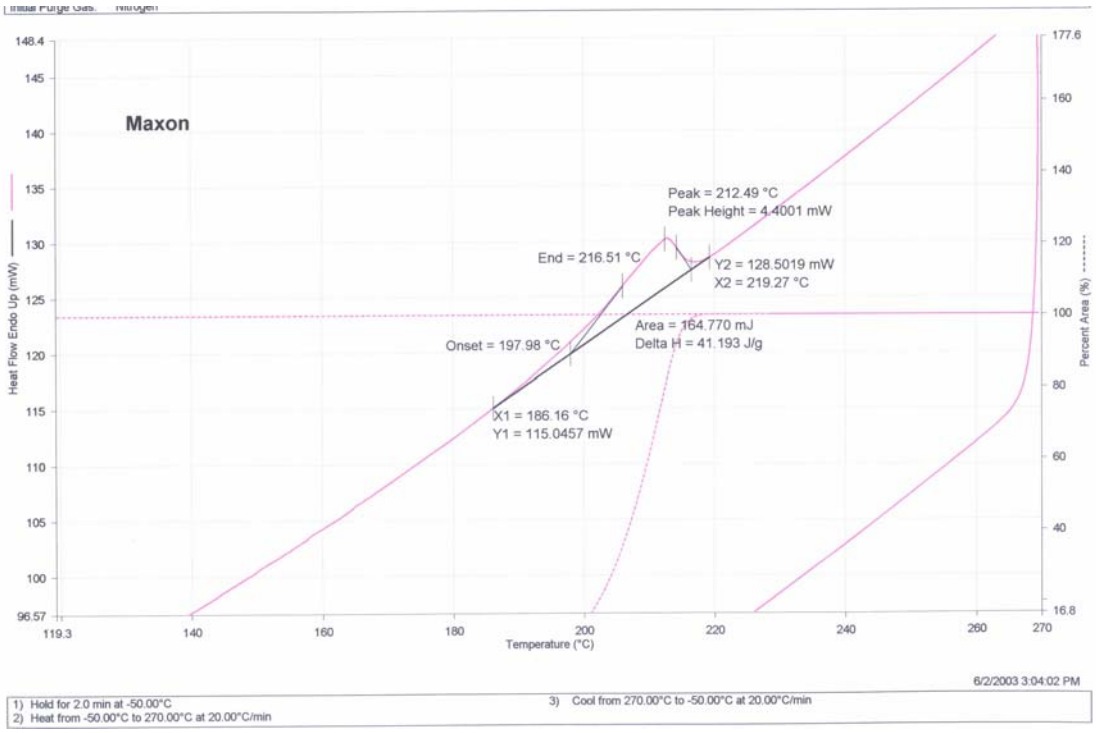

Figure 7. 10: DSC curve for Maxon

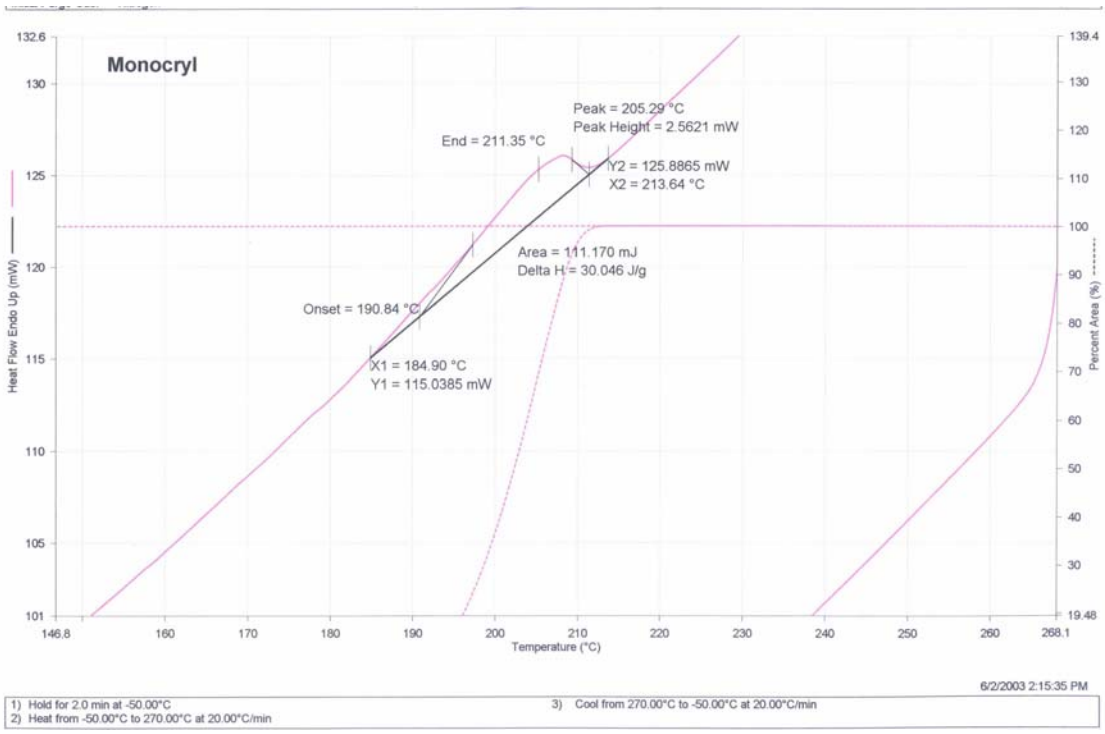

Figure 7. 11: DSC curve for Monocryl.

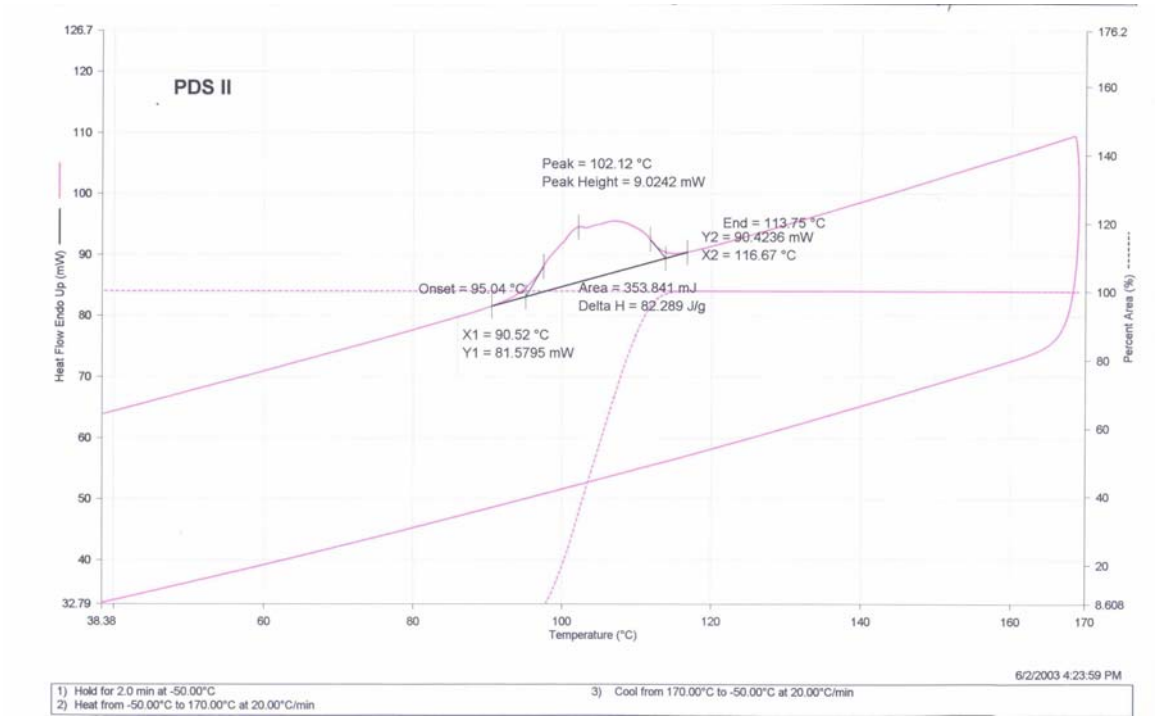

Figure 7. 12: DSC curve for PDS II

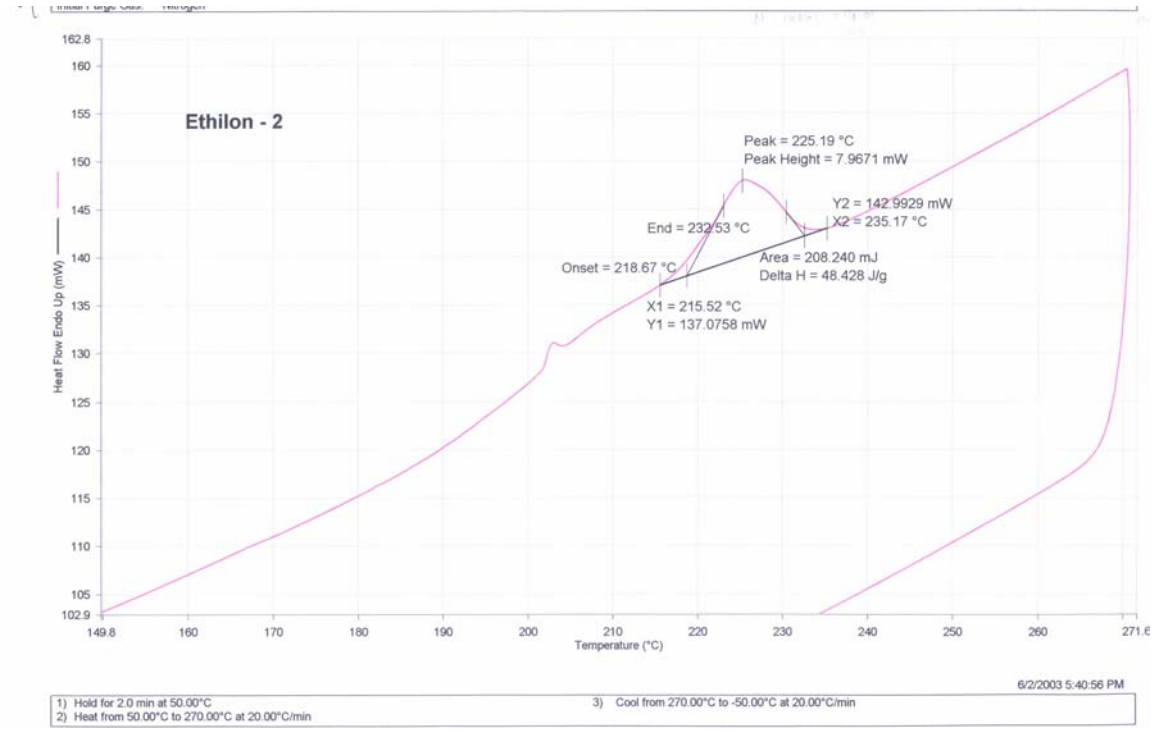

Figure 7. 13: DSC curve for Ethilon

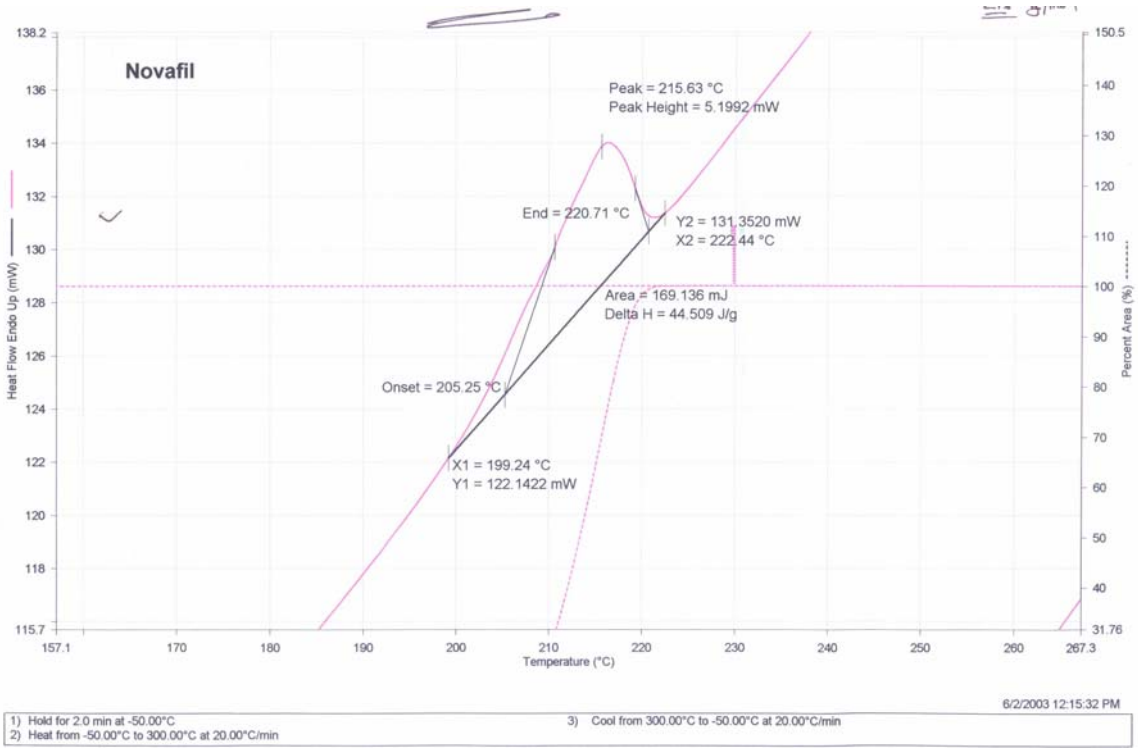

Figure 7. 14: DSC curve for Novafil

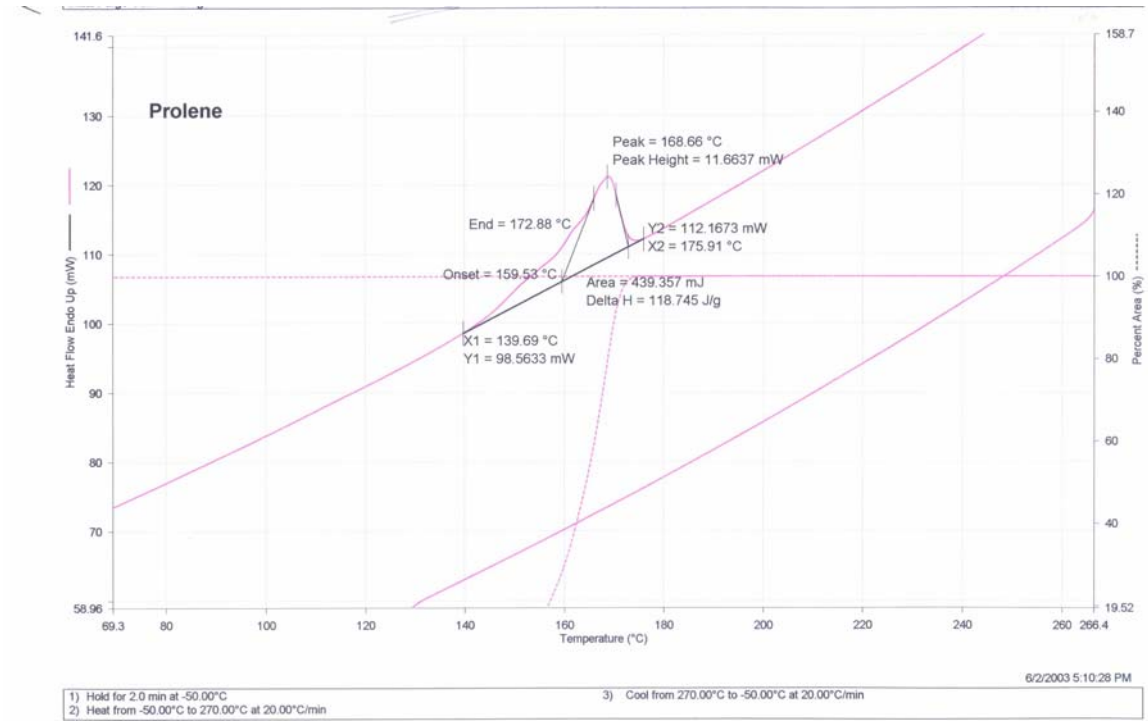

Figure 7. 15: DSC curve for Prolene

7.3 Tensile Curves

7.3.1 Barbed Sutures:

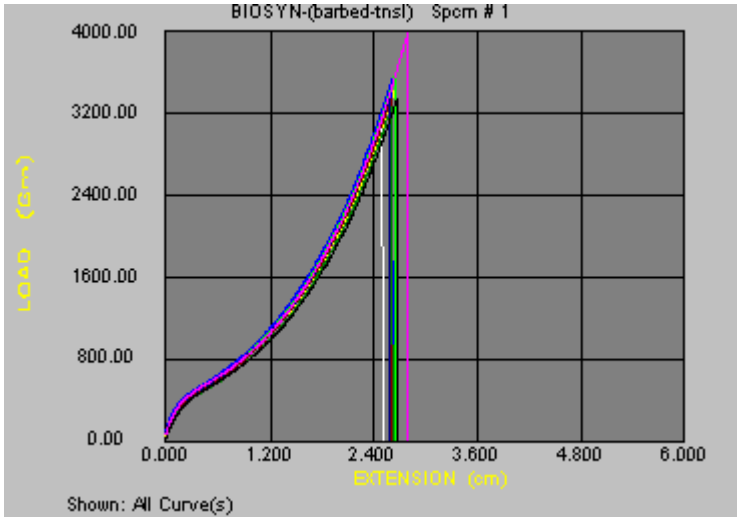

Figure 7. 16: Load-elongation curve for barbed Biosyn suture.

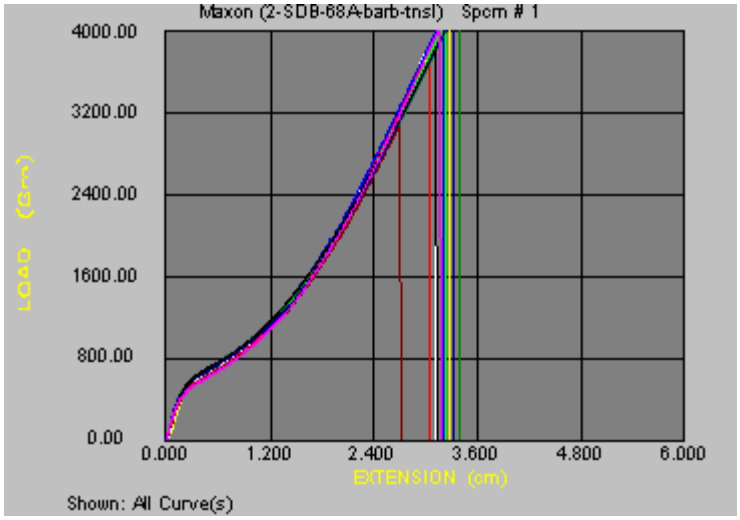

Figure 7. 17: Load-elongation curve for barbed Maxon suture.

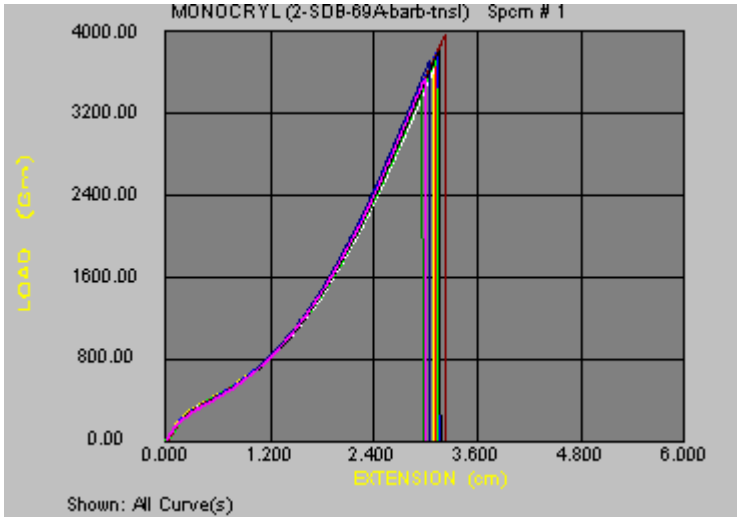

Figure 7. 18: Load-elongation curve for barbed Monocryl suture.

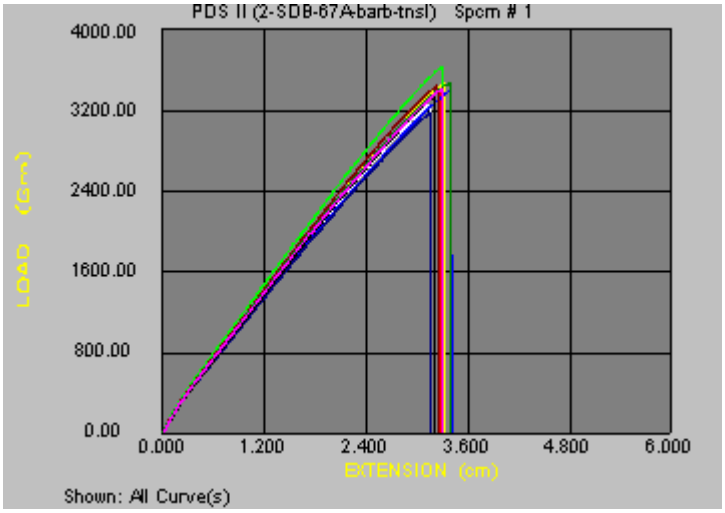

Figure 7. 19: Load-elongation curve for barbed PDS II suture.

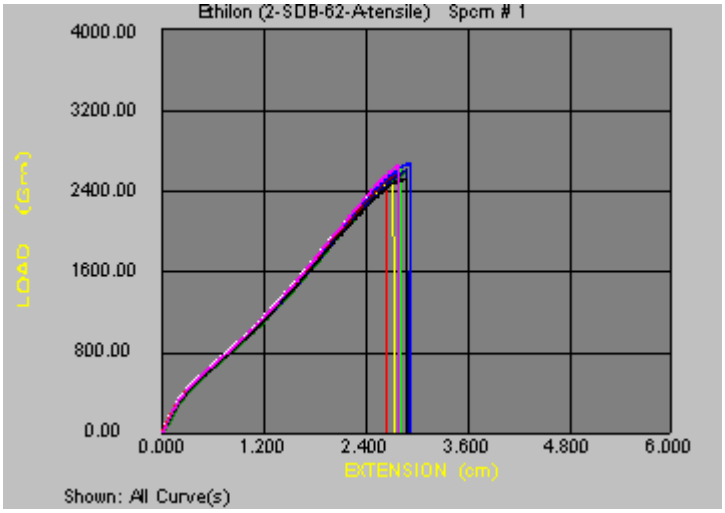

Figure 7. 20: Load-elongation curve for barbed Ethilon suture.

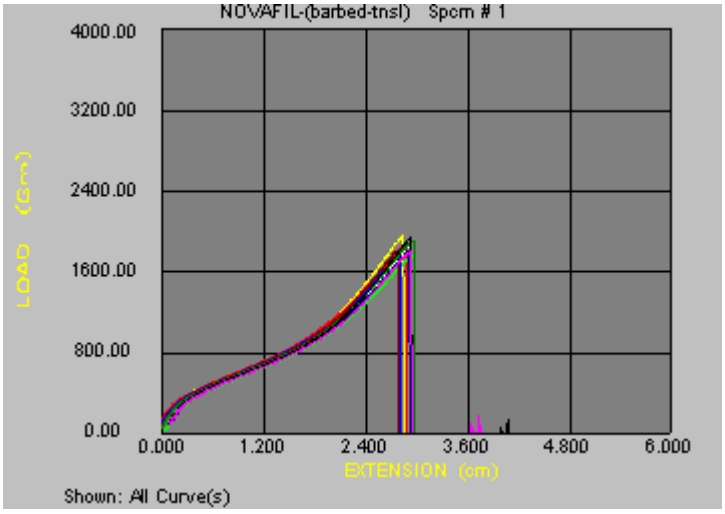

Figure 7. 21: Load-elongation curve for barbed Novafil suture.

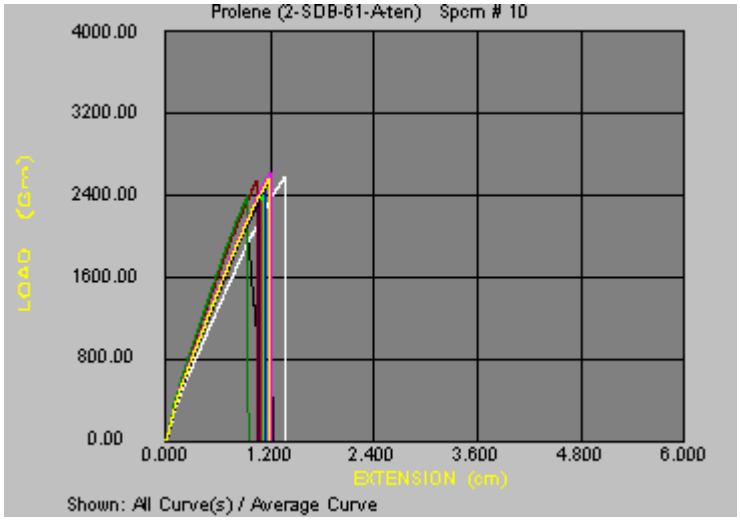

Figure 7. 22: Load-elongation curve for barbed Prolene suture.

7.3.2 Unbarbed Sutures

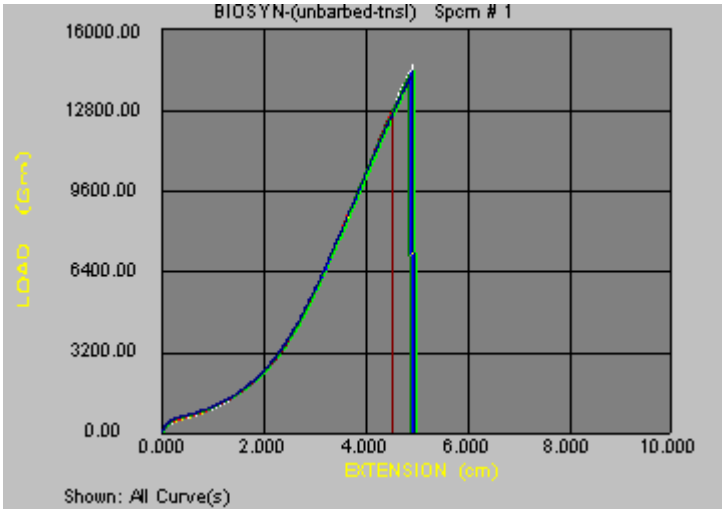

Figure 7. 23: Load-elongation curve for un-barbed Biosyn suture.

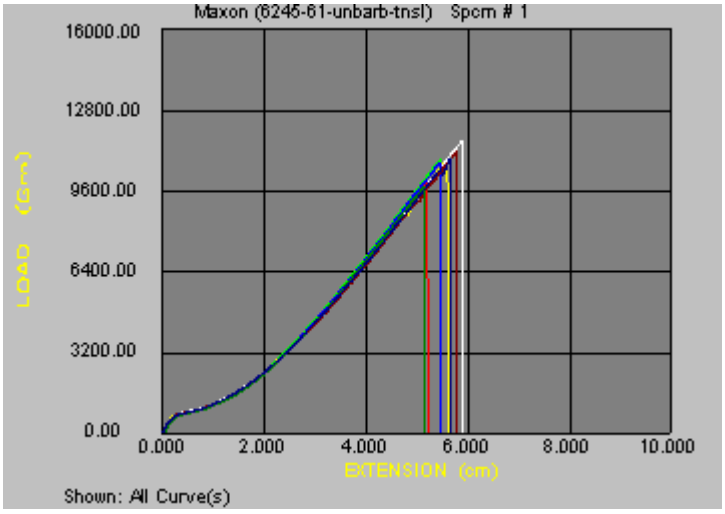

Figure 7. 24: Load-elongation curve for un-barbed Maxon suture.

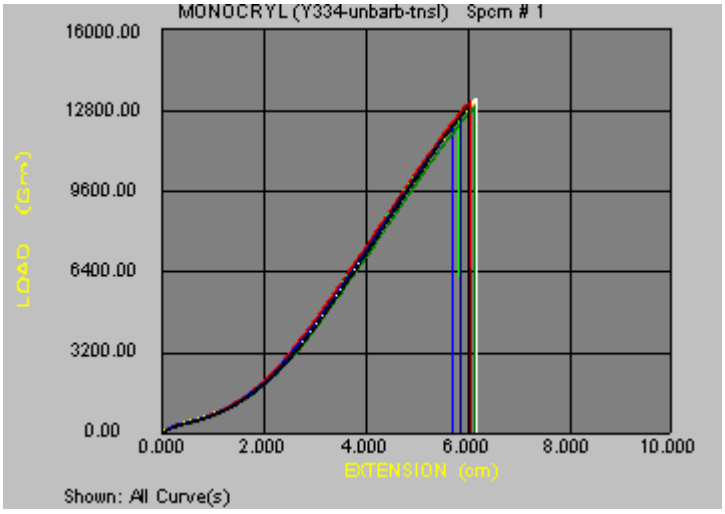

Figure 7. 25: Load-elongation curve for un-barbed Monocryl suture.

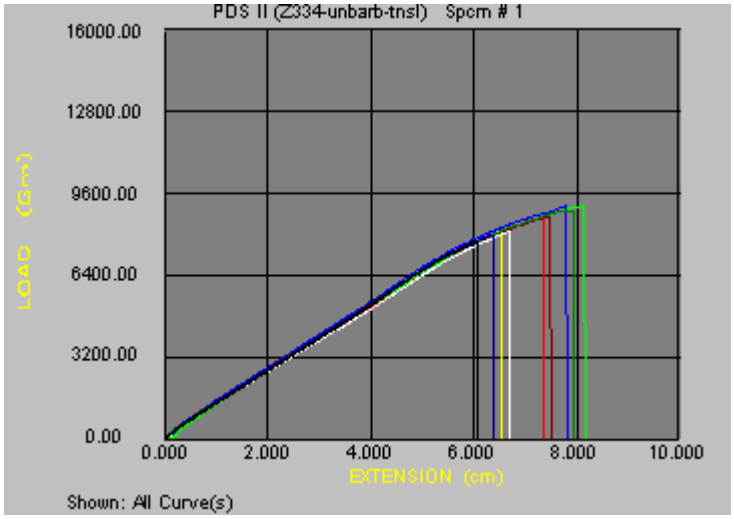

Figure 7. 26: Load-elongation curve for un-barbed PDS II suture.

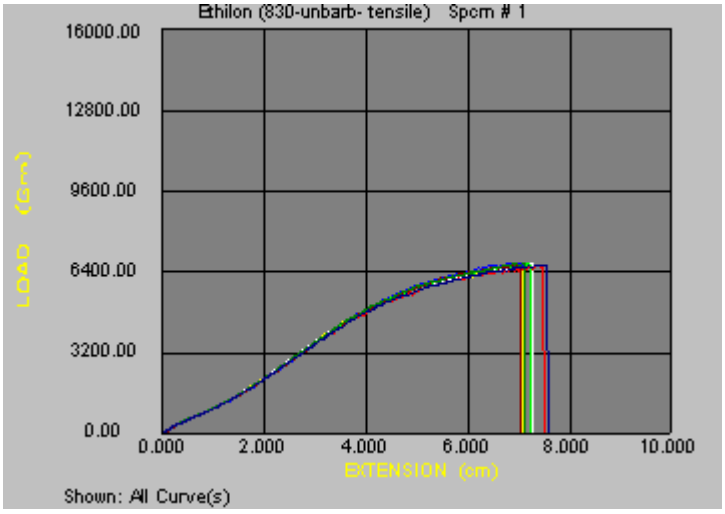

Figure 7. 27: Load-elongation curve for un-barbed Ethilon suture.

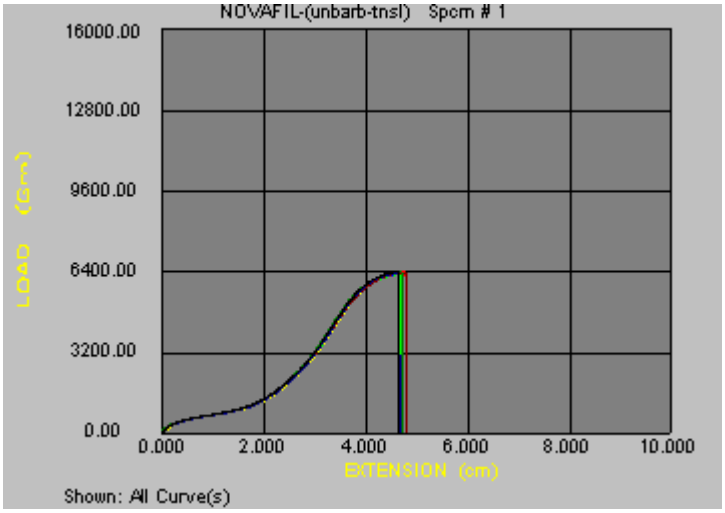

Figure 7. 28: Load-elongation curve for un-barbed Novafil suture.

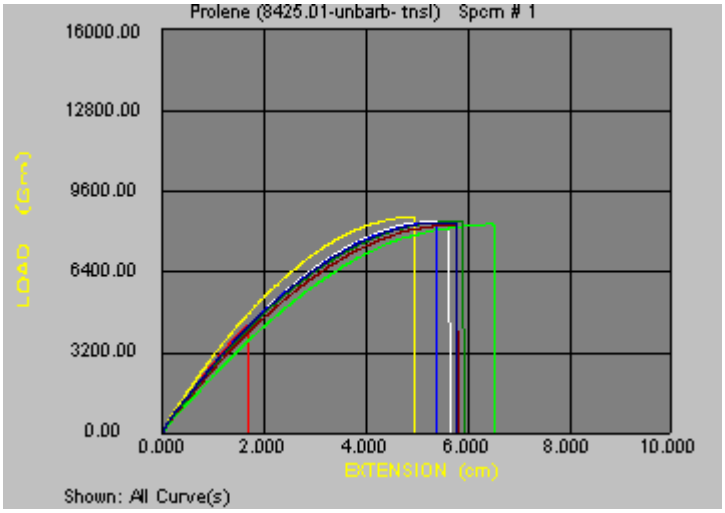

Figure 7. 29: Load-elongation curve for un-barbed Biosyn suture.

7.4 Suture/tissue pull-out curves

7.4.1 Barbed sutures

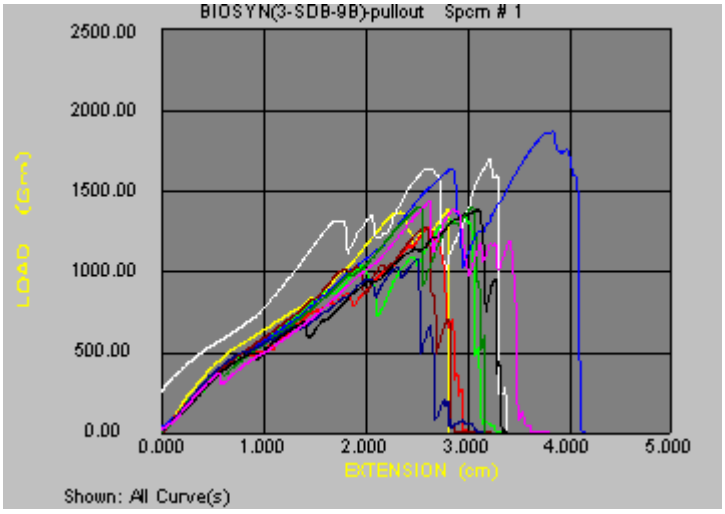

Figure 7. 30: Suture/tissue pull-out peak load curve for barbed Biosyn suture.

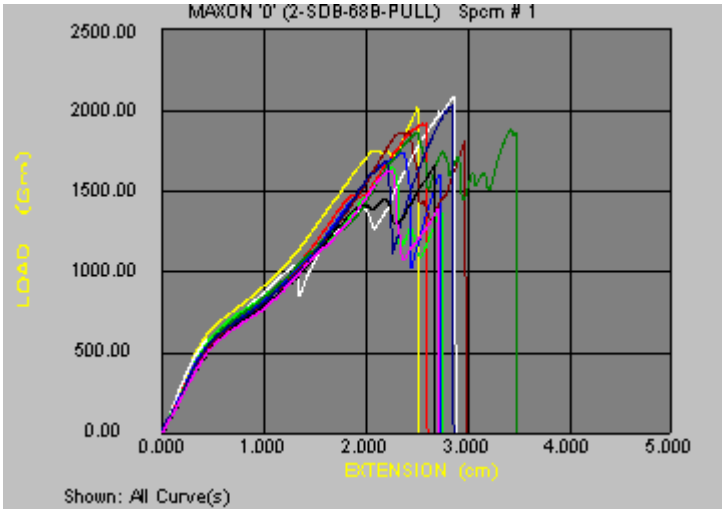

Figure 7. 31: Suture/tissue pull-out peak load curve for barbed Maxon suture.

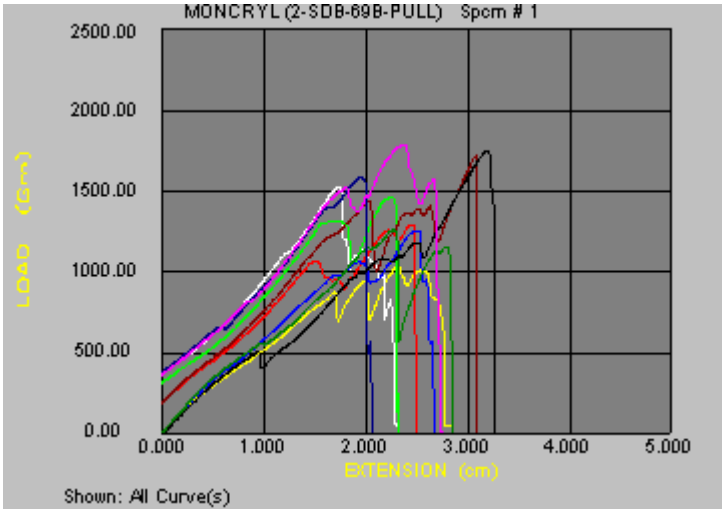

Figure 7. 32: Suture/tissue pull-out peak load curve for barbed Monocryl suture.

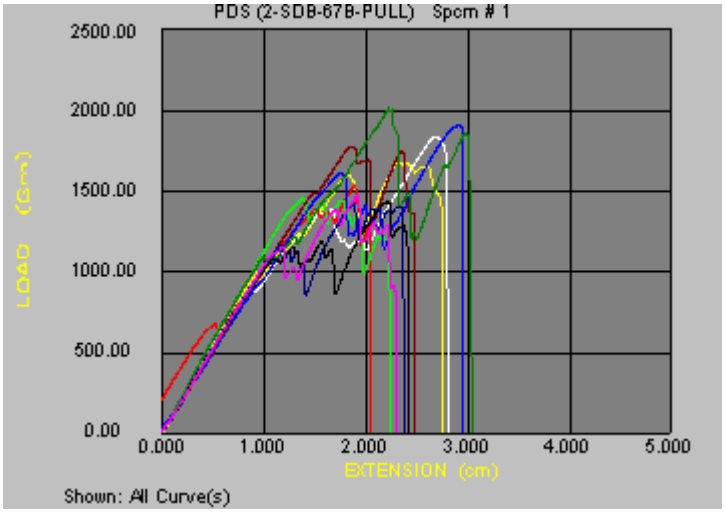

Figure 7. 33: Suture/tissue pull-out peak load curve for barbed PDS II suture.

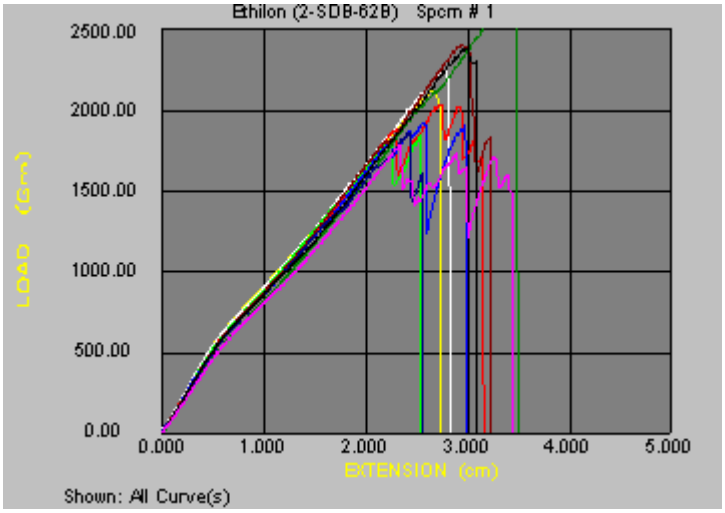

Figure 7. 34: Suture/tissue pull-out peak load curve for barbed Ethilon suture.

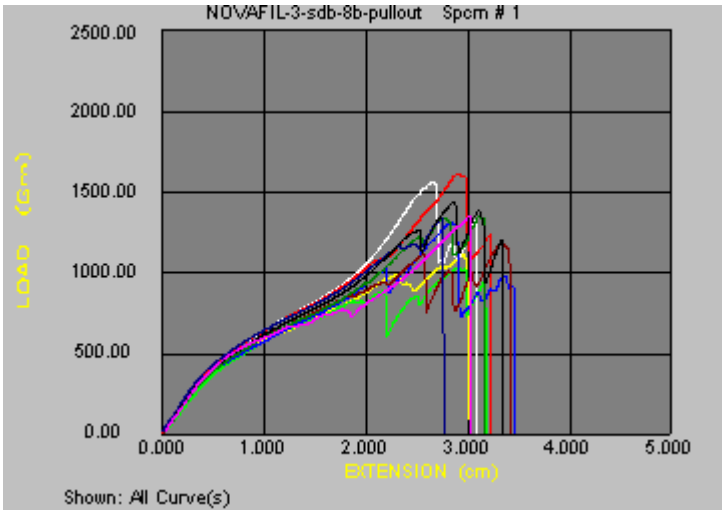

Figure 7. 35: Suture/tissue pull-out peak load curve for barbed Novafil suture.

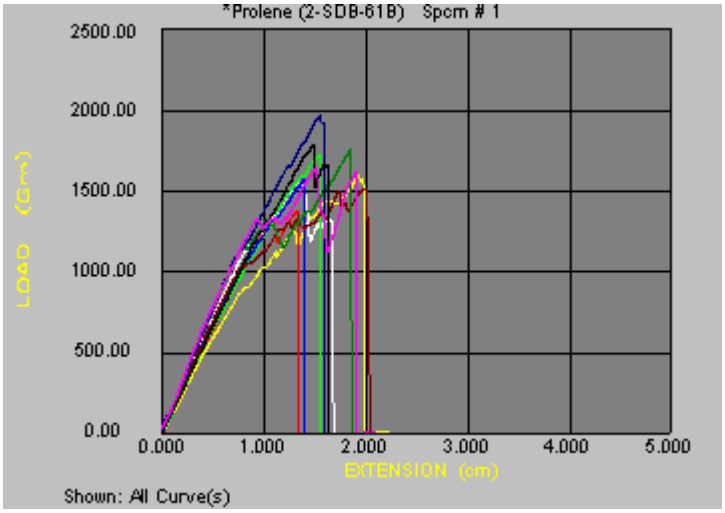

Figure 7. 36: Suture/tissue pull-out peak load curve for barbed Prolene suture.

7.4.2 Unbarbed sutures:

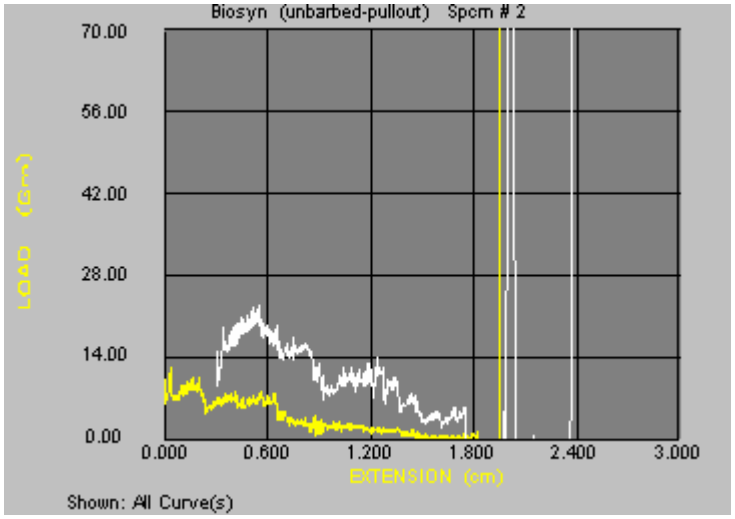

Figure 7. 37: Suture/tissue pull-out peak load curve for barbed Biosyn suture.

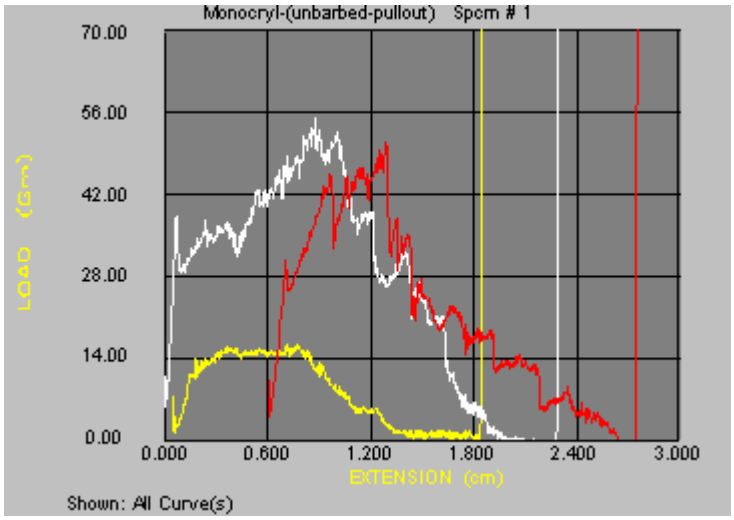

Figure 7. 38: Suture/tissue pull-out peak load curve for barbed Monocryl suture.

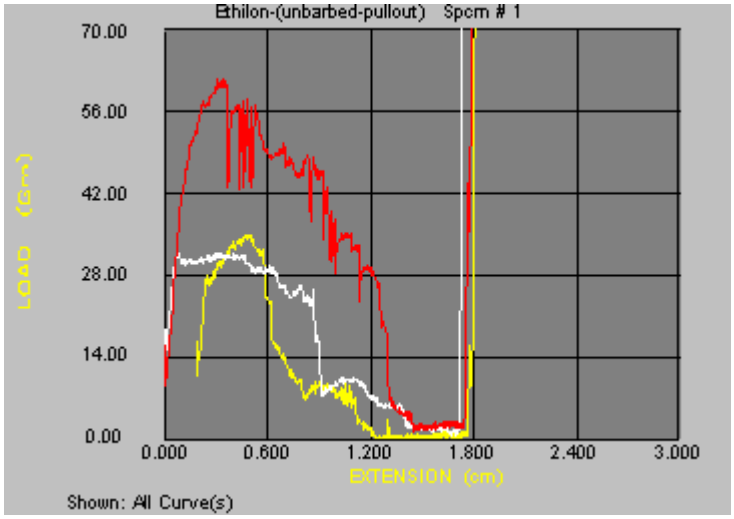

Figure 7. 39: Suture/tissue pull-out peak load curve for barbed Ethilon suture.

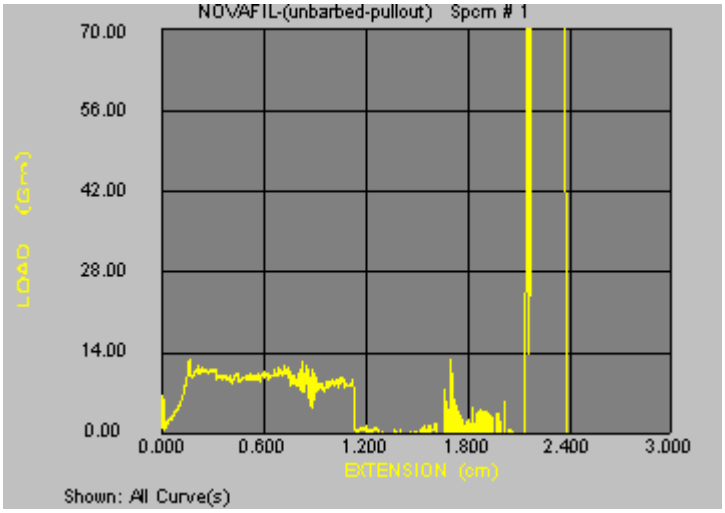

Figure 7. 40: Suture/tissue pull-out peak load curve for barbed Novafil suture.

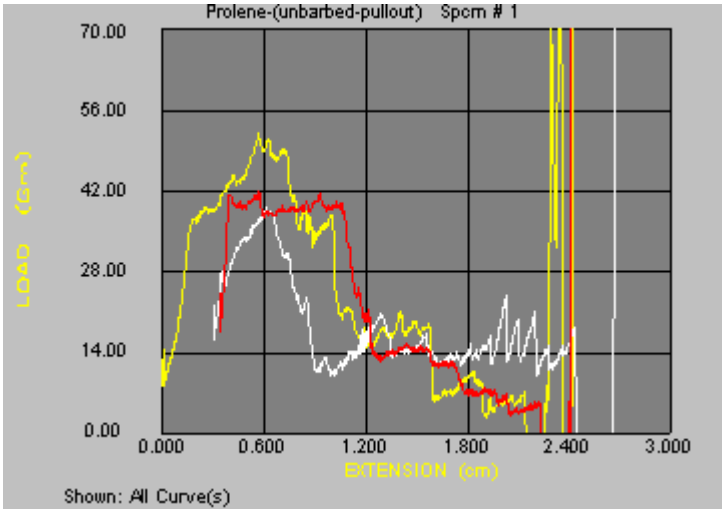

Figure 7. 41: Suture/tissue pull-out peak load curve for barbed Prolene suture.

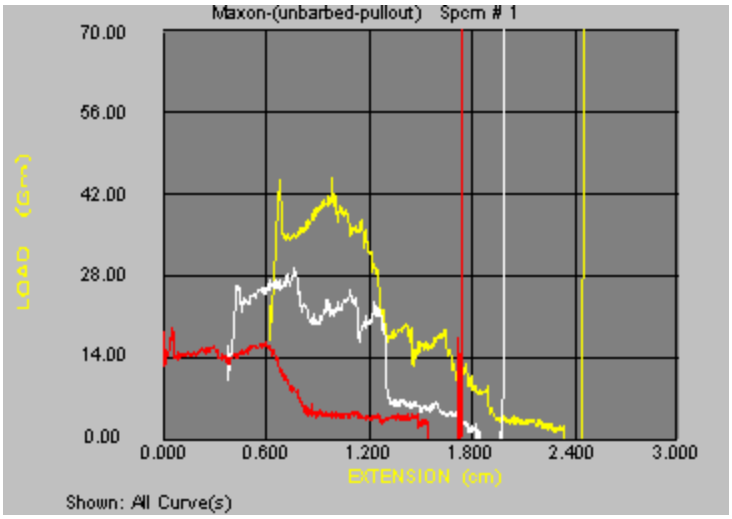

Figure 7. 42: Suture/tissue pull-out peak load curve for barbed Maxon suture